Transfer Mechanisms for Low Molecular Weight Lipid Insoluble Molecules into the Developing Brain

by

Carl Joakim Ek

Submitted in fulfilment of the requirements for
the Degree of Doctor of Philosophy

University of Tasmania, December 2001

Forewords and Acknowledgements

I came to Tasmania without knowing the nature of my research project or when I was going to start. At first I wondered why I should undertake research in a field I never heard much about before, using baby marsupials as my animal model. Nevertheless, I thought I should give it a go and did some preliminary experiments with the help of Dr Graham Knott. Even though I had my doubts, it was possible to carry out experiments in such small animals. So I sat down with Professor Norman Saunders and Associate Professor Katarzyna Dziegielewska and we made a research plan for the next three years. The first part of the project was supposed to be reasonably straightforward experiments using radiolabelled markers and measuring their uptake into the brain. The second part was to involve a tracer that we could visualise in the brain but the exact nature of these experiments we were not really sure about yet. However, as I realised later, nothing is straightforward when you have hands that are more designed for digging up potatoes than handling tiny animals. Just to take a sample of cerebrospinal fluid without contaminating it with blood took a while to learn, and to give injections into the pups often required the help of somebody else while I was guiding the micropipette under a microscope. I suppose it was straightforward once all that was sorted out.

After about one and a half years it was time to start familiarising myself with the electron microscope. So I wandered down to the EM suite with Rob Tennant. Rob made up a recipe for fixing choroid plexus tissue that was almost an instant success. However, I did have to learn the art of cutting ultra-thin sections. No textbook can teach you this and when I came to Rob for help I always got the answer "try this or try that". No rules. No definite solutions. So I tried everything but it still didn't work and so I went back to Rob for more hints. Come back tomorrow and it will probably work, was the answer - and it often did! After showing that I could handle the microtome using glass knifes I was finally given a diamond knife. An old one, but still, a diamond knife. One scratch in the middle and a smaller one just to the left. As long as you knew that, you were fine. I still remember those first pale gold sections coming off the knife. I just stared in amazement, totally frozen and then almost collapsed because I had forgotten to breath for a whole minute. The first part of the project progressed well and I had plenty of data to analyse. However, it felt like a long standstill when I started up the electron

microscopic study. It took a long time just to learn how to cut sections and develop a protocol to achieve satisfactory preservation and staining of tissue. And still, in order to get some results it was endless hours of cutting and trying to stay awake in a dark room with only the green light of the electron microscope.

My project could not have been completed without the help of many people. First of all I would like to thank my supervisors Professor Norman Saunders and Associate Professor Katarzyna Dziegielewska for letting me come to Tasmania and taking me on as a student without actually knowing me. Secondly, I would like to thank Dr Graham Knott and my research supervisor Dr Mark Habgood for patiently teaching me the intricate work of handling opossum pups. I would also like to thank other people in the department: Ann Potter for cutting endless sections without complaining, Dr Niels Andersen for keeping my computer at maximum speed, Rob Tennant for the help with the electron microscopy, and Michael Lane for that instant help during crucial experiments and the endless jugs of coffee.

This work would also have been impossible without somebody caring for the opossum colony. I am therefore grateful to Alan Norris and colleagues in the Animal House who has been keeping our opossums happy.

And last but not least I would like to thank Elizabeth for luring me over to this beautiful Island.

Abstract

The internal environment of the central nervous system (CNS) is protected from its surrounding milieu by barriers, which selectively facilitate and restrict the entry of molecules in and out of the CNS. These barriers form early during development, however, their selectivity in the developing brain appears to be different from those that protect the adult brain. The reasons for the differences in the CNS barriers between young and adult animals are still unclear. The experiments in this thesis were performed in order to obtain morphological and physiological explanations for the changes in the transfer of lipid insoluble molecules into the CNS that occur during development. Quantitative studies with radioactive markers in parallel with experiments using a tracer that could be visualised were conducted in an attempt to correlate physiological uptake with the structural studies. A marsupial species, the grey short-tailed South-American opossum (*Monodelphis domestica*), was used in all experiments since it is born at an early stage of brain development, and thus is a more accessible model than any eutherian animal during a similar developmental period. The transfer of lipid insoluble molecules has previously not been studied at such early stages of brain development. All experiments were carried out in accordance with NHMRC guidelines and with the approval of the University of Tasmania Ethics Committee. Lipid insoluble radioactive markers were injected into opossum pups and blood, cerebrospinal fluid (CSF) and brain samples were collected to assess initial rate of uptake and steady-state CSF/plasma and brain/plasma ratios. These experiments showed that the steady-state ratios for small lipid insoluble molecules were high in early development compared to the adult and that they decreased during development due to a reduction in CNS barrier permeability with age. Possible routes by which lipid insoluble molecules enter the brain were investigated using a 3000 molecular weight biotin-dextran and visualising it under the light and electron microscope. This tracer allowed localisation of a small inert lipid insoluble molecule at the blood-CNS interfaces. Quantitative measurements of CSF uptake showed that the dextran penetrates across the brain barriers to an extent similar to other small lipid insoluble molecules and thus validates the dextran as a suitable tracer. Under the electron microscope, it appeared that cells of the blood-CSF interface at birth already exhibited tight-junctions, which are the fundamental structures of the brain barriers. These junctions seemed to impede the intercellular movement of the biotin-dextran. Uptake into cells at the blood-CSF interface and lack of extracellular

biotin-dextran in the brain suggest that in the immature brain the route of penetration from blood to brain may be predominantly via the CSF rather than directly across the cerebral vessels of the developing brain.

Abbreviations

BUI	–	Brain uptake index
CNS	–	Central nervous system
CPM	–	Counts per minute
CSF	–	Cerebrospinal fluid
CVO	–	Circumventricular organ
DAB	–	Diaminobenzidine tetrahydrochloride
DPM	–	Disintegrations per minute
E	–	Embryonic day
ECF	–	Extracellular fluid
EM	–	Electron microscopy
ER	–	Endoplasmic reticulum
HRP	–	Horseradish peroxidase
LS	–	Liquid scintillation
MRP	–	Multi-drug resistant protein
MP	–	Microperoxidase
P	–	Postnatal day
PBS	–	Phosphate buffered saline
Pgp	–	Phospho-glycoprotein
SAS	–	Subarachnoid space
TER	–	Tubulo-cisternal endoplasmic reticulum
TLC	–	Thin layer chromatography
ZO	–	*Zonulae occludentes*

Statement

The work in this thesis has been undertaken exclusively for the use of a PhD in the area of Anatomy and Physiology, and has not been used for any other higher degree or graduate diploma in any University. All written and experimental work is my own, except where due reference is given.

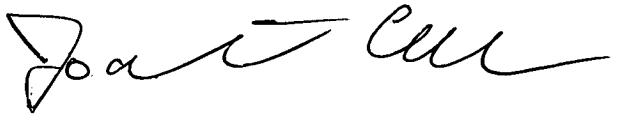

Carl Joakim Ek

Authority of access

This thesis may be available for loan and limited copying in accordance with the Copyright Act 1968.

Carl Joakim Ek

Contents

Chapter 1

*

General Introduction

This thesis starts with a general introduction to the field in Chapter 1. Chapter 2 describes experimental procedures that were common to a majority of the studies. Chapter 3 describes and evaluates the animal model that was used in the experiments of this thesis. Chapter 4 presents quantitative uptake studies of several small lipid insoluble molecules from the blood into the brain and CSF. Chapter 5 presents experiments with a small lipid insoluble dextran that was visualised in the brain under the light and electron microscope and Chapter 6 is a general discussion of all the results obtained. Part of the work in this thesis has been presented in Saunders et al. (1999c), Dziegielewska et al. (2001) and Ek et al. (2001). Copies of these publications are found in the back of this thesis.

Brief historical background

The earliest experiments that led to the concept of a barrier mechanism between blood and brain were made around the turn of the 19th century (Ehrlich, 1885; Lewandowsky, 1900 as cited by Habgood, 1990; Goldmann, 1909). These experiments involved small molecules that could easily be visualised eg. potassium ferrocyanide or dyes (such as trypan blue) that, after systemic injection, coloured almost the whole body but left the CNS unstained. On the other hand, when the dyes where injected directly into the brain the neural tissue became widely stained (Goldmann, 1913). These experiments also demonstrate the caution that has to be taken when interpreting the results of tracer experiments. Many of the dyes that were used in these early experiments were later found to bind to plasma proteins (Tschirgi, 1950), thus while in the plasma most of the dyes probably existed as dye-protein complexes. However, when injected directly into the CSF the dyes possibly existed as free dye to a much larger extent due to the low protein concentration in CSF. At the same time it was also noted that bile and sodium ferrocyanide, which had little effect when delivered vascularly, could have dramatic effects when delivered directly into the CNS (Biedl and Kraus, 1898; Lewandowsky,

1900 as cited by Habgood, 1990). Goldmann and Lewandowsky interpreted these experiments as an existence of barrier systems that restricted the entry of these dyes between the blood and the brain, and Lewandowsky coined the term "bluthirnschranke" (blood-brain barrier); however, at that time this concept was not widely accepted. Basic dyes did have the ability to stain central nervous tissue whilst acidic dyes did not stain the brain after systemic administration. This lead to the incorrect assumption that it was the affinity for neural tissue, and not its capacity to reach the brain, which explained the dyes ability to stain the CNS (Ehrlich, 1887; King, 1939 as cited by Habgood, 1990). The most obvious sites for a CNS barrier were the brain blood vessels, which could have properties denying the entry of dyes into the brain. During this time, however, using light microscopy, it was not possible to find any difference between the capillaries in the CNS and those of other parts of the body (Goldmann, 1913; Broman, 1941). It was not until the introduction of electron microscopy in the 1960's, revealing specialised ultrastructural properties in the brain capillaries, that a physical barrier to blood solutes was identified (Reese and Karnovsky, 1967; Brightman and Reese, 1969) (see below for more details about these experiments).

Ehrlich (1904) noted that in general the dyes staining the brain also stained adipose tissue. This was probably the first indication that lipid solubility plays a role in the ability of blood solutes to reach brain tissue. The use of lipid soluble narcotics, which had a rapid central action, supported this hypothesis (Krogh, 1946). When better analytical techniques, such as radioisotopes were introduced, the use of basic dyes could be abandoned and the range of compounds used in experiments increased. This also meant that it was possible to measure tracer levels of solutes in a quantitative way. With the use of these new techniques Davson (1955) published a series of comprehensive studies with a number of small molecules, electrolytes and non-electrolytes, and confirmed that lipid-solubility was a main determinant of penetration from blood to brain. These studies also showed that charged molecules such as cations and anions

penetrated from blood into the brain very slowly.

The earliest experiments investigating possible barriers in the developing animal were carried out in the 1920's (Wislocki, 1920; Behnsen, 1927; Stern and Peyrot, 1927 as cited by Møllgård and Saunders, 1986; Penta, 1932 as cited by Møllgård and Saunders, 1986). These studies used similar dyes and small markers that were used in the early experiments demonstrating barrier mechanisms in the adult animal (see above). Nearly all these studies showed that these markers penetrated into the developing brain in contrast to the lack of staining in the adult brain. These studies therefore lead to the misconception that the barriers were poorly developed until late in development. However, as was pointed out by Møllgård and Saunders (1986), these early experiments indicating barrier immaturity injected huge amounts of dye that probably affected the integrity of the fetal and embryonic barrier mechanisms. As became clear later (see references below) and is also shown in the experiments presented in this thesis, the developing brain is indeed protected by barriers that are present very early in development.

Current concept of the brain barriers

The term blood-brain barrier (BBB) is widely used as a collective term describing several barrier mechanisms in the CNS. However, scientists working in the field use the more exact definition of this term to define the restriction to the passage of molecules from the lumen of blood vessels inside the brain to the surrounding brain tissue (see Figure 1.1). In this thesis the term brain barriers will be used as a collective term for all barrier mechanisms regulating the penetration of blood solutes into the brain. The current concept of the brain barriers includes multiple systems that control the internal environment of the brain, both by restricting and by facilitating the entry of solutes (Saunders and Dziegielewska, 1997). These systems include outward transporting

systems, such as the P-glycoprotein and multi-drug resistant protein, which exclude molecules by active transport out of the endothelium (Borst and Schinkel, 1998). These specialised transporting systems within the barriers will be discussed separately later.

The brain barriers can be divided into four principal interfaces: 1) the endothelium of the cerebral blood vessels (blood-brain barrier), 2) the epithelium of choroid plexus tissue in the brain ventricles (blood-CSF barrier), 3) the ependymal lining of the ventricles and the pia-glia limitans (CSF-brain barrier), 4) and the meningeal barrier (a second blood-CSF barrier). The structures associated with these barriers will be described in detail below, first in the mature and then in the developing CNS (see also Figure 1.1).

Figure 1.1

The brain barriers in the developing and in adult animal. The central picture is a schematic diagram of the three main compartments in the central nervous system (CSF, brain and blood). These compartments are separated from each other by four separate barriers in the developing brain. **1**) The blood-brain barrier, which is situated between the lumen of the blood vessels in the brain and the brain tissue itself. Arrow points to the location of tight-junctions between the endothelial cells that restricts the intercellular passage of molecules. **2**) The blood-CSF barrier, which is situated between the lumen of the blood vessels in the choroid plexus and the cerebrospinal fluid (CSF). Arrows point to the position of the tight-junctions that impedes the paracellular passage of molecules in between the choroidal epithelial cells. **3**) The CSF-brain barrier, which is situated at the ventricular surface and the pia-glia limitans, between the CSF and brain tissue. This has only been shown to be a functional barrier in the early developing brain (Fossan et al., 1985) where the neuroependymal cells form a pseudostratified layer and are connected to each other by strap-junctions (arrowheads). **4**) The meningeal barrier, which is situated between the CSF filled subarachnoid space (SAS) and the overlaying blood circulation. The cells in the outer surface of the arachnoid have tight-junctions that hinder the extracellular movement of molecules. The dura mater has fenestrated blood vessels whereas the blood vessels in the arachnoids and on the pial surface have functional barrier characteristics similar to the blood vessels inside the brain. Likewise to the ventricular CSF-brain interface, a functional barrier seems to exist on the outer pial surface of the brain (arrowheads) during early development but disappears later. **5**) The mature ventricular surface is made up of a flat layer of ependymal cells. These ependymal cells are connected to each other by gap-junctions and lack tight-junctions so there is a free passage of molecules between the CSF and the extracellular fluid of the brain. Abbreviations: D – Dura mater, OA – Outer Arachnoid, SAS – Subarachnoid space. Modified from Saunders et al. (1999b), Habgood (1990) and Krisch et al. (1984).

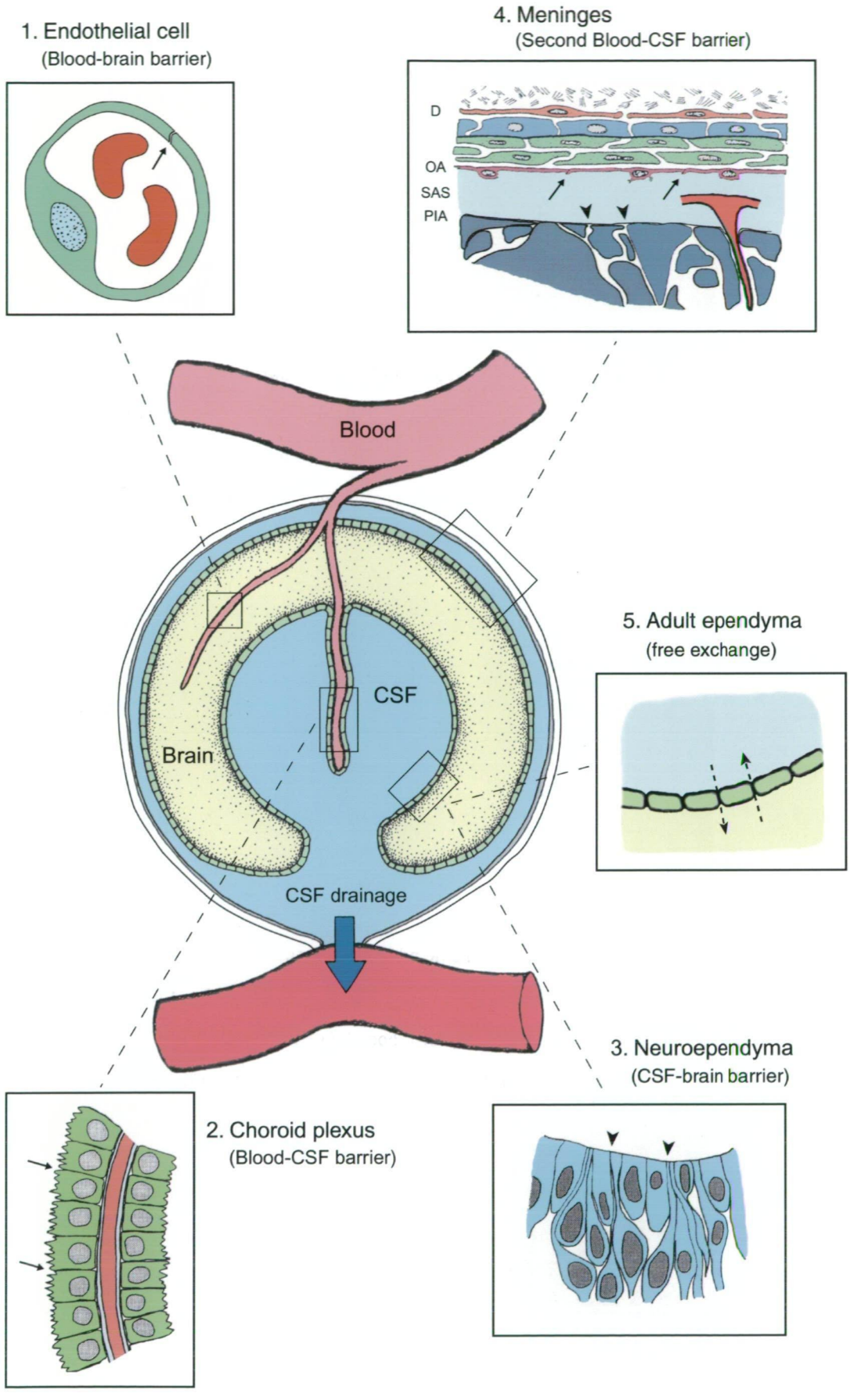
1. Endothelial cell
(Blood-brain barrier)
4. Meninges
(Second Blood-CSF barrier)
D
OA
SAS
PIA
Blood
CSF
Brain
CSF drainage
5. Adult ependyma
(free exchange)
3. Neuroependyma
(CSF-brain barrier)
2. Choroid plexus
(Blood-CSF barrier)

Barriers in the adult brain

I. *Blood-brain barrier*

In blood capillaries in the brain, the cell membranes of endothelial cells come together at the luminal side to form *zonulae occludentes*. *Zonulae occludentes* refers to a region of the intercellular cleft where the opposing cell membranes fuse at multiple points to form tight-junctions that obliterate the intercellular space. In freeze-fracture it has been shown that these tight-junctions form a continuous fusion and completely encircle the endothelial cells (Connell and Mercer, 1974; Dermietzel, 1975a; Shivers et al., 1984). These tight-junctions are believed to form a physical barrier to compounds and thus forming the structural basis for the blood-brain barrier. That the barrier was situated between the endothelial cells was first shown by Karnovsky (1967) and in further studies by Brightman and Reese (1969), who injected horseradish peroxidase (HRP), a 40 000 MW protein, into mice and visualised it under the electron microscope. HRP was confined to the lumen of the capillaries. It could penetrate the space in between the endothelial cells until it reached the tight-junction where it was stopped. An inverse image was found when HRP was introduced into the ventricles. HRP could penetrate brain tissue all the way to the endothelial cells, but was stopped in the interendothelial clefts. The tight-junctions of the endothelial cells have also been found to be impenetrable to other tracers such as cytochrome *c* (Milhorat et al., 1973; Milhorat et al., 1975), lanthanum (Brightman and Reese, 1969; Bouldin and Krigman, 1975), and microperoxidase (MP) (Reese et al., 1971). The latter molecule was later found to bind to plasma proteins so the barrier was to a MP-protein complex, which would be considerably larger than MP itself (Milton Brightman, personal communication). In contrast to the above-mentioned studies, Nag et al. (1982) found that lanthanum could penetrate the intercellular cleft in some cerebral arterioles but not in cerebral capillaries or venules. However, studies using lanthanum as a tracer has to be interpreted with caution because of its toxicity and also because of the differences in methods used in

experiments. For instance, Bouldin and Krigman (1975) perfused the brain with a lanthanum solution for 15 minutes *in vivo* before fixing the brain whereas Nag et al. (1982) first perfused the brain with an aldehyde solution and then with a lanthanum solution. The use *in vivo* has to be questioned since it is toxic (Milhorat et al., 1975), whereas the relevance of experiments in fixed tissue to *in vivo* penetration may be limited because it is not known whether channels and pores remain intact in the process of fixation.

Another way to study the permeability of the blood vessel wall is by measurements of electrical resistance over the endothelium. An electrode inside the vessel produces a small current and the fall in voltage with distance to the current source is partially affected by the leakage of ions through the vessel wall (indirect measurement of ionic permeability). Studies with electrical resistance in blood vessels have revealed that the brain capillaries have the highest resistance recorded for any endothelium. For example, transmembrane resistance of 2000 Ωcm^2 in capillaries on the surface of the brain in frogs compared to 20-30 Ωcm^2 in skeletal muscle endothelium (Crone and Olesen, 1982; Crone, 1984). Because of technical problems, however, measurements have so far only been made in the pial vessels which are accessible from the outside of the brain. It is still debatable if these vessels are a good representative of the vessels found deeper inside the cortex (for review see Allt and Lawrenson, 1997). In addition to restricted paracellular pathways, the endothelial cells in the nervous tissue also have low pinocytotic activity (Brightman and Reese, 1969; Sedlakova et al., 1999).

II. *The blood-CSF barrier*

This barrier is situated between the blood vessels of the choroid plexus and the CSF. Choroid plexus tissue is found in the roof of each of the ventricles as an invagination of

the ventricular ependyma forming lobulated structures and is believed to be the main producer of CSF (Johanson, 1988). Unlike blood vessels in other parts of the brain, choroidal vessels seem to lack the continuous membrane-membrane fusion found in cerebral endothelial tight-junctions (van Deurs, 1979). The choroid plexus is one of the circumventricular organs (discussed later) and shows similar fenestrated vessels, i.e. the capillary membrane appears to be reduced at certain points and this characteristic has been associated with higher permeability (Peters et al., 1991) (see Figure 5.6). The vessels are surrounded by connective tissue and leptomeningeal cells that have loose, discontinuous tight-junctions which are believed not to have a significant barrier function (van Deurs, 1979). This has been confirmed with tracer molecules that easily diffuse past the cells to reach the basement membrane of the choroidal epithelial cells (cytochrome *c* study by Milhorat et al., 1975; HRP study by Becker et al., 1967 and Brightman, 1968; MP study by van Deurs, 1978). HRP and MP seem to cross the endothelium of the choroid plexus by both interendothelial passage and pinocytosis but which process is the more important is not known. Outside the blood vessels in the choroid plexus is a layer of connective tissue and overlaying this is a layer of epithelial cells resting on a basement membrane (see Figures 5.3-5.6). At the apical (CSF) side the epithelial cells are fused together to form *zonulae occludentes* thereby minimising the paracellular pathway (Brightman and Reese, 1969; Dermietzel and Schunke, 1975). The transitional ependymal cells in the borderline between choroidal epithelia and the ventricular ependyma also seem to possess tight-junctions at their apical side (Krisch, 1986). It is these tight-junctions between epithelial cells that are believed to form the ultrastructural basis of the blood-CSF barrier. This has been confirmed by tracer studies using HRP (Becker et al., 1967; Becker and Almazon, 1968; Brightman and Reese, 1969; Krisch, 1986), MP (van Deurs, 1978) and cytochrome *c* (Milhorat et al., 1973; Milhorat et al., 1975). After administration into the blood, the tracers leaked out of the choroid plexus blood vessels into the interepithelial cleft, but the intercellular movement of tracers was stopped at the apical tight-junctions. The much smaller

lanthanum has been reported to be able to cross the epithelial tight-junctions of choroid plexus of rats and cats (Castel et al., 1974; Bouldin and Krigman, 1975). This would indicate that the tight-junctions in the choroidal epithelium are 'leakier' than those of the cerebral endothelium, which have been shown to be impermeable to lanthanum (Brightman and Reese, 1969; Bouldin and Krigman, 1975). However, as has been discussed above the suitability of lanthanum as an *in vivo* tracer has to be questioned since it is toxic.

Most of the transcellular transport across the epithelial cells is believed to be from the basal to apical direction, by pinocytosis in vesicles and multivesicular bodies. This transport seems to be lower in the choroid plexus epithelial cells compared to other epithelia of the body (van Deurs et al., 1978; Peters et al., 1991).

III. *CSF-brain barrier*

Krogh (1946) proposed that the composition of the brain extracellular fluid (ECF) in the adult resembles very closely that of the CSF, the implication being that they are in open communication with each other. It is generally known that polysaccharides and proteins present in the CSF readily penetrate into the ECF (Johanson, 1993). The ventricles are lined with a single layer of ependymal cells, which lack tight-junctions and are joined to each other by gap-junctions (see Figure 1.1). Gap-junctions are believed not to serve as excluding structures but to form channels for exchange between adjacent cells. Hydrostatic and osmotic forces therefore determine the net flow of solutes between the CSF and brain ECF, and this interface is unlikely to pose a significant barrier in the adult (Johanson, 1993). Similarly to the ventricular ependyma, the outer pial surface of the adult brain does not seem to constitute an impediment for macromolecules to diffuse between the CSF of the subarachnoid space and brain tissue (Saunders et al., 1999a).

IIII. *The meningeal barrier*

The outer lining of the brain and the subarachnoid space are the least studied of the blood-brain interfaces despite the fact that they constitute a major interface between blood, CSF, and brain (Bohr and Møllgård, 1974). This interface can be considered as part of the blood-CSF barrier but because of its anatomical segregation it is normally regarded as a separate barrier. In this thesis the name meningeal barrier will be used but it is sometimes referred to as the outer blood-CSF barrier. The meninges consist of an outer thick dura, the arachnoid, and the pia mater that surrounds the whole CNS (Johanson, 1998). Because it is sometimes difficult to structurally distinguish between the pia and arachnoid, they are collectively known as the leptomeninges (Peters et al., 1991). In between the arachnoid and the pia is the subarachnoid space, which is filled with CSF, collagen, and many blood vessels. In an adult human the subarachnoid space holds about 60% of the total CSF volume (Johanson, 1995). This is also where the arachnoid villi are situated which allow CSF to pass back into the blood of the venous sinuses by bulk flow. Some of the blood vessels in the dura are fenestrated, and cells at the inner surface of the dura facing the subdural space seem to lack tight-junctions and have been shown to be leaky to HRP; thus the dura is not believed to constitute a significant barrier (Nabeshima et al., 1975; Krisch et al., 1984; Balin et al., 1986). Instead, the outer layer of the arachnoid consists of leptomeningeal cells, which have tight-junctions in between them (Dermietzel, 1975b; Rascher and Wolburg, 1997). A barrier at this level would isolate the CSF in the subarachnoid space from the outer blood circulation. Studies with HRP have shown that this is stopped at the outer surface of the arachnoid, which is where the arachnoid cells are linked by tight-junctions (Nabeshima et al., 1975; Balin et al., 1986). However, Balin et al. (1986) reported species differences. Blood borne HRP was stopped at the arachnoid in rat and monkey, but could enter the subarachnoid space in mouse. Some authors have also shown that

there are species-dependent characteristics of the meninges including the presumed barrier layer of the arachnoid. Angelov and Vasilev (1988) reported that the electron dense band between the dura and the arachnoid membrane is less prominent in the cat compared to other species and also only observed occasional tight-junctions in the presumed barrier layer of the outer arachnoid. Further studies by Angelov (1990a) compared the structure of the dura-arachnoid layers in rats, rabbits, cats and humans. The author could not give a general description of the tissues because of the heterogeneity between the different species. For instance, in the rat the dura-arachnoid membranes comprised of four distinct layers whereas in the cat and especially in humans these layers were difficult to differentiate. The arachnoid itself seems to lack blood vessels but in the reticular tissue of the subarachnoid space there are numerous vessels which have endothelial cells fused together by tight-junctions (Nabeshima et al., 1975). This constitutes an endothelial blood-CSF barrier. The blood vessels at the pial surface of the brain are also known to have tight-junctions and have been extensively used as an accessible place to study brain blood vessels *in vivo* (Crone and Olesen, 1982; Butt et al., 1990). The meningeal barrier has also been shown to be impermeable to MP but possible transport systems have not been studied (Cserr and Bundegaard, 1984).

Barriers in the developing brain

It was noted early on that the CSF in the developing brain had a higher concentration of protein than in the adult (Flexner, 1938). This was first interpreted as a simple reflection of less developed barriers, however, as the development of the brain barriers has been studied in more detail, a somewhat different picture has emerged (Johanson, 1989; Saunders, 1992). Instead of being immature it seems that the developing CNS, with its own requirement for growth, maintains a different environment from that of the adult CNS. Rather than being immature the barriers seem to be specialised during

development, including additional barriers, not present in the adult (Fossan et al., 1985). Since tight-junctions have been found to be the structural basis for the brain barriers, most studies have focused on the development of these in order to find correlations between changes in structure and permeability during development. When the literature is scrutinised it becomes apparent that most studies have not been successful in correlating changes in morphology with changes in permeability of the brain barriers during development. In addition there are contradictory results in defining the functional onset of the different brain barriers. Possible explanations for these contradictions are discussed below.

I. The blood-brain barrier

The origin of cerebral vessels in the developing brain is from the perineural plexus. This consists of fenestrated vessels that form a network around the outer surface of the entire neural tube and which sends long sprouts with abundant branches down to the ventricular zone of the neuroectoderm. It has been shown in the mouse that at around embryonic (E) day 10, these vessels lose their fenestrations and also that *zonulae occludentes*-like junctions appear between the endothelial cells (Bauer et al., 1993). In the rat, intraneural vessels have been reported to lose their fenestrations at around E12-E13 but the perineural vessels retain their fenestrations longer until around E17 (Stewart and Hayakawa, 1994). Another study in the same species found fenestrated intraparenchymal vessels as late as E17 (Yoshida et al., 1988). During growth of the CNS, the cerebral blood vessels undergo several other characteristic changes. There is an increase in the density of brain capillaries (Caley and Maxwell, 1970; Stewart and Hayakawa, 1987), a decrease in the thickness of the endothelial wall (Stewart and Hayakawa, 1987; Simionescu et al., 1988), changes in the tight-junctional structure (Schulze and Firth, 1992; Stewart and Hayakawa, 1994; Kniesel et al., 1996) and a decrease in pinocytotic activity (Bauer et al., 1993; Xu and Ling, 1994), however, other

studies have shown low pinocytotic activity even in early development (Stewart and Hayakawa, 1987). The induction of brain vessels to form barrier characteristics early in development appears to come from the surrounding nervous tissue. This was shown by Stewart and Wiley (1981) who transplanted avascularised embryonic quail tissue into embryonic chicks. When brain tissue was transplanted into the coelomic cavity this promoted barrier distinctiveness in the invading host vessels. In contrast, when somites where grafted into the embryonic chick brain ventricle, the invading cells seemed to lack barrier characteristics. What the molecular signals are that stimulate the vessels invading CNS tissue to develop barrier characteristics is still not clear (Risau et al., 1998).

Some of the first studies of the immature CNS claimed that the tight-junctions in the cerebral endothelium were incomplete compared to the adult and this was thought to be the reason for dyes staining the brain (for references see Saunders, 1992). Improved fixation techniques for fetal tissue have, however, produced evidence contrary to this view and demonstrated complex tight-junctions present between the endothelial cells at early stages of brain development (Møllgård and Saunders, 1975; Xu and Ling, 1994). Møllgård and Saunders (1975) reported a high complexity of the endothelial tight-junctions in human (10-13 weeks old) and sheep fetuses (E125) using freeze-fracture techniques. Xu and Ling (1994) found that in 1-day old rats the cerebral endothelial cells already exhibited tight-junctions with several contact points. There have been several other more recent studies on the structural development of junctions of brain endothelium in the rat. Schulze and Firth (1992) studied cerebral tight-junctions in thin-sections using the goniometric tilting device and found changes in the 'narrow zone' (close contact between the cell membranes) relative to the entire length of the tight-junction between developing and adult cortical vessels of rats. Embryos and postnatal rats showed high variability in this ratio and also prominent membrane separation whereas the adult tight-junctions appeared more uniform in structure. At various ages

between E17 and postnatal (P) day 16, however, there was little systematic change in these features of the tight-junctions. Stewart and Hayakawa (1994) also studied developmental changes in cerebral endothelial tight-junctions using transmission electron microscopy and found no differences in either the length of the tight-junctions or the cleft index (proportion of unfused cell membrane) between embryos and adults. However, they did find a decrease in the proportion of junctions with expanded cleft with age. The authors suggested that these larger clefts might be the ultrastructural basis for the apparently more permeable vessels in embryos. Kniesel et al. (1996) made a freeze-fraction study of cerebral vessels in rats from E13 to adulthood. They reported an increase in the complexity of the tight-junction network between E13 to P1, with the most significant increase between E18 and P1, but found no further changes after birth. This finding did correlate well with changes in the transendothelial resistance in developing rat pial vessels during development (Butt et al., 1990). At P17 the pial vessels resistance was around 310 Ωcm^2, which increased dramatically to 1130 Ωcm^2at P21, but increased little further after birth (1490 Ωcm^2 at P28-P33). Butt et al. (1990) also studied the penetration of lanthanum in the pial vessels and found that these vessels appeared impermeable to the small particle lanthanum *in vivo* even in fetal animals. The observation that the tight-junctions stop the paracellular penetration of lanthanum in pial blood vessels at early stages of development was later also shown for vessels in the corpus callosum (Xu and Ling, 1994). Xu and Ling (1994) also investigated the transfer of ferritin, a large protein tracer (molecular weight 900 000 Da), in blood vessels of the corpus callosum and found that it was transported in vesicles at earlier stages of development (P1 and P7), but one week later (P14) this transfer mechanism could not be detected. The authors suggested that the main route by which exogenous material is transported across the cerebral endothelium is by trancytosis in pinocytotic vesicles, and that a reduction in this activity is responsible for the decrease in vessel permeability with age. There have also been morphological studies of endothelial tight-junctions combined with HRP experiments in mice (Stewart and Hayakawa, 1987) and chicks

(Delorme et al., 1970; Wakai and Hirokawa, 1978) during development. Stewart and Hayakawa (1987) reported a parallel decrease in the tight-junction index and permeability of HRP in mouse embryos, and suggested a "tightening" of the paracellular route is responsible for the decrease in permeability with age. However, the largest drop in permeability index occurred between E15 and P10 when there was little change in the tight-junctional cleft index. Moreover, when HRP was visualised under the electron microscope, they could find no evidence of a paracellular route even at the earliest age studied. Delorme et al. (1970) found that there was free passage of HRP out of the telencephalatic vessels up to E10 in the chick but later in development the paracellular route for HRP seemed to be blocked as a result of the formation of tight-junctions of mature appearance. This is somewhat in disagreement with a later study by Wakai and Hirokawa (1978) which reported that the blood-brain barrier to HRP is not fully developed until E15 in the chick. As pointed out by Wakai and Hirokawa (1978) the discrepancy between these two studies may be due to the differences in the amount of HRP injected. As will be discussed below, the study of Wakai and Hirokawa (1978) has to be questioned in relation to the rather high quantity of HRP that was injected into the chick embryos. It is not clear from the description by Delorme et al. (1970) what quantity and volumes were injected into the embryos.

The two most popular explanations for the higher permeability across the developing brain endothelium have been a higher paracellular permeability or an augmented vesicular transport across these cells in development. Møllgård and Saunders (1975) suggested an alternative explanation in that the higher transfer of proteins during development could be due to transport in the endoplasmic reticulum of endothelial cells but did not further investigate these structures. As discussed later a similar transporting system has also been suggested to be developmentally regulated at the blood-CSF barrier interface. Lossinsky et al. (1986) found that both HRP and ferritin were stopped by the endothelial tight-junctions, but were found in tubulo-canalicular structures inside

the endothelial cells in neonatal mice. This transporting system was not found in adult mice suggesting that transport in these structures during development could be responsible for the apparent higher permeability of developing brain vessels.

II. *The blood-CSF barrier*

The blood-CSF barrier in the developing brain has probably been characterised better than any other of the blood-CNS interfaces. A primitive ventricular system is first formed when the neural tube is closed and fluid is trapped within the central canal. Interestingly this closure is associated with a subsequent increase in the intraventricular fluid pressure and coincides with an onset of brain enlargement. That the ventricular system might provide an essential driving force for normal brain expansion and morphogenesis was demonstrated by Desmond and Jacobson (1977) and Desmond (1985). These two studies showed that intubation of the embryonic ventricular system in the chick, that lowers the CSF pressure, resulted in less tissue volume in all parts of the CNS and only about 50% of the normal cell number in the brain. That the pressure and composition of the ventricular fluid is important for brain development raises interesting questions about developmentally regulated changes at both the blood-CSF barrier and the CSF-brain barrier, since these two barriers control the composition of this fluid. At the time of neural tube closure, the choroid plexus has not yet formed, so a blood-CSF barrier as such does not exist. Some other tissue presumably forms the fluid inside the expanding ventricular system, and this is believed to be the neural tissue itself (Catala, 1998). The choroidal epithelial cells arise from the neural tube whereas the more central structures of the choroid plexus form from the paraxial mesenchyme (Wilting and Christ, 1989). The different choroid plexuses appear in the order of 4th, lateral, and last the 3rd ventricular plexus in all mammalian species studied (Catala, 1998). The 4th ventricular plexus appears at E13 in both rat and mouse, at E5-6 in chick, at E24 in sheep, and during week 7 in humans (Catala, 1998), so this is the first

time a proper blood-CSF barrier can be considered. An important point to note is that the choroid plexus is much larger relative to brain tissue in the developing than in the adult animal (Johanson, 1995). Therefore it is possible that the choroid plexus plays an important role in providing nutrition for the brain during development (Johanson, 1999).

Junctions between the epithelial cells of the choroid plexus, that resemble the *zonulae occludentes* in the brain endothelium, have been shown to be present very early during development in mice (Zaki, 1981), rats (Dermietzel et al., 1977), sheep (Møllgård and Saunders, 1975; Møllgård et al., 1979), rabbits (Tennyson and Appas, 1968), humans (Tennyson and Appas, 1968; Bohr and Møllgård, 1974), and chicks (Delorme, 1972 as cited by Møllgård and Saunders, 1986). Changes in epithelial tight-junction complexity during development have been studied in the rat by Tauc et al. (1984). They showed that as early as E14 the junctions are structurally similar to those in the mature animal forming continuous belts around the epithelial cells. This study also investigated the localisation of HRP in the choroid plexus after intravenous injections. Similar to the adult choroidal vasculature, HRP easily leaked out of the vessels to reach the basolateral membrane of the epithelial cells and into the intercellular space but appeared to be stopped at the apical tight-junctions as early as E14. A similar study by Lu et al. (1993) showed that the tight-junctions of 1-day old rats impeded the intercellular flow of HRP and suggested that the transcellular route for HRP was in vesicles at this age. However, since only 1-day old rats were studied, no comparisons could be made with other developmental ages. Freeze-fracture studies on sheep embryos have shown that complex tight-junctions are present as early as the E30 (Møllgård and Saunders, 1975) and that the minimum number of strands and junctional depth of the tight-junctions only changed to a minor extent between E40 and E125 (Møllgård et al., 1976). Further studies in sheep fetuses by Møllgård et al. (1979) using an improved freeze-fracture technique also found no evidence for discontinuous strands or a change in the

proportion of complex strands between E30 and E125 (sheep are born around E150). The blood-CSF barrier of the chick has also been extensively studied during development. Wakai and Hirokawa (1981) reported that a proper functional barrier to HRP is established at E10. This study showed that HRP injected intravenously penetrated the tight-junctions of the choroidal epithelial cells freely until E8, was blocked by most junctions at E9, but was never found to penetrate the junctions at E10. Furthermore, HRP was never found to be transported in vesicles from blood into the CSF. A similar study by Bertossi et al. (1988) showed comparable results except that the timing of the apparent junction tightening was slightly later. At E10 HRP appeared to be stopped by most of the tight-junctions but a few still seemed to be leaky and at E15 HRP never penetrated the junctions. This study also found little vesicular transport of HRP in the blood-CSF direction, but after an intraventricular injection, HRP was taken up in vesicles and was actively endocytosed and degraded in the epithelial cells. They concluded that at E15 the barrier to protein is functionally and structurally very similar to the adult. As described below in more detail, the studies by Wakai and Hirokawa (1981) and Bertossi, et al. (1988) claiming a poorly developed barrier early in development can be questioned in regard to the physiological state of embryos as a result of the large volumes and high concentrations of solutions that were injected.

The concentration of proteins in CSF reaches a peak early in development, thereafter it gradually decreases with age (Saunders and Dziegielewska, 1997). This generally occurs during fetal development in eutherian mammals reaching a total protein concentration that is 10-20 times the adult level. This has been interpreted by some (Adinolfi, 1985) as a reflection of immature barriers, but with further studies it has become clear that this is probably not the case (Dziegielewska et al., 1991; Habgood et al., 1992). If the reduced permeability of proteins with age were a reflection of tight-junction development between the epithelial cells, the structure of the tight-junctions would be expected to change. The reported minor changes in tight-junction complexity

during development (Møllgård et al., 1976) are unlikely to account for the dramatic changes in permeability of proteins that have been reported (Dziegielewska et al., 1980). When endogenous albumin, exogenous albumin from other species, and chemically modified derivates of albumin were injected into sheep fetuses, native protein reached the highest concentrations in the CSF. Similar studies in neonatal rats (Habgood et al., 1992) and opossums (Knott et al., 1997) found similar results. Thus a possible transporting system seemed to be able to distinguish between different kinds of albumin. It was also found that the greatest number of choroidal epithelial cells containing albumin coincided with the peak in CSF protein concentration in opossums (Knott et al., 1997). The authors suggested that the route for albumin is intracellular through the epithelial cells of the choroid plexus in a process that can distinguish between native and modified albumins. This selective transporting mechanism seems to only be present during early development since in the more mature brain there was no difference in the penetration between different species of albumin (Knott et al., 1997). Møllgård and Saunders (1977) investigated the tubulo-cisternal endoplasmic reticulum (TER) in the immature choroidal epithelial cells in sheep and found that this system had close contact with the cell membrane both at the basolateral and apical sides. In contrast, later in development the TER was separated from the cell membrane and the authors suggested the TER could constitute a transcellular pathway between blood and CSF for larger molecules such as albumin during early development. Later Balslev et al. (1997b) showed using EM immunocytochemistry that albumin can be found in the TER of the immature choroid plexus in sheep after administering it into the blood. They found no albumin passing the interepithelial cleft and proposed that the TER is the main route of transfer for albumin from blood into CSF in the immature animal.

III. *The CSF-brain barrier*

Brightman and Reese (1969) showed that in adult animals, solutes such as HRP diffuse unhindered from the CSF into the extracellular fluid (ECF) of the brain. However, when Fossan et al. (1985) perfused HRP through the fetal sheep ventricles at E60 it did not penetrate into the brain but did so later in fetal development at E125. This restricted entry into the brain at early stages of development was suggested to be accounted for by novel type of junctions found between cells in the neuroependyma of the ventricular zone (Møllgård et al., 1987). These single strand junctions differed in their freeze-fracture appearance from tight-junctions in that they produced wider ridges and E-face grooves filled with particles, and were orientated perpendicular to the CSF surface rather than in a circumferential belt. These junctions were believed to be an uncharacterised type of junction and not simply precursors of gap-junctions, and were named strap-junctions. These strap-junctions were only present in early stages of sheep brain development (eg. E20-E60), and later, as the neuroependyma is replaced by an ependyma with adult characteristics, the cells are connected with gap-junctions exhibiting the normal 20 nm intercellular cleft. This novel barrier was postulated by the authors to contribute to creating a high osmotic pressure gradient between the CSF (containing a high protein concentration) and the ECF of the brain (containing a low protein concentration). The physiological importance of this barrier has therefore been hypothesised to provide an essential force for normal brain growth and development (Møllgård et al., 1987). A similar CSF-brain barrier has been reported in the neuroependyma of a developing marsupial species, the Australian tamar wallaby (Dziegielewska et al., 1988). Ultrastructurally the neuroependymal cells had the same strap-junctions in between them as reported for sheep (Møllgård et al., 1987). When HRP was administered intravenously into the developing wallaby, it was found in the CSF but the strap-junctions in the neuroependyma appeared to stop HRP from penetrating from the CSF into the extra cellular fluid (ECF) of the brain. The

neuroependyma was not studied in later stages of development in the wallaby so whether the strap-junctions disappear later in development, similar to the sheep, is not known.

Similarly to the interior barrier between CSF and brain, Fossan et al. (1985) found that the outer pial surface of the brain was less permeable to HRP in fetal sheep at E60 than later in gestation (E125). This interface has also has also been shown to be impermeable to endogenous albumin at E60 in sheep (Balslev et al., 1997a). Fetal rats have been shown to have complex junctions (non tight-junctional type) between the glial end feet from around E14 and these were suggested to be a supplementary barrier for macromolecules between the subarachnoid space and the ECF of brain in early development (Balslev et al., 1997b). These junctions might be precursors of gap junctions, which in their fetal form exclude proteins from the ECF.

IV. *The meningeal barrier*

The origin of the mammalian meninges is still not clear. This is because dye and marker studies carried out in order to follow the destiny of specific cells has in mammals proven complicated, since the tissue is formed by several embryonic layers. However, the early differentiation of this tissue has been examined in birds and amphibians. In amphibians the dura has mostly a mesodermal origin whereas the leptomeninges are formed from the neural crest. In the chick, the spinal meninges have a mesodermal origin but the cephalic meninges seem to have a more complex origin in birds (Catala, 1998). It is uncertain, however, if the composite structure of the mammalian meninges is similar to that of amphibians and birds (Catala, 1998), and they have been suggested to have both neuroectodermal and extra-neural origins (Weston, 1970; Angelov and Vasilev, 1989).

Balslev et al. (1997b) showed that the blood vessels in the pia and subarachnoid space are fenestrated early in development of the rat (E12) but soon become non-fenestrated vessels exhibiting tight-junctions between endothelial cells (E14-E16). This observation is contradictory to a study by Stewart and Hayakawa (1994) who reported that pial vessels are fenestrated as late as E17 in the rat. Only one study seems that have investigated the tight-junctions in the outer arachnoid membrane, that are thought to make up the external barrier to the CSF in the subarachnoid space, during development. Rascher and Wolburg (1997) quantitated the changes in the complexity of the tight-junctional network between the arachnoid cells in rats and chickens during development using freeze-fracture techniques. The complexity index was calculated as the total length of the tight-junctional strand divided by the total number of branching points. They found a successive increase in arachnoid tight-junction complexity between E10 and adulthood in chicks, whereas the complexity index decreased slightly between P2 and adulthood in the rat. In the adults, the complexity index was approximately double in the chicks compared to that of the rat. However, as pointed out by the authors, there is a lack of permeability studies of this specific barrier during development, so structural changes cannot be compared with permeability studies in order to deduce whether they are of significance for the functional development of this barrier.

Structural aspects of the brain barriers in comparison to permeability of lipid insoluble molecules during development

Even though the exact timing of the maturation of the brain barriers is somewhat unclear, the structural basis for these barriers seems to be well established by birth in all eutherian mammals studied. In mouse and sheep, the first blood vessels that invade the brain seem to possess structural and functional barrier characteristics (Møllgård and Saunders, 1975; Bauer et al., 1993; Xu and Ling, 1994; Bauer et al., 1995). In the sheep,

the junctional morphology can be compared with proper quantitative permeability studies for a range of differently sized lipid insoluble markers. The steady-state concentrations of various lipid insoluble molecules have been shown to significantly decrease during development in sheep fetuses (Evans et al., 1974; Dziegielewska et al., 1979). These studies showed that between the E60 and the E125 the steady-state CSF/plasma concentration for sucrose and inulin fell from 23% to 7% and 11% to 3%, respectively. As pointed out by the authors, this reduction in steady-state ratios could be explained by other factors than a decrease in barrier permeability, such as an increase in the CSF turnover. The continuous production of CSF flushes out solutes in the CSF and hinders them from equilibrating with the concentration in the blood; this effect has been named the CSF sink (Oldendorf and Davson, 1967; Davson and Segal, 1969) and an increase in CSF sink could account for the age-related decline in steady-state ratios. Evans et al. (1974) reported a large increase in the CSF secretion rate between E60 and adulthood in the sheep (2.8 to 118 µl/min). However, when the secretion rate is related to the total CSF volume (which also increases during development) and is calculated as a turnover rate of CSF per minute, this only increased from 0.62% at the E60 to 0.83% in the adult. Furthermore, by dividing the CSF turnover rate by the brain mass at each age, the CSF sink for the brain was estimated; this was shown to significantly decrease during development from 0.32% at E60 to 0.01% min^{-1} g^{-1} brain weight in the adult sheep. Evans (1974) therefore proposed that it seems unlikely that the decreases in steady-state ratios can be explained by an increase in CSF sink, but rather by a decrease in the intrinsic permeability of the brain barriers. Structural investigations of the fetal tight-junctions of both endothelial and epithelial cells have reported that they closely resemble those of the mature sheep (Møllgård and Saunders, 1975; Møllgård et al., 1979). It therefore seems that there is a significant decrease in barrier permeability long after mature tight-junctions are present. Changes in permeability of lipid insoluble molecules have not been studied in the mouse so similar comparisons cannot be made. In the rat, the exact onset of the structural characteristics for the brain barriers is still

disputed, however, nearly all studies show that the barriers are structurally mature at birth (Kniesel et al., 1996). However, the steady-state concentration of small lipid insoluble molecules have been shown to decrease significantly after birth (Ferguson and Woodbury, 1969; Habgood et al., 1993) when the structure of the tight-junction has been reported to be indistinguishable from the adult rat (Kniesel et al., 1996). Ferguson and Woodbury (1969) explained the falling ratios with age by an increase in the CSF sink, but did not present experimental evidence for this statement. The CSF turnover rate in rats as summarised by Saunders (1992) showed that this remained rather stable between P3 and P21-P23, and that the sink effect on the brain decreased over the same developmental time. Furthermore, Habgood et al. (1993) argued that if there was an increase in CSF sink with age this would reduce the time to approach steady-state. However, since this did not change between P2 and adulthood this was ruled out as an explanation for the age related decrease in ratios. It therefore seems that the permeability changes to small lipid insoluble molecules during development in sheep and rats is not a reflection of either maturation of the tight-junctions or an increase in CSF sink, but by other factors that are still to be identified.

Difficulties in correlating barrier morphology with its function during development

Possible explanations for the difficulty of correlating physiological permeability of inert lipid insoluble molecules (or the penetration of tracers) with structural studies of the barriers during development are discussed below. There is an obvious lack of good quantitative physiological studies of barrier permeability during development. In rats (Ferguson and Woodbury, 1969; Habgood et al., 1993) and sheep (Dziegielewska et al., 1979) the permeability to various sized lipid insoluble markers has been extensively investigated. However, these types of studies are lacking in other species such as the mouse and chick in which the ultrastructure of the barriers have been studied

comprehensively (Doolin and Birge, 1969; Zaki, 1981; Stewart and Hayakawa, 1987; Bauer et al., 1993; Rascher and Wolburg, 1997). In these species, the permeability has only been studied by histological visualisation of some proteins, including HRP, in brain tissue (Delorme et al., 1970; Wakai and Hirokawa, 1978; Lossinsky et al., 1986; Roncali et al., 1986; Stewart and Hayakawa, 1987; Bertossi et al., 1988). The lack of physiological permeability studies in several species has lead to the confusion in the field such that comparisons have been made across species, but it is uncertain if those kind of comparisons are appropriate. Added confusion has also been brought about by the fact that birth is not a comparative developmental stage across species but appropriate comparisons have to be based on knowledge about general and specific stages of brain development (Stonestreet et al., 1996).

Ultrastructural studies of cells at the barrier interfaces can only examine a very small proportion of all the cells even though a large amount of work is undertaken. This is especially true for thin-section electron microscopy, whereas freeze-fracture studies can examine much larger areas of tissue at one time. Freeze-fracture is the only practical way to establish that tight-junctions are continuous all around the cell or if they have gaps at certain points. Just to follow one junction in serial thin-sections around the cell would involve an enormous amount of sectioning and examination. This has lead to the problem that ultrastructural studies of the endothelium have only been carried out in certain parts of the brain, or studies have focused on the endothelium from a particular type of blood vessel. However, when a permeability marker is injected into the blood, the brain barrier permeability determined will be related to the permeability of all blood vessels in the brain. The problem is to know whether the blood vessels that have been examined ultrastructurally are representative for all vessels. Because of technical problems it has sometimes only been possible to study vessels that are easy to access, such as the pial vessels on the surface of the brain.

When the ultrastructure of tissue is studied from different developmental ages, the choice of fixation technique can also affect the outcome. Most studies have tended to use the same fixation techniques for all ages, but this is not always appropriate since it does not give satisfactory preservation of tissue. For instance, most fetal tissue is small and fragile and it is therefore not always possible to fix by perfusion, whereas adult tissue often requires perfusion fixation in order to preserve tissue adequately. Fixation is an important consideration because it can affect cell volumes and thus the appearance of cell junctions. Another aspect of studies with fetal animals is that extra care has to be taken in order to minimise physiological interference during experiments. This is especially important when markers are injected systemically or intraventricularly. If the volume injected is not carefully considered in relation to the volume of the compartment that it is injected into, this can have disastrous effects on the fetus. Equally important is to consider the changes in osmotic balance that the injection solution might produce in the fetus. As pointed out by Saunders (1992) several developmental studies have injected HRP in such high concentrations that it would have increased the total protein concentration in the blood by up to 2-3 times. For example, Wakai and Hirokawa (1978, 1981) injected HRP intravenously into chick embryos in a concentration of about 50-100 mg/ml. The injection volume was one tenth of the total blood volume, which would have resulted in approximately doubling the protein concentration in the blood. Other examples are the studies by Roncali et al. (1986) and Bertossi et al. (1988) in which HRP was injected intracardially into chick embryos aged between E10 and E21 in a concentration of 0.3 mg per gram body weight in 0.1-0.3 ml saline solutions. A chick embryo at E10 weighs approximately 2 grams (based on weights given by Davis and Garrison, 1968 for a chick embryo at Hamburger and Hamilton stage 36) and can therefore be expected to have a blood volume of about 0.2 ml. Such an injection would increase the systemic volume by about 50% and the protein concentration by about 30% in an embryo at E10 (plasma protein concentration is 7.1 mg/ml at E10 as reported by

Birge et al. (1974). Furthermore, in the same study HRP was also injected intraventricularly in the same concentration but in a slightly smaller volume (0.05-0.1 ml). To the author's knowledge nobody has estimated the CSF volume in a 10-day old chick but it can be expected to be only a fraction of the total blood volume. It is therefore difficult to imagine that the brain barriers could remain intact after adding such a large volume of fluid into the ventricular system. Yet another example is the study by Angelov (1990b) in which 1 and 10 mg of HRP were injected into the arachnoid space of adult rats and cats, respectively. This amount can be estimated to be 10 times the total protein content in the CSF and would thus have significantly changed the osmotic balance in the brain.

The permeability of the brain barriers has been extensively studied by the penetration of markers which can be visualised in tissue after fixation. The ideal marker should be physiologically inert, homogenous in particle size and structure, immobilised in its real position by fixation, and directly or indirectly capable of being visualised at low concentrations in the electron microscope. It would also be very useful if it were available in different molecular sizes and easy to quantify. The first tracer used for electron microscopy was horseradish peroxidase (HRP, mw 40 000), and it is still widely used as a marker for barrier integrity. However, it is not known if it is a good representative of other large lipid insoluble molecules such as plasma proteins. It is also a disadvantage that it is an enzymatic reaction product that is electron dense enough to be visualised under the electron microscope rather than the actual protein. Thus there are likely to be problems of interpretation due to diffusion of the reaction product. Other larger tracers suitable for electron microscopy such as ferritin (mw 900 000) and cytochrome *c* (mw 12 000) have been used but there has been a lack of low molecular weight tracers. Lanthanum, a very small electron dense particle, has been used in fixed tissue, but because of toxicity it is not suitable *in vivo*. Small heme-peptides, called microperoxidases, were introduced in the early 1970's (Feder, 1971), but they were later

found to bind to plasma proteins. The use of low molecular markers is essential when investigating small intercellular channels or cellular compartments. With the recent introduction of several smaller lipid insoluble tracers (such as the biotin-dextrans), the *in vivo* penetration of such molecules can be investigated in order to find out the route of transfer that molecules take across the brain barriers and how this compares to that of larger molecules.

Studies that have tried to find correlations between morphology and physiology have concentrated on the ultrastructure of the paracellular route, namely the tight-junctions, as the structural determinant of barrier permeability. Claude and Goodenough (1973) correlated the transepithelial resistance of epithelia from different parts of the body of various species with the tight-junctional morphology. High resistance epithelia, such as the urinary bladder, showed high strand numbers and junctional depth whereas low resistance epithelia, such as the proximal tubule, had few strands and had little junctional depth. From this study it therefore appears that the morphology of the tight-junctions does determine the electrical 'tightness' of a cell layer. As discussed above, however, tight-junctional structure and brain barrier permeability of lipid insoluble molecules do not always correlate well in the developing animal. Moreover, Martinez-Palomo and Erlij (1975) used a hypertonic solution in order to make the intestines of rabbits more permeable. This treatment resulted in an increase in the permeability of the intestines, however, they could not find any change in the tight-junctional network in freeze-fracture replicas. It therefore seems that other aspects to a high degree also determine the permeability of cell layers such as other cell-cell junctions, transcellular routes, or other, still un-characterised attributes. There is also the possibility that the resolution of freeze-fracturing and thin-section electron microscopy, used to study tight-junctional structure is not high enough to see small molecular differences that may underlie developmental changes in cell junction permeability. The molecular structure of tight-junctions is still not clear. Several tight-junction associated proteins have been

identified including ZO-1, ZO-2, ZO-3, 7H6, several claudins, cingulin, and occludin (Kniesel and Wolburg, 2000). Most attention has been given to the transmembrane protein occludin and some studies have found correlations between occludin appearance in postnatal rat development and the maturation of the blood-brain barrier (Hirase et al., 1997 as cited by Rubin and Staddon, 1999). Several mutant occludin epithelial cell lines and also mice with null mutations have been developed in order to elucidate the role of occludin as a tight-junctional protein. Mutant cell lines have provided evidence both for and against occludin as a crucial transmembrane protein of the tight-junctions (Saitou et al., 1998; Bamforth et al., 1999). Mice lacking the occludin gene developed abnormally with retardation of several organs, however, barrier morphology and function in the intestine appeared normal (Saitou et al., 2000). Because of these and other experiments it is now believed that occludin is not the pivotal tight-junctional protein but only one of several proteins that can form strand structures, and attention has been switched to the family of claudins (Goodenough, 1999). It is now known that the tight-junctions are not as static as was first believed and that the junctional proteins probably change during CNS disorder such as multiple sclerosis (Bolton et al., 1998). Recently it has been shown that tyrosine phosphorylation of the junctional proteins can dramatically change the permeability of endothelial and epithelial cell cultures, however, the results are contradictory (Rubin and Staddon, 1999; Takeda and Tsukita, 1995 as cited by Chen et al., 2000; Chen et al., 2000). Other factors that seem to be able to influence the structure and function of the tight-junctions are cAMP, Ca^{2+}, and GTPase levels (Kniesel and Wolburg, 2000). Maybe the molecular assembly and modulation of the tight-junctions are critical for understanding the paracellular permeability changes of the barriers during development.

The circumventricular organs

As the name implies, these tissues are situated around the ventricles of the brain and

include area postrema, median eminence, neurohypophysis, the pineal gland, the choroid plexus, and the subfornical organ (Prescott and Brightman, 1998). They are characterised by a lack of a blood-brain barrier and seem more adapted for exchange of solutes since they have fenestrated blood vessels, increased capillary density, thinner endothelium and a high level of vesicular transport (Prescott and Brightman, 1998). All these organs are believed to act as portals into or out of the brain via a signalling system which often includes hormones. The penetration of solutes from the circumventricular organs (CVO) to other parts of the brain is somewhat unclear. However, the ependymal cells overlying the CVO seem to possess tight-junctions that have been shown to stop the transfer of HRP (Madsen and Møllgård, 1979; Prescott and Brightman, 1998). Thus it is unlikely that the CVO act as routes of entry for the brain as a whole.

Characteristics of barrier selectivity

Influence of lipid solubility and molecular size

The main determinant of a molecule's ability to enter the CNS is its lipid solubility (Oldendorf, 1974; Levin, 1980). Lipid solubility is important since it determines how easily a molecule can pass through cell membranes and to what extent it can form electrostatic bonds with water molecules. Consequently, the more polar groups a compound contains, the greater number of bonds it can form with water molecules which will effectively retain the compound in the aqueous phase (blood). In order for a compound to leave the aqueous environment (blood) and enter into the non-polar environment of the cell membranes, it needs to break these electrostatic bonds with water molecules. Lipid-solubility of a substance can easily be determined *in vitro*, by its partitioning between a non-polar and a polar phase. The partition coefficient obtained between octanol and water ($LogP_{oct}$) has been widely used as a predictor of *in vivo* brain barrier permeability (Rapoport and Levitan, 1974). However, $LogP_{oct}$ values have been found to be a fairly poor predictor of a molecule's *in vivo* steady-state concentration in

the CNS or brain barrier permeability. For instance, compounds with similar $LogP_{oct}$ values can, *in vivo,* vary by two to three orders of a magnitude in their permeability across the brain barriers (Levin, 1980). A possible reason why Log_{oct} has not always been a good predictor of brain uptake may be that the partitioning coefficients are greatly affected by the experimental conditions under which they are measured. $LogP_{oct}$ measurements are attempted to be made under conditions so that all molecules are in their neutral form. However, the conditions of these measurements may be very different from those *in vivo*. Temperature and pH will directly affect the proportion of a compound in ionised form and thus will affect the rate of uptake into the brain.

It might be expected that smaller molecules would penetrate the brain barriers more easily than larger molecules, however, this does not always appear to be the case. When the uptake into CSF is measured of compounds with low and similar lipid-solubility, this have shown that there is a strong inverse correlation between molecular size and steady-state concentrations in the CSF (Felgenhauer, 1974). The rate of entry in to the CNS for these compounds appears to be determined by the diffusion coefficient and since this is inversely related to molecular size, smaller molecules penetrate faster. However, if a much wider range of compounds is examined there is no correlation between brain-barrier permeability and molecular size. This suggests that molecular size per se does not have a major influence on blood-brain barrier permeability compared with lipid solubility. Furthermore, if structurally related compounds are compared, it appears that increasing the size of a molecule can in fact both increase its lipid solubility and entry into the CNS (Habgood et al., 1999). For instance, adding extra non-polar methyl groups to the carbon chain of methyl alcohol (to make ethanol, propanol, butanol etc) will increase the size, however, each extra methyl group will also make the molecule more lipid soluble (Habgood et al., 2000).

Enzymatic barriers

There are also specific brain barrier mechanisms that are capable of controlling the entry of substances that are lipid soluble and thus could be expected to have a high rate of entry into the brain. These barrier mechanisms include enzymes that degrade substances as they cross the barriers and transport systems that actively transport the molecules back into the circulation (see below). The degradation of neuroactive substances such as L-dopa and tryptophan (precursors of dopamine and serotonin) by decarboxylases prevents them from accumulating in the brain to large extent. In clinical treatment of Parkinson's syndrome, it is necessary to saturate these enzymatic systems and this can be accomplished by administering large doses or by co-administration of a decarboxylase inhibitor. There are also several peptidases and angiotensin-converting enzymes present in the brain endothelial cells (Johansson, 1997).

Active transport out of brain

The concentration of a molecule in the brain is affected by both its influx into and efflux out of the brain. Many essential molecules for normal brain function such as glucose and amino acids would have a very slow penetration into the brain if it was not for active transport into the brain. These systems will be discussed in more detail later on in this Chapter. There are also several compounds, such as the drugs vinblastine and cyclosporine A, that have been found to have much slower uptake into the brain than could be expected from their lipid-solubility. The explanation for this was first found in a family of multi-drug resistant phospho-glycoproteins (Pgp) found in the vasculature of the brain and later also in a multidrug resistant protein (MRP) which has been found in the choroid plexus. These proteins are believed to function as a defence of the CNS against certain lipid soluble molecules. They are often highly expressed in brain tumours leading to reduced drug accumulation, and are therefore responsible for the clinical ineffectiveness of several anti-tumour drugs (Borst and Schinkel, 1998).

Tumours can also build up resistance to certain drugs because the exposure of a drug may lead to increased expression of both Pgp and MRP. The mechanism by which these proteins exclude some drugs from the brain is still not clear but is known to be energy dependant. Pgp and MRP both are have membrane spanning domains and can transport drugs from the cytosol of the cell or from the cell membrane itself to the external (blood) side of the membrane. These two proteins only share about 15% amino acid homology and substrates for them vary a great deal (Lautier et al., 1996). One way to overcome Pgp related drug resistance is to co-administer a known substrate or an inhibitor of Pgp function, leading to an increase in drug delivery (Borst and Schinkel, 1998). However, because of the lack of good substrates for MRP, this approach has not yet been effective against MRP dependant drug resistance (Lautier et al., 1996).

The importance of studying the brain barriers

The knowledge about brain barrier selectivity is vitally important for estimating the entry of centrally acting drugs into the CNS. Equally important is to be able to estimate the CNS uptake of peripherally acting drugs with neurotoxic side effects. Therefore, accurate modelling of a drug's entry into the CNS could be very useful in predicting the prospective therapeutic success of a drug. However, at present it does not seem that drug companies have appreciated the full potential of understanding brain barrier selectivity. According to Pardridge (1999) more than 95% of all drugs are denied access to the brain but less than 1% of drug development effort is committed to improving brain delivery. Instead, more than 99% of all the effort goes to the discovery of new drugs. This is especially extraordinary since drugs against CNS disorders are one of the fastest growing areas in therapeutics. Some strategies to improve drug delivery have involved the utilisation of endogenous transporting systems, osmotic opening of the brain barriers, and the lipidisation of drugs. These have all been successful to a limited extent but there is still a huge scope for improvement, and also an enormous potential

benefit for new more specific CNS targeting drugs. Since some of the barrier mechanisms in the developing brain appears to be different, it is possible that knowledge of barrier mechanisms of the immature brain will lead to the development of new drug targeting strategies for the brain.

Many pollutants, food additives and drugs in the mother's blood circulation may be harmful to the fetus if they are able to cross the human placenta. In the human placenta, the mother and fetal blood are only separated by a single layer of transfer-limiting cells (syncytiotrophoblasts). Compared with many other mammals, the human placenta is more permeable to small lipid insoluble molecules (Bain et al., 1988; Schneider, 1991) and is also believed to be a rather weak barrier to most drugs (Audus, 1999). It is often a challenge for clinicians to prescribe drugs for pregnant women because there is very limited knowledge of how these drugs may affect the unborn child. In addition, women often use drugs before they realise they are pregnant, during the first crucial time of pregnancy when the organs develop (Gilstrap, 1997). The problem might be even more challenging when the pregnant mother suffers from a chronic medical disorder such as asthma, diabetes, hypertension or various cardiac diseases, and the intake of a certain drug cannot be avoided not to jeopardise the health of the mother (Rayburn and Lavin, 1986). Even though the brain barriers seem to form early in development, as have been described above, the barrier mechanisms in the immature brain are different from the adult. Therefore is it not always possible to know how or to what extent foreign substances can access the developing brain. This is especially a concern since the developing CNS may be particularly sensitive to exogenous material. The knowledge about fetal CNS barrier function is not only important when trying to predict possible adverse effects of substances on the unborn child but could also be of interest for fetal drug therapy. With better understanding of drug uptake into the fetal circulation and drug penetration into the developing CNS, this could be a growing field of therapy.

Possible routes of entry for lipid insoluble molecules into the CNS

Paracellular pathway

In vessels outside the brain, lipid insoluble molecules are believed to be transferred across the endothelium by filtration through pores. These pores have been suggested to be the intercellular cleft between endothelial cells with a radius of 40-70 Å. Karnovsky (1967) showed that, at least for HRP, the endothelial cleft in heart and skeletal muscle is indeed a functional pathway across the endothelium. However, it has been difficult to explain how larger lipid insoluble molecules cross the endothelium since they would be too large for the normal interendothelial cleft. One hypothesis has been that they cross through pores which are considerably larger (200-300 Å) but the structural basis for these larger pores is still not known. The reason these large pores have never been localised has been proposed to be that they are rare in the vasculature, or if ever found, may have been believed to be artefacts (Rippe and Haraldsson, 1987). In the brain, however, the paracellular route is severely restricted by the continuous tight-junctions between endothelial cells. As has been described above it seems likely that these effectively stop the penetration of most proteins from blood into brain. Whether smaller molecules can penetrate the tight-junctions has still not been established, but this has often been considered to be the case (Goodenough, 1999).

Transcellular pathways

I. *Active transport*

Normal functioning of the brain requires a higher rate of delivery of certain compounds than can be achieved by passive transfer. For instance the brain is in constant need of D-

glucose, which is delivered by the blood as an energy source for all the cells. Transporters for D-glucose within the brain were first described in the middle of the 1980s and today six functional transport proteins have been identified, all related structurally and with similar function but expressed differently in various tissue (Drewes, 1998). Other molecules that are dependant on active transport into the brain are amino acids, peptides and ions. Amino acids are transferred into the CNS by several transporting systems that do not seem to be specific for one amino acid but prefer amino acids of particular size and charge (Smith and Stoll, 1998). Ions are either positively or negatively charged and would therefore have very low brain barrier permeability if not transported into the brain actively. They are transported by ATPases or antiporters with different transporting mechanisms at the luminal and abluminal membrane both in the endothelial cells of the brain capillaries and in the epithelial cells of the choroid plexus (Frelin and Vigne, 1998; Speake et al., 2001). Whether the movement of a specific ion in/out of the barrier cells is important for transcellular transport, or the need for the endothelial and epithelial cells to keep an ion gradient between themselves and the surroundings, is difficult to determine. At least for the choroid plexus, which is known to play a major role in CSF secretion, the mechanism by which CSF is produced is dependant on the existence of an ion gradient between the epithelial cell and blood/CSF (Johanson, 1995).

II. *Vesicular transport*

The plasma membrane can invaginate at both the luminal and abluminal side giving off membrane coated spheres called vesicles that can travel across the cell in a process called trancytosis. In these vesicles any molecule can be engulfed as long it is smaller than the size of the vesicle. Under normal circumstances the vesicular transport in brain endothelia is low compared to other endothelia (Connell and Mercer, 1974; Stewart, 2000), but has been shown to be higher during development (Xu and Ling, 1994). The transport in vesicles has been found to be polarised in both the choroidal epithelia and

brain endothelia with greater uptake from the luminal membrane (van Deurs et al., 1978; Balin et al., 1986). How important vesicular transfer is in endothelia is still debatable but it is believed to be only important for larger lipid insoluble molecules, since the process is rather slow. Stewart (2000) only found a weak correlation between vesicular density and protein permeability in several endothelia throughout the body including the brain. The author suggested that protein transfer is more dependant on receptor-mediated trancytosis. Three different mechanisms of vesicular transcellular transport have been proposed (Nag, 1998). Firstly, the vesicles are suggested to bud at the luminal cell membrane, move across the cell and empty their contents at the opposite side of the cell by fusing with the abluminal cell membrane, or by a similar process in the reverse direction. The second hypothesis is that vesicles only move a short distance within the cell and then fuse with another vesicle mixing their interior contents and then separate again. Eventually a substance will reach the other side of the cell as observed by Clough and Michel (1981) with ferritin transport in frog endothelium. The third hypothesis is that a whole row of vesicles fuse together and thereby form an extracellular channel through the cell in which fluid can move in either direction. This has been demonstrated by Simionescu et al. (1975) in rat muscle capillaries and was also suggested by Clough and Michel (1981). To the author's knowledge such vesicular channels have never been observed within brain endothelium or choroid plexus epithelium.

III. *Transfer in other subcellular structures*

Møllgård and Saunders (1977) studied the choroid plexus of the immature sheep and reported that the endoplasmic reticulum (ER) during early fetal development is in close contact with both the basolateral and apical membranes of choroidal epithelial cells. The ER could directly be linked with the membrane via a tubulo-cisternal system or vesicles. It was suggested that this system could constitute a transcellular pathway, which seemed to be developmentally regulated since it was not present in late fetal

development. This pathway was later suggested to be the route by which albumin crosses the epithelial cells of the choroid plexus (Balslev et al., 1997a). The ER has also been suggested to transport protein in the endothelial cells of the brain (Møllgård and Saunders, 1975). This is in contrast to Balin and Broadwell (1988) who found HRP in tubular structures in the epithelial cells after systemic administration but suggested that these structures are components of lysosomal or endosomal systems and are not involved in trancytosis of HRP. The authors opposed the view by Møllgård and Saunders (1975, 1977) that the ER could constitute a pathway through the choroidal epithelium or the cerebral endothelium. Similar tubular structures were proposed to form functional pathways through the brain barriers by Lossinsky et al. (1983, 1986). These studies showed that in states of increased brain barrier permeability, HRP and ferritin were found in channel like structures in endothelial cells which the authors referred to as tubulo-canalicular structures.

IIII. *Absorptive-mediated transfer*

More recently it has been discovered that certain peptide sequences are rapidly internalised into cells. This phenomenon was first observed for transcription factors of the *Drosophila* (Derossi et al., 1998), but has also been found for protein domains of viruses (Schwarze et al., 1999). The mechanism of the internalisation of the peptide is not clear, but has been suggested to involve electrostatic attraction between positive amino acids in the peptide and negative lipid or sugar components in the cell membrane (Derossi et al., 1998). The membrane is thought to destabilise and produce inverted micelles so that the membrane lipids form a ring around the peptide that can travel across the membrane and release the peptide into the cytoplasm. The findings have led to the development of so-called Trojan peptides, which can deliver other peptides into the cell when they are linked to the Trojan peptide. For example, these peptides have been shown to increase the transport of the anticancer drug doxorubicin into the brain parenchyma (Rousselle et al., 2000).

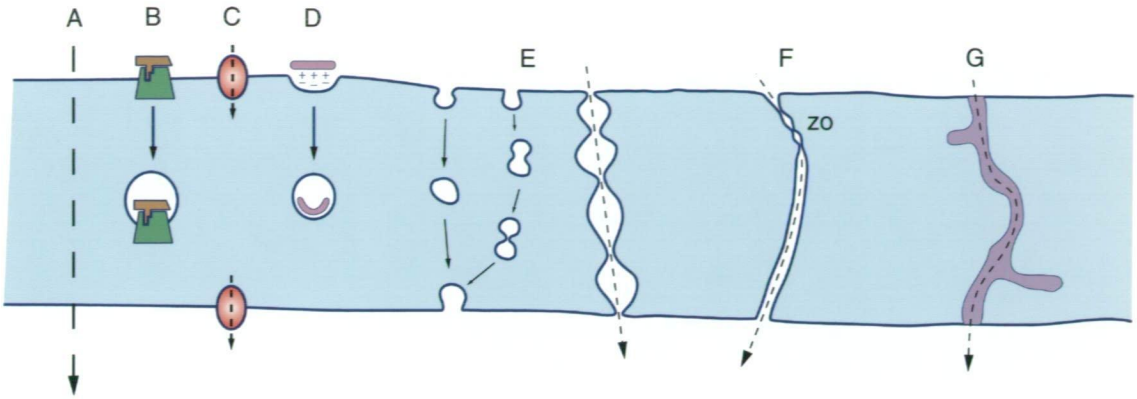

Figure 1.2

Schematic diagram representing possible pathways across endothelial (blood-brain barrier) and epithelial cells (blood-CSF barrier) in the brain. **A**) Diffusion. Lipid soluble (non-polar) compounds can diffuse through cell membranes and enter the brain. **B**) Receptor-mediated trancytosis. Some larger proteins such as the iron transporter transferrin bind to specific receptors at the luminal side of the cell membrane and the protein-receptor complex is then endocytosed. **C**) Carrier-mediated trancytosis. The cell membrane at both the luminal and abluminal side contains transporters that facilitate the transport of molecules such as D-glucose, ions and amino acids. **D**) Adsorptive trancytosis. Certain small peptides with a positive moiety can interact with the negative cell membrane and is then internalised into the cell. **E**) Vesicular transport. Vesicles are produced by an invagination of the cell membrane and can contain large molecules. Vesicular transport has been suggested to work by either vesicles moving from one side the opposite side of the cell, or by shuffling of contents from one vesicle to the next inside the cell, or by several vesicles fusing and forming an extracellular channel through the cell. **F**) Paracellular route. Most of the intercellular cleft is wide enough to all through all but very large molecules; however, at the luminal side of the endothelial cells and at the abluminal side of epithelial cells a *zonulae occludentes* (zo) is present, which severely restrict this pathway. **G**) Channels in subcellular structures. Certain tubulo-canicular structures in endothelia, and endoplasmatic reticulum in epithelia have been proposed to form functional pathways through the cell.

Present study

The present study was undertaken in order to understand the mechanisms of transfer for small lipid insoluble molecules across the brain barriers during development. This was investigated in an integrated approach which combined both quantitative physiological permeability studies and morphological tracer studies in the same species over a similar developmental period. This has the significant advantage over previous studies in that the results from both approaches are directly comparable.

In the present experiments, the blood-CSF and blood-brain uptake in very young (postnatal day 6) to newly weaned (postnatal day 65) South-American opossums (*Monodelphis domestica*) were investigated for several small lipid insoluble compounds. This is the earliest stage of brain development that such studies have been carried out in any species. Just how the present study of the brain barriers compares with previous studies can be illustrated by comparing the age at which the choroid plexuses appear in other species with the opossum. In the rat, the 4th choroid plexus appears at E12, the lateral at E13-E14, and the 3rd at E16 (Chamberlain, 1973). In sheep, the choroid plexus appears in the 4th ventricle at E18-21, in the lateral ventricles at E21-E24, and in the 3rd ventricle at E30-E36 (Jacobsen et al., 1983) (sheep are born around E150). The earliest age at which permeability studies with inulin and sucrose have been carried out in these species is E18-P2 in rats (Ferguson and Woodbury, 1969; Habgood et al., 1993) and E40-E60 in fetal sheep (Evans et al., 1974; Dziegielewska et al., 1979; Cavanagh et al., 1983). In contrast, the South-American opossum is born with only rudimentary lateral ventricular choroid plexuses, no 3rd ventricular plexus, and only a small 4th ventricular choroid plexus (Dziegielewska et al., 2001).

In parallel to these permeability studies, an attempt has been made to visualise the route for small lipid insoluble molecules from blood into the brain. Only electron microscopy

could give high enough resolution to define any such route at the cellular level and it was therefore necessary to use a tracer that was or could be made electron dense. For larger molecules, horseradish peroxidase (a 40 000 molecular weight soluble protein) has been extensively used as a marker (Graham and Karnovsky, 1966; Bouchaud and Bouvier, 1978; van Deurs et al., 1978; Balin et al., 1986; Sedlakova et al., 1999 and many others), but not until quite recently has a low molecular weight electron dense marker been available. Microperoxidase (MP) was introduced in the early 1970's (Feder, 1971) as a low molecular weight marker (molecular weight 1500-1900 Daltons) but it was later found to bind to plasma proteins (Milton Brightman, personal communication). This means that it cannot be used as a small tracer in the blood, however, its usage as a small tracer might be valid when administered directly into the CSF since the CSF contains low levels of proteins. Biotin-dextrans have successfully been used as axonal tracers because of their inertness and low lipid-solubility (for references see Köbbert et al., 2000). In the present study, a low molecular weight biotin-dextran was used as an external tracer for small lipid insoluble molecules and was visualised both at the light and electron microscopic level. In addition, its penetration from blood to CSF was also measured in order to directly compare its CSF uptake with other small radiolabelled markers. Its penetration from blood into the CSF and brain was studied at comparable ages to the quantitative permeability studies using radiolabelled markers.

Aims

There were two main aims of this thesis:

- The first aim was to quantitate, *in vivo*, changes in the transfer of small lipid insoluble molecules from blood to brain and blood to cerebrospinal fluid (CSF) that occur during development, particularly at very early stages.

- The second aim was to visualise the transfer route for such molecules into the developing brain.

Chapter 2

*

General Methods

Review of techniques used to study brain uptake

There are a number of methods used to study the uptake of molecules from blood into the CNS. The most commonly used *in vivo* and *in situ* methods are described below and are also briefly discussed in relationship to their applicability to the present studies. There have also been several *in vitro* models developed, but since it is difficult to mimic what is occurring during development *in vivo* with an *in vitro* model, such models were ruled out in the current investigations.

In *in situ* methods the uptake into brain is determined after arterial infusion of test substance in anaesthetised or in animals immediately after death (Begley, 1992). The perfusate normally contains one or several test substances and an impermeable molecule, and is infused by a motor driven syringe pump normally through the common carotid. The impermeable molecule is used to estimate vascular space. From this the amount of test substance still trapped inside blood vessels in the brain can be determined and is subtracted from brain samples in order to obtain true concentrations in brain tissue. The perfusion can last from a few seconds up to hours. The technique can determine the unidirectional uptake constant (K_{in}; usually expressed as $\mu l\ g^{-1}\ min^{-1}$) either by using single or multiple time points. Multiple time point analysis gives a more accurate estimate but a larger number of animals must be used. The advantage with this method is that the medium containing the test substance can be precisely controlled so problems with protein binding or competition with endogenous compounds do not exist. Since *in situ* brain perfusion is more technically challenging than other methods this was judged not suitable in the present experiments due to the very small size of the animals.

The brain uptake index (BUI) is a simple and fast technique which calculates the uptake of test substance in relation to a reference molecule into one or both hemispheres after a

single arterial (normally carotid) bolus injection (Cornford, 1998). The injectate normally consists of a ^{14}C labelled test substance, a ^{3}H reference isotope and $^{113}Indium$ (binds to transferrin and is therefore impermeable in short-term experiments). A few seconds after the injection the animal is decapitated and the brain dissected out and prepared for scintillation counting. The ^{3}H reference isotope eg. tritiated water is almost completely cleared from blood during a single pass through the brain. The brain uptake index is calculated as $[Extracted_{test\ substance} - Extracted_{indium}]/Extracted_{reference}$ and the ratio given as a percentage. BUI is only appropriate for test substances that have a fast uptake into the brain and could therefore not be used in the present experiments involving slowly penetrating lipid insoluble markers. Furthermore, it would be extremely difficult to give intra-arterial injections into small pups.

Analysing the uptake rate into the CNS after peripheral injections of test substance in awake animals is probably the most physiological technique available (Egleton and Davis, 1997). The technique is experimentally simple, but it is more difficult to interpret the data obtained. The injection solution is prepared in a similar way to the infusate in perfusion experiments with an impermeable marker to determine vascular space. Blood samples are collected throughout the experiment until the animal is killed and brain tissue obtained. The data can be either analysed as a single time point or multiple time points. In the former analysis brain samples are collected at one time point and in the latter at several time points. The advantage of this method is that the test substance's uptake into brain can be measured in awake animals that have been minimally manipulated. The uptake rate is determined under the influence of all components in the blood and the test substance is allowed to pass the vascular bed many times. However, it can sometimes be difficult to interpret the results just because the uptake rate determined is influenced by factors such as protein binding or metabolism. A combination of an *in situ* and an *in vivo* technique will give the best understanding of a substance's uptake into CNS, because the uptake can be measured with or without the

influence of blood components. Since the present study was carried out in small, delicate, developing animals, a minimal invasive technique was required and therefore the single bolus injection method was chosen. Because of the very small size of animals it was not possible to give them intravenous injections and the uptake of markers was instead measured after a single intraperitoneal injection.

Animals

The grey short-tailed South-American opossum (*Monodelphis domestica*)

The grey short-tailed South American opossum (*Monodelphis domestica*) was used in these experiments. The animals were obtained from the colony established at the Central Animal House, University of Tasmania. *Monodelphis domestica* is a small pouchless marsupial native to South-America, from eastern Panama to central Argentina. In the wild the animal is nocturnal, terrestrial or semi-arboreal. The adult male weighs about 120-150 g and the female slightly less. Animals are housed in individual boxes (30X40X16 cm) with a smaller nesting box inside (20X12X10 cm) and males and females are kept in separate rooms except for breeding. The box is filled with paper pellets for ground cover and shredded paper supplied for nest bedding. The room temperature is kept at 25-28°C with a reversed day/night cycle with 14 hours of light. The diet consists of cat food (fortified with meat meal, milk powder, high protein cereal, peanut oil, and multivitamin mix), dry cat pellets, fresh fruit such as banana or kiwi, and live meal worms and crickets. The female reaches sexual maturity at 6 months and the male at 8 with a breeding life of approximately 2 years for both sexes. Two days before breeding the male and female swap cages in order to pheromonally promote oestrous and decrease aggressive behaviour between the pair. The pair remains together for two weeks and afterwards the female is monitored for weight gain in order to check if the mating was successful.

Like all marsupials, this species is born at an earlier stage of brain development than any eutherian mammal, after a gestational period of only 14 days (Saunders et al., 1989). The new born pup weighs approximately 0.1 grams (crown-rump length ~10 mm) and is in terms of general development equivalent of a E13-14 rat, a E35-E40 sheep or pig, or a 6 week human embryo (Saunders et al., 1989). The main precursor of the cortex, the cortical plate appears at around postnatal day 3 in the *Monodelphis*, which in the rat can be first seen on E16, in sheep at E34, or in the human at E50 (Saunders et al., 1989). As an animal used for biomedical research it has the advantage over other marsupials that it breeds all year around, gives birth to large litters that range from 1-14 pups, and can be housed in rather small areas because of its size. It has been successfully used in other areas of neurobiological research such as regeneration of immature spinal cords (Saunders et al., 1998), and studies of spinal cord, cortex and olfactory bulb development (Saunders et al., 1989; Brunjes et al., 1992; Molnár et al., 1998; Knott et al., 1999; Cabana, 2000). The only disadvantage is that the time of mating cannot be exactly established which make developmental studies of embryonic opossums difficult.

Care of pups

Monodelphis pups are constantly attached to mother's teats until 15-20 days after birth. While attached to mother, it is very difficult to make delicate injections into young pups. This can be made easier by lightly anaesthetising the mother during injections, however, this would have enforced another problem since mothers are known to eat their pups when disturbed. Instead in the present experiments, to avoid the risk of cannibalism, pups were detached from mother before injections and kept in a humidicrib (65-75% relative humidity) until terminally anaesthetised. The mother was briefly anaesthetised with isoflurane (see below) while the pups were detached. The

maximum time young animals were kept in the humidicrib did not exceed 4½ hours. Newborns were wrapped in a tissue to minimise heat loss. A temperature probe was kept with the pups in the humidicrib and the temperature was maintained at 27.5-29.5°C. Normal adult body temperature in the opossum is lower (32°C) than in eutherians (Kraus and Fadem, 1987). All experiments were conducted in accordance with NHMRC guidelines and approval of the University of Tasmania Ethics Committee.

Figure 2.1

The grey short-tailed South-American opossum (*Monodelphis domestica*). **A**) Close-up of a 7-day old opossum pup. **B**) Female with 1-day old pups attached to her teats. The opossum is a pouchless marsupial which makes access to the pups easy. It can give birth to up to 14 pups but normal litter sizes range from 5 to 10 animals. The newborn opossum only weighs approximately 0.1 g with a crown-rump length of about 10 mm. **C**) Female with 6-day old pups attached to her teats. The pups weigh approximately 0.3 g at this age. **D**) 35-day old opossum weighing approximately 6-7 g. **E**) Cage and nesting box. The nesting box is filled with shredded paper which the animals use to build a nest. Adults are kept in separate boxes except for during mating. **F**) Adult opossum. The adult male weighs 100-120 g and the female weighs slightly less


A


B


C


D


E


F

Anaesthesia

Surgery, such as nephrectomy, was performed under gaseous anaesthesia with isoflurane (2.5-3.5%; Abbott). This anaesthetic was chosen because of its superior safety margin over other anaesthetics and also its short duration of action, which means quick recovery. The depth of anaesthesia was evaluated by tail and toe pinch throughout the time of anaesthesia. Before collecting blood, CSF or brain samples animals were terminally anaesthetised with inhalation of halothane (Zeneca).

Nephrectomy

Some experiments in this thesis involved injections of radioactive markers into the intraperitoneal cavity of young opossums in order to measure the uptake from blood into the CSF and brain. The model which will be described in detail in Chapter 3 was based on uptake measurements determined by steady-state concentration ratios between CSF/plasma and brain/plasma several hours after the injections. Samples of plasma showed that the plasma concentration increased quickly after the injections, but after an initial peak the concentration gradually fell over time, which possibly was a result of clearance through the kidneys. Urine samples after the injection showed high concentrations of isotopes which confirmed that large amounts of the marker were lost from the blood by filtration out of the kidneys. In order to avoid renal clearance of markers, opossums at P37 and P65 were bilaterally nephrectomised. This was done on a heated operating table under isoflurane anaesthesia. Pups were laid ventrally and the skin was cut along the dorsal midline. After a small cut through the back muscles the kidneys were located and adipose tissue removed so the kidneys could easily be manipulated. The renal artery and vein were then ligated using a suture and the skin was sealed with superglue. Pups were left to recover on a heated table until awake and then left with their mother before final anaesthesia for sample collection.

Injections of radioactive markers

Radioactive markers were obtained from Amersham International and are listed in Table 2.1. All isotopes for injection were prepared in sterile 0.9% NaCl solution. The final activity of each marker was 4.2 - 5.0 KBq μl^{-1} of ^{3}H and 0.42 - 0.58 KBq μl^{-1} of ^{14}C. The activity of injection solution was always measured before the experiment to ensure reproducibility between the experiments. Standardised injections (6 µl/g body weight) were made into the intraperitoneal cavity with a Hamilton syringe fitted with either a 29-gauge needle or a glass micropipette. The intraperitoneal injection avoided the possibility of sudden osmotic or volume changes in the blood system. Inulin, sucrose and L-glucose were chosen as small lipid insoluble test molecules of permeability since they are minimally metabolised in the body (Habgood, 1990) and are believed to only distribute in extracellular compartments. As will be discussed in Chapter 5 this may be true for the adult animal, however, results presented in this thesis suggest that it may not be the case in the developing animal. The use of glycerol was restricted to short-time experiments only (less than 25 minutes) to minimise possible metabolism. The degree of possible glycerol metabolism *in vivo* during such an experiment was checked 30 minutes after an intraperitoneal injection by thin-layer chromatography (see below).

Table 2.1

Radiolabel	Marker	Code No	Molecular Weight
[U-^{14}C]	Sucrose	CFB-146	342
[^{3}H]	Inulin	TRA-324	~5200
[1-^{14}C]	L-glucose	CFA-328	180
[1(3)-^{3}H]	Glycerol	TRA-244	92

Radioactive markers used in permeability experiments. All markers were either ^{14}C or ^{3}H radiolabelled.

Tissue and fluid samples

Blood samples

As soon as a deep level of anaesthesia was obtained, blood was immediately sampled with a glass micropipette by mouth suction. Each pipette was prepared 1-3 days before usage by filling it with heparin and gently blowing out so a film of heparin was formed on the inside of the pipette to prevent blood clotting. In older pups (older than P10) the rib cage was opened and blood collected from the left ventricle of the heart. In younger pups blood was collected by drainage from the left subclavian/axillary artery. The artery was carefully dissected out and any fluid around it was removed with a cotton tip. The blood vessel was cut and blood collected from the groove after the dissection. This artery was chosen since it avoids any possibility of blood mixing with intraperitoneal fluid. Blood samples were transferred to a plastic tube and kept on ice until plasma was separated by centrifugation (5 minutes, 5000 rpm).

CSF and brain samples

After blood samples were taken the heart was cut to lower the systemic pressure and minimise the risk of blood contamination in CSF samples. CSF was taken from the *cisterna magna* of the hindbrain by gentle mouth suction using a glass micropipette. The tip of the pipette was carefully pushed to penetrate through the *dura mater* at an angle to avoid damaging small blood vessels. CSF was transferred to a plastic tube and spun at 5000 rpm for five minutes. Every tube was inspected for blood contamination by examining it under a dissecting microscope over a white background. Blood contamination as low as 0.1% can be detected in this manner (Habgood, 1990). Any tube with visible blood contamination was discarded. After CSF collection the whole brain was dissected out and immediately frozen.

Radio-scintillation counting

In liquid scintillation (LS), radioactive compounds are dispersed in a liquid medium, which is called scintillation fluid. This fluid converts the radioactive decay particles into photons, which can be detected by photomultiplier tubes and a voltage is produced. The LS counter can be set to only count voltage pulses within a set lower and upper limit and this normally defines a 'counting channel' or 'counting window'.

Ideally the rate of counts per minute (CPM; counts seen by the LS counter) is proportional to the disintegrations per minute (DPM) of the radioactive compound. However, quenching can reduce the number of photons produced by the radioactive emission. Quenching is commonly an intrinsic property of plant or animal tissue and thus can be different from sample to sample. Therefore the correct number of counts (DPM) can be calculated by knowing the counting efficiency, which is defined as

$$\text{Counting efficiency} = \frac{\text{CPM}}{\text{DPM}}$$

Quenching of any sample is determined by the LS counter by exposing the sample to a standard gamma ray emitting isotope. It is therefore necessary to make a series of samples with a standard radioactivity but different quench which will give a standard quench-efficiency curve (see Figure 2.2). A quench-efficiency curve has to be constructed for each different isotope since the counting efficiency changes with the energy of the β-decay. At high quenching the counting efficiency is not linearly related to quenching and therefore high quenching in samples should be avoided. From the quench-efficiency curve the DPM from any sample can be determined from the CPM. It is also necessary to determine if the counting efficiency changes with increasing activity (DPM) in the sample solution. By measuring a series of samples with the same quench but increasing DPM this can be determined. As seen in Figure 2.3 the counting efficiency did not change up to at least 700 KDPM, which is well above the activity in any of the sample solutions used in this study.

Any radioactive material produces decaying particles within a certain energy spectrum and the counting channel can be set to only count particles within this spectrum. With the right channel settings, two or more radioactive substances can be counted in the same medium as long as their energy spectra do not overlap. Even if the spectra do overlap to some degree, is it possible to determine the relative activity from each radioactive compound. The lower energy β-decay emittance for ^{3}H overlaps with the higher energy emittance of ^{14}C (see Figure 2.4A). The amount overlapping can be determined as follows. Two counting channels are set so the lower one (channel A) includes all the counts from ^{3}H and a small proportion from ^{14}C. The other channel (channel B) is set to include all other counts from ^{14}C (See Figure 2.4B). A series with a standard amount of ^{14}C but different quench is counted with the channels set as above.

The ratio of counts falling into channel A and B is calculated with different quench (see Figure 2.4B). Quench will reduce the pulse height and shift the energy spectrum to the left and a higher A:B ratio is obtained with quench, ie. the portion of counts is smaller in channel B (see Figure 2.4). A sample with both ^{3}H and ^{14}C can now be counted since the amount of counts produced by ^{14}C in channel A can be estimated from the counts seen in channel B. By subtracting the estimated counts from ^{14}C in channel A from the total counts, the CPM for ^{3}H is determined. The error of estimating the CPM for ^{3}H by this method can be minimised by having 5-10 times more ^{3}H label than ^{14}C. This is especially important when a sample is heavily quenched since the efficiency of ^{3}H decreases proportionally more than ^{14}C (see Figure 2.2).

Sample handling for radio-activity measurements

Aliquots of plasma and CSF were weighed and 5 ml of scintillation fluid (Packard) added. Brains were homogenised and aliquots weighed. To each aliquot of brain 0.5 ml of tissue solubiliser (Soluene-350, Packard) was added and aliquots were left in a low heat oven (40°C) overnight to ensure complete solubility of tissue. 5 ml of scintillation fluid was then added. Tubes were counted for five minutes in a liquid scintillation counter (Beckman LS3801) with window settings as above to allow determination of both ^{14}C and ^{3}H activity. Background counts for CSF and plasma were estimated by vials with only scintillation fluid and background for brain samples by tubes with scintillation fluid plus 0.5 ml soluene (Soluene-350, Packard). These counts were subtracted from all other tubes. The counting-efficiency curve constructed for each isotope converted the CPM determined by the counter to DPM. In order to estimate the true activity in brain tissue the amount of isotope still trapped within the vascular system of the brain was subtracted from the total activity. The residual vascular space was estimated from the initial distribution space of inulin (approximately 1-2 min) in P15 pups (n=5; used to correct values in animals between P6-P15) and P40 (n=5; used

to correct values in animals between P32-P65). Concentration of isotope in each sample was calculated as DPM/g.

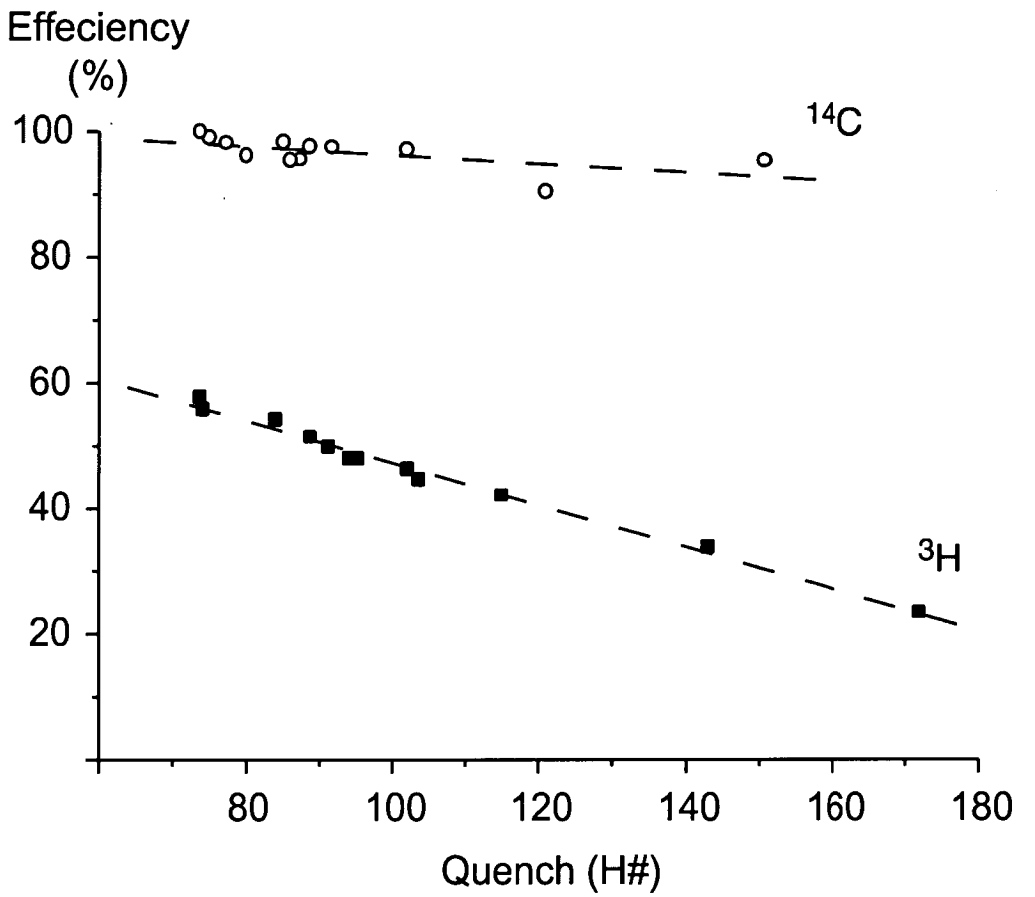

Figure 2.2

Counting efficiency (y-axis) for ^{3}H and ^{14}C against quench (x-axis). Quench reduces the ^{14}C counting efficiency little whereas the ^{3}H counting efficiency decreases considerably with increasing quench. Linear regression lines have been fitted to the data. These lines were used to determine counting efficiency at a given quench. The counting efficiency was necessary to know in order to convert the CPM measured by the scintillation counter to DPM.

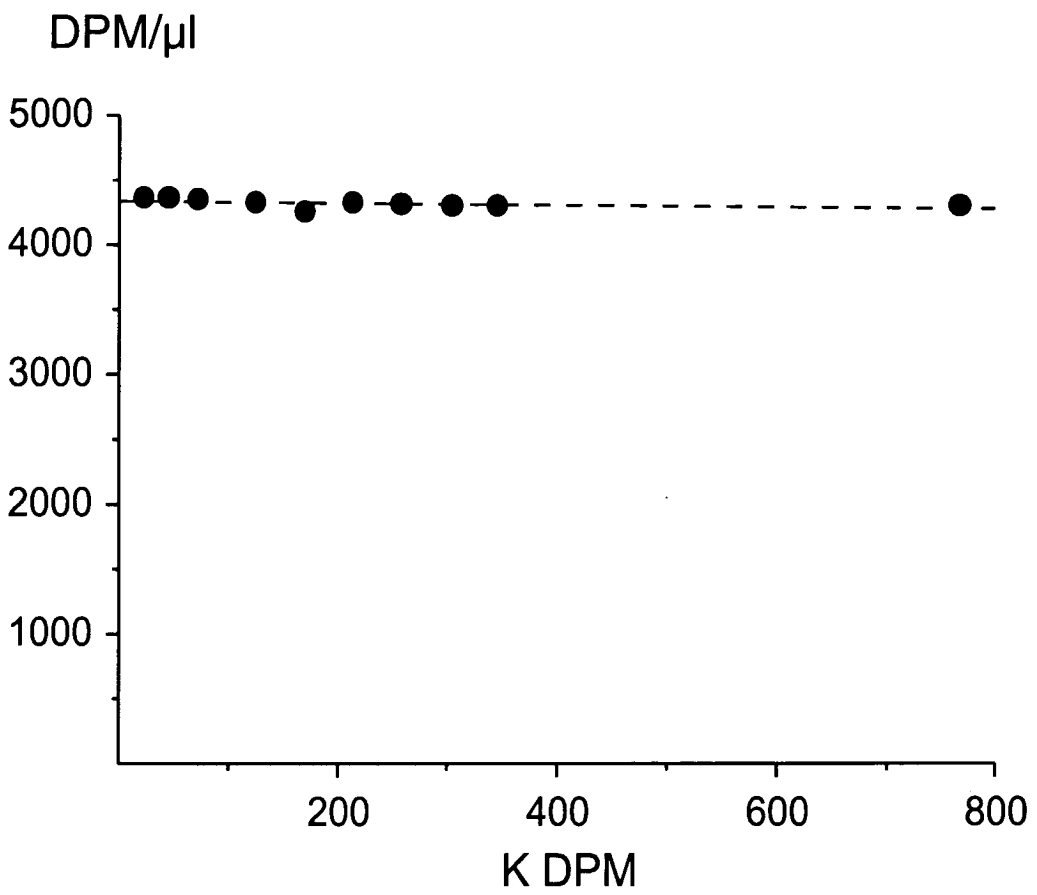

Figure 2.3

The radioactive concentration (DPM/µl) on the y-axis against the total amount of DPM in sample (x-axis). The same solution of ^{14}C was pipetted into scintillation vials in increasing volumes (5-180 µl). The measured concentration of radioactivity (DPM/µl) was the same in all samples. This experiment showed that the counting efficiency did not change with either increasing sample volume or total amount of radioactivity. Both the sample volume and total amount of radioactivity were greater in these experiments than in any of the samples collected from animals.

Figure 2.4

A is a schematic drawing of ^{14}C and ^{3}H spectra and illustrates changes in spectra with (dashed line) or without (solid line) quench. As seen quench will shift the energy spectrum to the left and also decrease the counts seen by the scintillation counter (reduced counting efficiency). The total energy pulse is decreased proportionally more for ^{3}H than ^{14}C with increasing quench (see also Figure 2.2). In order to determine the counts produced both by ^{14}C and ^{3}H in a sample, the scintillation counter was set to count energy within two windows, window A (0-400) and window B (400-660). With these settings, in a sample with little quench, all counts produced by ^{3}H will fall into window A and the counts produced by ^{14}C will mostly fall into window B with a small amount in window A. Since quench shifts the energy spectrum for ^{14}C to the left this will increase the proportion of counts produced by ^{14}C that falls in window A. A series of samples containing the same amount of ^{14}C label but different quench were counted with the windows set as above. The results are shown in *B*. This graph shows the ratio between counts in window A and B (y-axis) with increasing quench (x-axis) for ^{14}C. A linear regression line was fitted to the data. Samples with both ^{3}H and ^{14}C can be counted since the amount of counts produced by ^{14}C in window A can be estimated from the counts seen in window B by the regression line. By subtracting the counts from ^{14}C in window A from the total counts in that window, the total counts for ^{3}H is determined

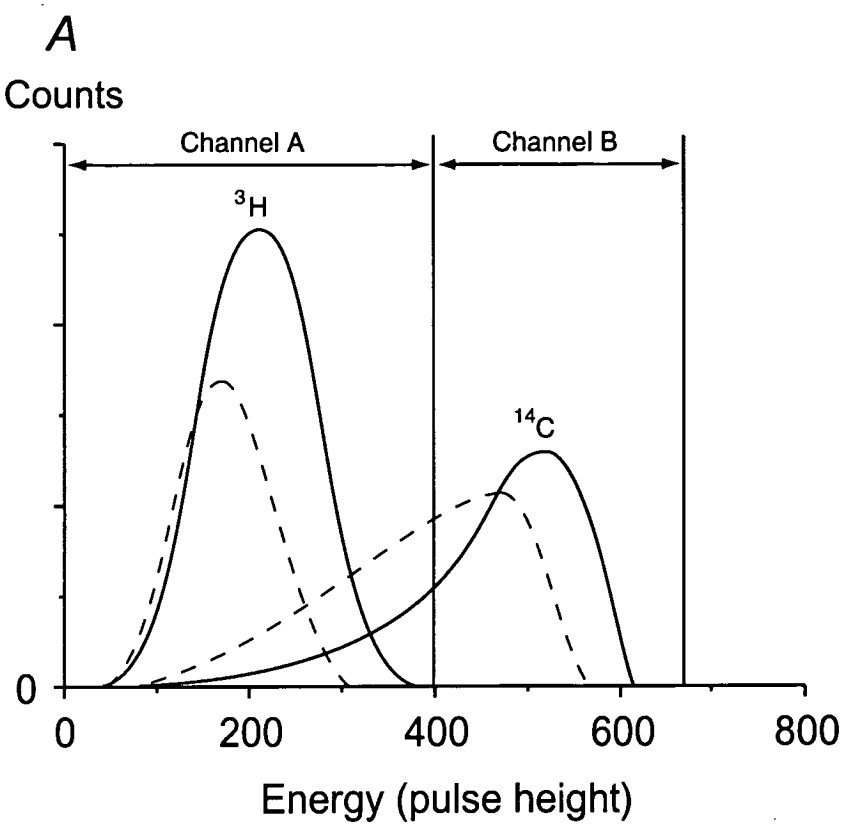
A
Counts
Channel A
Channel B
^{3}H
^{14}C
0
0
200
400
600
800
Energy (pulse height)

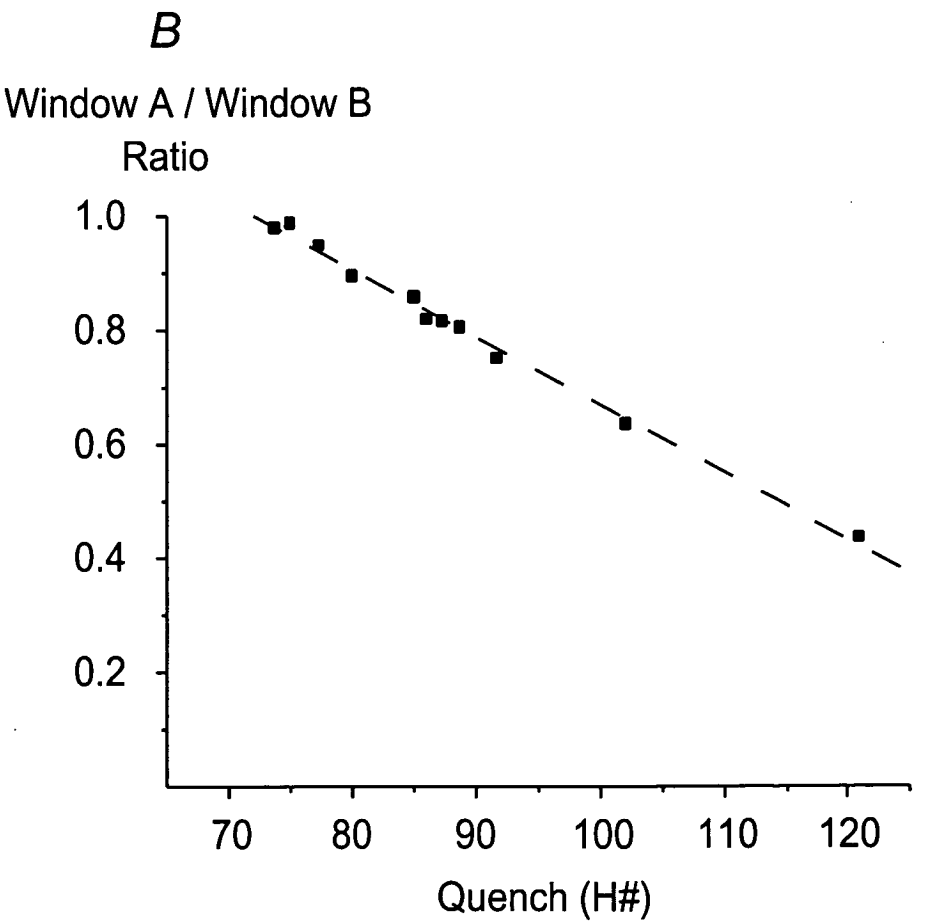
B
Window A / Window B
Ratio
1.0
0.8
0.6
0.4
0.2
70
80
90
100
110
120
Quench (H#)

Lipid solubility of markers

As mentioned in Chapter 1, lipid solubility is a principal molecular property determining rate of uptake into the CNS. Blood solutes, which are in an aqueous environment are believed to enter the CNS by crossing the lipid cell membrane of the endothelium, diffusing through the cytosol and crossing the abluminal cell membrane into an aqueous medium on the other side of the endothelium. This hypothesis could explain the high rate of penetration for lipid soluble blood solutes across the brain barriers, since they leave the aqueous phase of plasma more easily and are less restricted in crossing lipid cell membranes. A solute's lipid solubility is measured by its partitioning in a lipid and in a water phase. A correlation of *in vitro* measurements of a substance's partitioning in hydrocarbon/water phases and brain uptake was found by Mayer et al. (1959). More recently the partitioning between octanol/water has been measured and found to predict brain uptake more accurately (Rapoport and Levitan, 1974). The permeability experiments (presented in Chapter 3) showed clear differences in brain uptake for inulin, sucrose, L-glucose and glycerol throughout development. Measurements of lipid solubility were conducted in order to check if differences in permeability of markers could be explained by their lipid solubility.

Measurement of a substance's lipid/water partitioning is greatly influenced by the medium in which the measurement is performed. A molecule can exist in both ionised and unionised forms, and the ionised form has much more difficulty leaving an aqueous environment because of its polarity. Therefore the ionised form crosses the brain barriers at a slower rate. Measurements of a compound's lipid/water partitioning coefficient as well as its fractional concentration between altered species in a whole range of different pH media will provide information of how lipid solubility changes with ionisation of the drug. From this the partitioning coefficient can be calculated for the unionised form of the compound and is referred to as Log P_{lipid}. This is quite

straightforward as long as it is possible to change the pH to drive the compound into its neutral form. Even if a smaller amount of the compound is in a charged form, the true Log P_{lipid} can be calculated by knowing the fractional concentration for different species. However, if the compound can both give and take protons it becomes more difficult, since it will be impossible to change the pH to get large amounts of the neutral form of the compound. Instead the measurements can be made under standardised conditions (ie. pH 7.4 and 37°C) and the partitioning coefficient is then referred to as Log D_{lipid}. It can be expected that the fractional concentration of different species under these conditions is similar to what would be found *in vivo*.

Radiolabelled markers were made up in 154mM phosphate buffered saline at pH 7.4, and 2 ml of each isotope was transferred to 2-5 separate mixing vials. The initial isotope concentration in buffer was measured by radio-scintillation counting, and the total amount of isotope in each vial ranged between 18.5 GBq – 130 GBq. To each mixing vial 2 ml of (2)-Octanol was added, and to assure proper partitioning between buffer and octanol phase, tubes were vigorously shaken overnight at room temperature. Vials were spun at 3000 rpm for 5 min and left for 30 min on bench. The isotope concentration in the two phases was determined by radio-scintillation counting. The partitioning coefficient ($LogD_{octanol,\ 25°C}$) for each marker is presented in Table 2.2.

Table 2.2

Marker	LogD ± SD	n
Inulin	-3.51 ± 0.02	5
Sucrose	-3.47 ± 0.01	5
L-glucose	-2.68 & -2.68	2

Log $D_{octanol,\ 25°C}$ values for each marker calculated from their partitioning between equal volumes of phosphate buffer and 2-octanol at 25°C. Values shown are mean ± SD (n=number of individual measurements). Since only two measurements were made for L-glucose both are listed here.

Possible metabolites of glycerol

In order to check possible metabolites or breakdown products of glycerol *in vivo*, a P30 opossum was injected intraperitoneally (ip) with ^{3}H-glycerol, and blood and CSF was collected 30 minutes after the injection. In comparison, the longest duration of any measurement of the *in vivo* glycerol permeability was 23 minutes. 5 µl samples were spotted and run, together with a standard (blood from an uninjected animal mixed with ^{3}H-glycerol), on 20 cm silica thin layer chromatography (TLC) plates (Merck, G60). Plates were run in an ascending fashion in a chloroform:methanol (1:2) mixture until the solvent reached up to ¾ of the plate. A non-radioactive standard was run at the same time to identify the glycerol position. At the end of the run, each plate was divided into seven equal fractions (approximately 1.5 cm each) and the gel was carefully removed into individual scintillation vials. The activity in each vial was determined by liquid scintillation counting. Background activity was measured in two vials containing only

the gel and was subtracted from sample vials.

The proportional activity (%) in each fraction to the total amount on each plate was calculated (see Table 2.3). Standard sample showed 96% activity in the two fractions (fraction 4 and 5) that corresponded to the glycerol spot. The same fractions in blood and CSF had 71% and 80% of the activity, respectively. Less than one percent of the activity was found in the fraction moving with the solvent front (fraction 7) in all samples. The first fraction (including the initial spot) constituted 8% and 2% of activity in blood and CSF, respectively.

Table 2.3

Fraction	1	2	3	4	5	6	7
Standard	0.2	1.0	2.5	36.7	59.2	0.4	0
Blood	8.4	10.8	6.9	20.5	50.3	2.3	0.8
CSF	1.7	9.2	6.3	16.2	63.4	3.1	0

TLC analysis of blood and CSF from a P30 opossum 30 minutes after intraperitoneal injection of ^{3}H-glycerol. The activity in separate fractions is expressed as the proportion (%) to the total on each plate (ie. the total of each plate is 100%). Standard was ^{3}H-glycerol mixed with control blood immediately prior to chromatography.

The first fraction corresponds to most hydrophilic substances such as water or glucose, the last (7^{th}) fraction to compounds that are most hydrophobic such as lipids. As seen in Table 2.3 small amounts of activity were found in the fractions above the glycerol

position, which indicates that little glycerol was converted in to more lipid soluble compounds. Instead, some glycerol seemed to have been transformed into more water soluble compounds found in fraction one to three. Since conversion products are almost uniformly lipid insoluble compounds, which would enter the CNS at a slower rate than glycerol, measurements of glycerol permeability should be little affected by these compounds.

Chapter 3

*

Experimental Model

Introduction

Traditionally the permeability across the brain barriers of slowly penetrating solutes (eg. lipid insoluble compounds) has been measured by maintaining a constant blood plasma level of test substance until a steady level has been reached in the CSF and brain (Ferguson and Woodbury, 1969; Dziegielewska et al., 1979). A constant plasma level can be obtained by infusion of test substance until the amount infused equals the amount lost from blood (by diffusion into other tissue or renal clearance) (Ueda et al., 1993). The concentration in brain will also slowly increase until a steady-state is reached. Samples of brain and plasma are taken and a ratio between the brain and plasma concentration is calculated and expressed as a measure of brain permeability. When only a single injection of marker molecule is possible, bilateral nephrectomy prevents renal clearance and a steady plasma level is obtained (Habgood et al. 1993). In both of these models, preliminary experiments have to be performed to determine the time scale of approaching the steady-state between CSF or brain and plasma. Steady-state ratios between CSF/plasma and brain/plasma are then measured as transfer rates across the brain barriers (Habgood et al. 1993).

For detailed procedures of methods described below such as nephrectomy, injections, and tissue sampling see Chapter 2. The experiments described in this Chapter were conducted in a sequential manner, where certain parameters in one experiment had to be established before the next was commenced. These parameters determined the procedures used in the following experiments. The results have therefore been described consecutively with respect to development of the underlying methodologies in order to understand the reasons for certain experiments and procedures The experimental model presented in this Chapter was used in further experiments, which are described in the Chapters 4 and 5.

Methods

Litter based model

Blood and CSF samples were obtained from opossum pups as early as P6. At this age the pups weigh 200-250 mg and presuming a similar blood to body weight ratio as in older animals, newborn pups would only have a blood volume of about 20-25 µl. This makes it impossible to use serial blood sampling from one animal in order to construct a plasma concentration curve of markers. This problem can be overcome by using a litter-based model that was described by Habgood (1990). Instead of taking serial blood and CSF samples from one animal, a whole litter is used and only one blood sample is taken from each animal at successive time points. This model assumes that every littermate behaves in a similar manner, and a sample from one animal can represent all other littermates at that time point (Habgood, 1990).

Newborn opossums model

The very small size of newborn opossums made it technically impossible to cannulate any vessels for infusion or nephrectomise animals in order to maintain a constant plasma concentration of markers. In the present study, near to steady-state ratios were estimated by dividing the CSF or brain activity by the mean plasma activity throughout the experiment following single injection, in non-nephrectomised animals (see equations below).

$$\text{CSF/Plasma Ratio} = C_{CSF} / \left(\int_0^T C_{plasma} / T \right) \qquad (3.1)$$

$$\text{Brain/Plasma Ratio} = C_{brain} / \left(\int_0^T C_{plasma} / T \right) \qquad (3.2)$$

The accuracy of estimating steady-state ratios with this method was evaluated in older postnatal animals by comparing steady-state ratios obtained from nephrectomised animals, with ratios from unoperated (intact) animals determined using the above equations. Preliminary experiments were necessary to determine the time it takes to approach a steady-state in nephrectomised animals. This was investigated in pups at P37 since it was found impossible to nephrectomise younger animals. It was also necessary to determine the plasma concentration curves at several developmental ages in intact animals in order to check if the plasma profiles for the markers changed with age.

Time to approach steady-state in nephrectomised animals

In order to determine the time it takes to approach steady-state between plasma, CSF and brain a group of P37 opossums (n=12) were bilaterally nephrectomised (for surgical details see Chapter 2). Animals were injected ip with a mixture of ^{14}C-sucrose and ^{3}H-inulin and killed with an overdose of halothane inhalation after 1, 2, 3 and 4 hours and blood, CSF, and brain samples were collected. Since a litter-based model was used, it was necessary to standardise the plasma concentrations between different animals in separate experiments. This was obtained by expressing plasma concentrations as a ratio between the activity in plasma and injection solution. For each experiment the isotope concentration in the injection solution was determined.

Plasma concentration curves in intact animals

Opossums at P9-10 (n=15), P15 (n=15), and P37 (n=12) were given a standardised injection of a mixture of ^{14}C-sucrose and ^{3}H-inulin. Animals were killed with an overdose of Halothane between ½ and 4 hours, and blood samples were taken in order to determine the plasma concentration curves of markers. The plasma concentration was plotted against the time after the injection. The integral of the plasma curve was used to

calculate the mean plasma concentration at any time point throughout the experiment. Ratios were calculated between the CSF/mean plasma concentration and brain/mean plasma concentration (see Equation 3.1 and 3.2.)

Results and Conclusions

Nephrectomised animals

Plasma concentration curve and time to approach steady-state

Animals at P37 were bilaterally nephrectomised in order to determine the time it takes to reach steady-state and to evaluate the novel model of estimating steady-state ratios in intact animals. Figure 3.1 shows the plasma concentration curve in nephrectomised animals after a standardised ip injection of sucrose and inulin. After nephrectomy the plasma concentration became stable within three hours for both inulin and sucrose. Sucrose being a smaller molecule with a faster diffusion rate reaches a steady level within one hour. Nephrectomy is therefore a suitable method of achieving steady plasma concentration of a substance when constant infusion is not practical. CSF/plasma ratios for sucrose and inulin in these animals approached a plateau by three hours after the injection (Figure 3.1). The brain/plasma ratios for sucrose also approached a plateau after three hours whereas inulin is not illustrated since it did not reach detectable levels (<1% of plasma concentration) within 4 hours.

Non-nephrectomised animals

Plasma concentration curves

Groups of opossum pups at P9-10, P15, and P37 were injected with markers without prior nephrectomy. As seen in Figure 3.2 the litter based model provides a useful method of monitoring plasma concentrations in very small animals, where it is not possible to obtain serial blood samples from one animal. The plasma concentrations of

inulin and sucrose reached a peak within 1 hour, thereafter they fell throughout the time of the experiment because of renal clearance. This was confirmed by finding very high isotope activity in urine. The markers were cleared from the blood at a slower rate at P9-P15 compared to P37. When possible a polynomial regression line was fitted to the plasma concentration time points, and was forced to cross 0 at the origin since at time 0 all of the isotope should be in the intraperitoneal cavity, and none in the blood. In other cases a computer fitted bezier curve was made to fit through the average plasma concentration at each time point. According to the litter-based model this was representative of the plasma concentration curve for all non-nephrectomised animals between 0 to 4 hours and the integral could then be used to estimate the mean plasma concentration at any time point.

Steady-state ratios in intact animals

In nephrectomised animals the time to approach steady-state had been determined to be at least three hours. According to the litter-based model the changes in plasma concentration curve from an individual sample could be approximated by the plasma concentration curve from the litter-based experiment. Steady-state CSF/plasma and brain/plasma ratios in intact animals were calculated using equation 3.1 and 3.2 at three hours. The accuracy of these ratios were determined by comparing them with ratios in nephrectomised animals at the same time point, which had been shown to approach a steady-state (Table 3.1).

Table 3.1

	Sucrose		Inulin	
	CSF/Plasm	Brain/plasma	CSF/plasma	Brain/plasma
Nephrectomised	15.0 ± 1.8	4.4 ± 0.8	6.9 ± 0.6	3.5 ± 0.9
Intact	14.2 ± 2.0	4.3 ± 0.5	7.3 ± 0.7	3.4 ± 0.4

Steady-state CSF/plasma and brain/plasma ratios for ^{14}C-sucrose and ^{3}H-inulin in nephrectomised (n=4) and intact (non-nephrectomised, n=5) P37 opossums. CSF concentrations were measured in samples collected from the cisterna magna. In nephrectomised animals, the CSF and plasma concentrations both approached steady-state by 3 hours after ip injection, whereas in intact (non-nephrectomised) animals the plasma concentration peaked at 30-60 min after the injection and then gradually fell. In these intact animals, the mean plasma concentration was determined from the integral of the plasma concentration curve over the entire time course of each experiment and ratios calculated as CSF/mean plasma concentration or brain/mean plasma concentration (see equation 3.1 and 3.2). These two different methods of determining steady-state ratios gave similar results. Values are mean ± S.E.M.

Figure 3.1

The left y-axes in A and B show the plasma/injectate (■) and the CSF/injectate (●) concentration ratios for sucrose (A) and inulin (B) following a single ip injection in nephrectomised opossums at P37. The right y-axes in A and B show the CSF/plasma ratios (△). The left y-axes in C show the plasma/injectate (■) and the brain/injectate (◆) concentration ratios for sucrose in the same animals. The right y-axes in C show the brain/plasma ratios (▽). The x-axes show the time after the ip injection. The concentration in plasma, CSF and brain were divided by the original concentration in the injection solution in order to obtain normalised data that were comparable between different animals and experiments. The plasma/injectate, CSF/injectate and brain/injectate concentration ratios are all approaching a steady level by three hours after injection for both markers. CSF/plasma ratios for sucrose (A) and inulin (B), and brain/plasma (C) for sucrose also approach a steady level by three hours after injection. The brain/plasma ratios for inulin were not illustrated because it did not reach appreciative levels in brain within three hours. All data points shown are means (n=3-4) and the error bars indicate ± SEM. Where no error bars are visible, they are contained within the symbol.

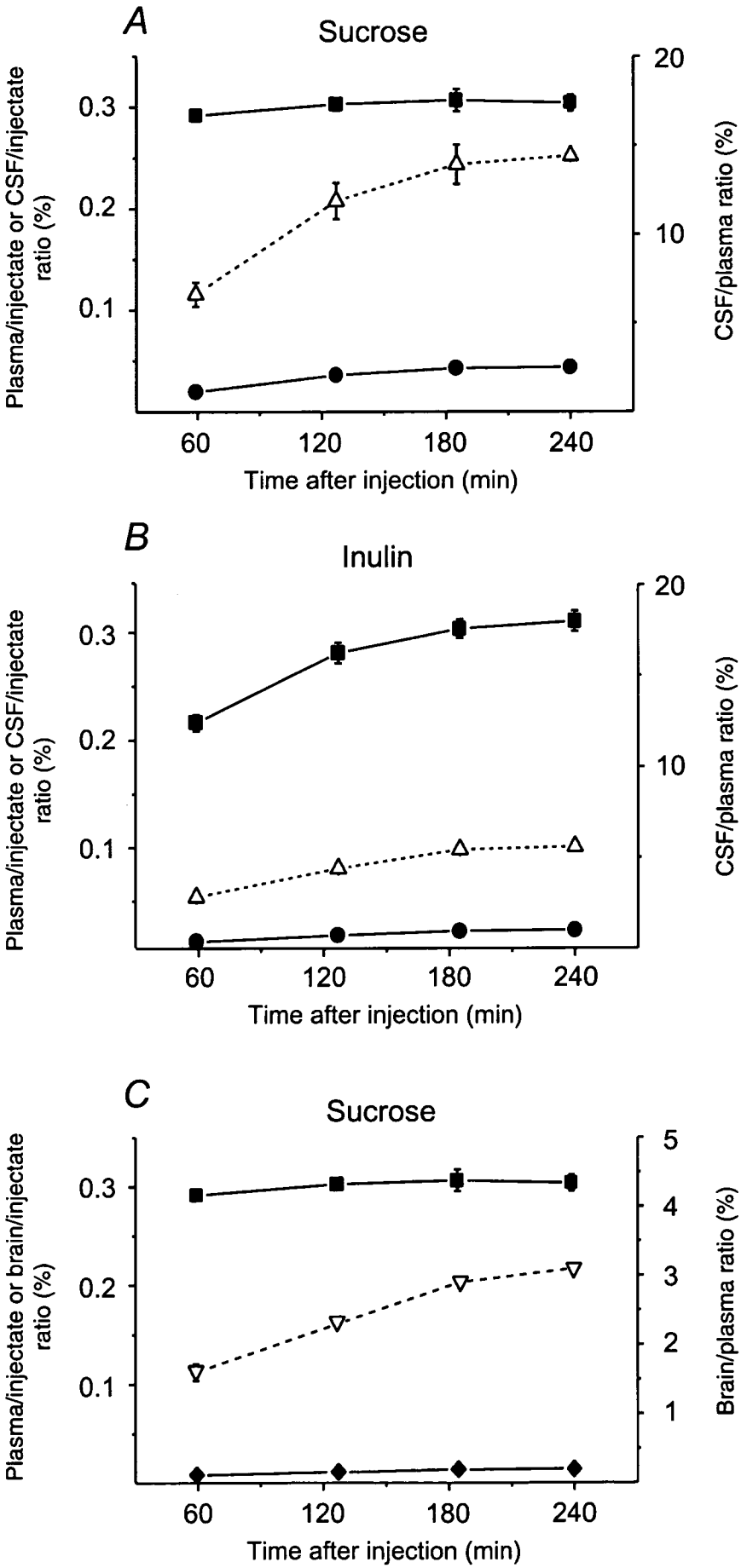
A
Sucrose
Plasma/injectate or CSF/injectate ratio (%)
0.3
0.2
0.1
20
10
CSF/plasma ratio (%)
60
120
180
240
Time after injection (min)
B
Inulin
Plasma/injectate or CSF/injectate ratio (%)
0.3
0.2
0.1
20
10
CSF/plasma ratio (%)
60
120
180
240
Time after injection (min)
C
Sucrose
Plasma/injectate or brain/injectate ratio (%)
0.3
0.2
0.1
5
4
3
2
1
Brain/plasma ratio (%)
60
120
180
240
Time after injection (min)

Figure 3.2

Plasma/injectate concentration ratios for ^{14}C-sucrose (A), ^{3}H-inulin (B) in plasma after a single intraperitoneal injection in non-nephrectomised animals determined at P9-P10 (△), P15 (●), and P37 (□). The x-axes show the time after the ip injection. The concentration in plasma, CSF and brain were divided by the original concentration in the injection solution in order to obtain normalised data that were comparable between different animals and experiments. The curves shown are bezier curves computer fitted to data points for each age and used to calculate mean plasma concentrations. The plasma/injectate concentration ratios in these non-nephrectomised animals all reach a peak and then gradually decline over time. The curves at P9-10 and P15 animals were very similar for inulin and sucrose, whereas the peak for P37 animals occurred somewhat later.

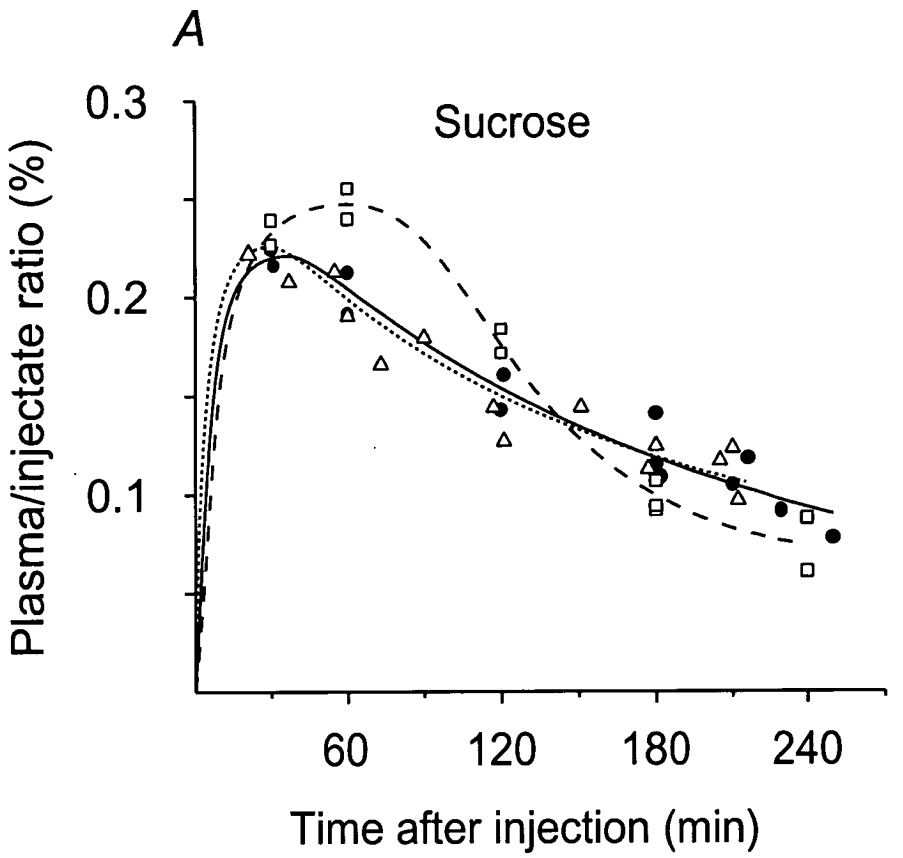
A
Sucrose
0.3
0.2
0.1
Plasma/injectate ratio (%)
60
120
180
240
Time after injection (min)

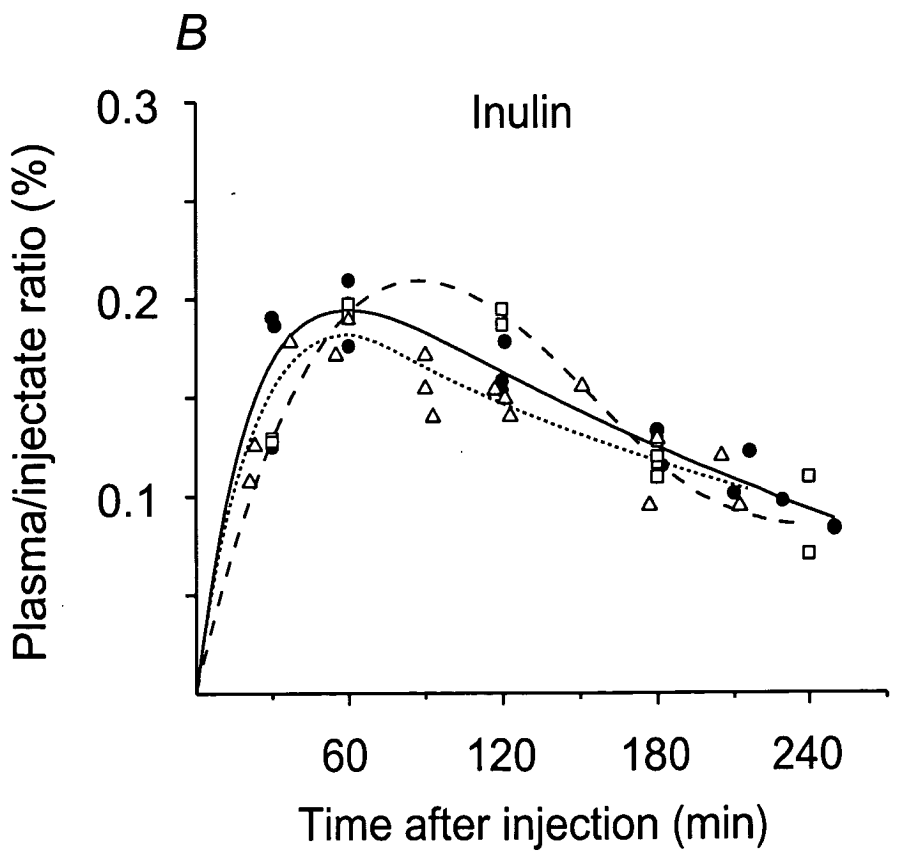
B
Inulin
0.3
0.2
0.1
Plasma/injectate ratio (%)
60
120
180
240
Time after injection (min)

Validity of model

The CSF/plasma and brain/plasma ratios of sucrose and inulin at 3 hours were very similar for nephrectomised and intact animals (see Table 3.1). Steady-state ratios from nephrectomised animals can therefore be accurately estimated from animals without prior nephrectomy. Nevertheless, there are a few considerations of the model when applying it to younger ages. Firstly, does the time to reach steady-state change with the age of the animals? If the equilibrating time is longer in younger animals the ratios would be under-estimated since the CSF and brain concentrations are still rising. This could not be tested in opossums since it is technically not possible to keep a steady plasma concentration at very young ages. However, it is unlikely that it would take a longer time in younger animals since lipid insoluble compounds seem to enter the CNS faster at younger ages (Ferguson and Woodbury, 1969; Dziegielewska et al., 1979; Habgood et al., 1993) and the time to reach steady-state should then be shortened (see Chapter 4 for discussion). Secondly, how do the differences in the plasma profile for markers at different ages affect the model? By calculating 3-hour steady-state ratios at P37 by applying the different plasma concentration curves at P9-10, P15, and P37 this could be determined. The data are presented in Table 3.2. By applying the P15 and P9-P10 plasma curve to the P37 data, the mean plasma concentration will be underestimated, giving higher ratios. The effect is very small on inulin ratios whereas it is greater on sucrose ratios especially when using the P15 concentration curve. The difference between using the P15 and P9-P10 concentration curves for inulin and sucrose is very small. It was therefore assumed that the plasma curve for P9-10 animals could also accurately represent the plasma curve for even younger animals.

Table 3.2

	P37	P15	P9-P10
Sucrose	14.2 ± 0.9	18.4 ± 1.2	18.6 ± 1.2
Inulin	7.4 ± 0.3	7.9 ± 0.3	8.3 ± 0.4

The steady-state 3-hour ratios for inulin (n=5) and sucrose (n=5) in P37 opossums by applying P37, P15, and P9-P10 plasma concentration curves. The ratios changes for sucrose by using the P37 and P15 plasma concentration curves whereas the difference is small between P15 and P9-P10 animals. Inulin shows small differences in ratios by applying any of the plasma concentration curves. Values are means ± SEM.

Chapter 4

*

Uptake of Low Molecular Weight Markers during Development

Introduction

Rapidly penetrating solutes will reach a CSF/plasma concentration ratio of 1 at equilibrium. Even slowly penetrating substances should at infinite time (equilibrium) reach the same concentration in the CSF as in plasma. Failure to reach a ratio of 1, as was reported in Chapter 3 for inulin and sucrose, could result from active transport from CSF to blood. However, this is unlikely in the case of substances such as sucrose or inulin that are supposed to be biologically inert within the body. A more likely explanation is a continuous replacement of CSF in the ventricles (ie. the flow of CSF), which could account for slowly penetrating solutes not equilibrating with the plasma concentration even after a long exposure in plasma. This is often referred to as the sink effect (Oldendorf and Davson, 1967; Davson and Segal, 1969). Slowly penetrating solutes will have a lower concentration in the newly formed CSF compared with plasma. The slower a substance penetrates the blood-CSF interface, the lower C_{CSF}/C_{plasma} ratio will be at steady-state. The steady-state level can therefore be a measure of permeability.

In Chapter 3 a model was described that estimated steady-state CSF/plasma and brain/plasma ratios in animals with varying plasma concentrations of marker after a single intraperitoneal injection. The model was found to accurately estimate steady-state ratios and this provided a way to study the penetration of markers with little manipulation of the animals. With further use of this model, steady-state ratios were estimated in *Monodelphis* pups at various ages between P6 to P65 for three small lipid insoluble markers sucrose, inulin, and L-glucose. The results are presented in this Chapter. In the current study, the penetration of lipid insoluble molecules has been measured in a quantitative way earlier in development than have previously been reported. The results of these experiments are compared with morphological studies using tracers presented in Chapter 5.

In order to investigate more directly the possible developmental changes that could give rise to age related differences in steady-state ratios, short time course uptake experiments were carried out (7-24 minutes). As explained in Chapter 2, K_{in} can be determined by the initial uptake into CSF and brain. The slow uptake of sucrose and inulin would be difficult to detect and therefore a smaller inert molecule was needed with faster penetration but still with hydrophilic characteristics. L-glucose with a molecular weight of 182 (about half the size of sucrose), metabolically inert because of its L configuration, and a $LogD_{octanol, 25°C}$ value of –2.68 (see Table 2.2) was used. For comparison, the short-term uptake rate of a moderately lipophilic molecule (glycerol, LogD –1.94) was studied. Such a molecule should pass the cell membranes of the epithelial cells of the choroid plexus and the endothelial cells in the brain blood vessels with relative ease. Blood flow and the vascular surface area available for exchange would therefore mostly determine the uptake rate into the CNS. A moderately lipophilic molecule was chosen because the rate of uptake would be difficult to measure for highly lipophilic compound, where the CSF would rapidly equilibrate with plasma. Glycerol with a $LogD_{octanol, 25°C}$ of –1.94 and which had been shown to be relatively stable *in vivo* during such a short duration (see Chapter 2) was chosen as a suitable test molecule.

Methods

Steady-state concentration ratios during development

Opossums at P5-P7 (n=9), P9-P13 (n=15), P15-P17 (n=5), P32-P37 (n=10), and P65 (n=3) were injected, ip, with a mixture of ^{14}C-sucrose and ^{3}H-inulin. Steady-state ratios between CSF/plasma and brain/plasma were estimated by the model described in Chapter 3 in animals killed between 3-3½ hours after the injection. The mean plasma

levels for ^{14}C-sucrose and ^{3}H-inulin of animals between P6-P10 were estimated from the plasma concentration curves for P9-P10 animals, and for animals aged between P13-P17 from the plasma curve for P15 animals; finally for animals aged between P32-P37 the plasma concentration curve from P37 animals was used (see Chapter 3 for plasma curves). Animals at P65 were nephrectomised prior to injection but were otherwise treated in the same manner and ratios were calculated assuming a steady plasma level.

Other groups of opossums were injected, ip, with ^{14}C-L-glucose at P18 (n=9) and P38 (n=10). Samples of CSF, blood and brain were collected approximately every 30 minutes between ½ and 4 hours in order to construct a plasma concentration curves at both ages. Plasma samples collected for initial uptake rate experiments (see below) were included as data points in the plasma concentration curves, however, this resulted in many data points between 0 and 30 minutes. For the clarity of presentation, data points were grouped within the same 10-minute interval (0-10, 10-20, 20-30 minutes etc) and the mean ± SEM was calculated for each group (Figure 4.1). Plasma concentration curves were constructed by computer fitting bezier curves to the data points. Steady-state ratios between CSF/plasma and brain/plasma were estimated by the model described in Chapter 3, in animals killed between 3 and 3½ hours (n=4 for both ages) after the injection. Differences in steady-state ratios were tested by unpaired t-test. For more detailed description of procedures used in these experiments see Chapter 2. Differences in steady-state ratios between P18 and P38 for L-glucose were tested by two-way unpaired t-test.

Short time-course experiments

Opossum pups at P18 (n=9) and P38 (n=13) were injected ip with a mixture of ^{3}H-glycerol and ^{14}C-L-glucose. The timing of tissue sampling was crucial in these

experiments, and therefore the procedure of taking CSF, brain and blood samples was modified. After anaesthesia, CSF was collected from the *cisterna magna* and the animal immediately decapitated to stop blood flow to the brain. Blood was then collected from the bleeding carotid artery and the brain removed. This procedure minimised the time delay between CSF and blood sampling. The starting and ending time of the blood collection was recorded and the average time calculated as the blood collecting time. The average difference in time between CSF collection and blood sampling was 26.3 ± 4.8 (Mean ± SD; n=8) seconds in P18 animals, and 18.5 ± 4.8 (n=10) seconds in P38 animals. All blood samples were collected between 7 and 24 minutes after injection. Since there was no blood flow to the brain after decapitation, the timing of brain tissue sampling was not considered critical but nevertheless it did not exceed one minute after decapitation. The amount of marker molecule entering the brain from blood between decapitation and brain tissue sampling will not effect the measurements since it will be compensated for by the deduction of the vascular space. The time for brain sampling was recorded as the time for decapitation. CSF/plasma and brain/plasma ratios were calculated and plotted against the blood collection times. Linear regression lines were fitted to data points with least square method. Differences in slope of the regression lines were tested with unpaired t-test. For more detailed description of procedures such as injections, collection and handling of tissue samples used in these experiments see Chapter 2.

Results

Steady-state concentration ratios during development

In order to estimate steady-state ratios for L-glucose with the model described in Chapter 3 a plasma concentration curve was first determined after single ip injection in non-nephrectomised animals at both P18 and P38. This showed that similar to inulin and sucrose (see Figure 3.2), the plasma concentration for L-glucose increased rapidly

and then gradually fell over time at both ages (see Figure 4.1). The changes in steady-state CSF/plasma and brain/plasma ratios for radioactive markers with age are shown in Figure 4.2. Ratios for sucrose were consistently higher than for inulin at all ages examined. Sucrose CSF/plasma ratios fell from 59.1 ± 2.9% (mean ± SEM) at P6 to 6.2 ± 0.9% at P65 and inulin ratios decreased from 29.7 ± 1.4% at P6 to 1.3 ± 0.2% at P65. Brain/plasma ratios for sucrose were reduced from 15.9 ± 0.8% to 4.0 ± 0.2% between P6 and P65 whereas inulin ratios declined from 9.5 ± 0.7% to 1.4 ± 0.1% over the same time. Ratios for the smaller molecule L-glucose were higher than inulin and sucrose at corresponding ages. There was a significant reduction in steady-state CSF/plasma and brain/plasma ratios for L-glucose between P18 and P38. The steady-state CSF/plasma ratios decreased significantly from 35.5 ± 1.9% at P18 to 14.2 ± 0.3% at P38 ($p<0.01$). In a similar way the brain/plasma ratios at 3 hours were reduced from 13 ± 1.0% at P17 to 7.1 ± 0.3% at P38 ($p<0.01$). Brain/plasma ratios were considerably lower than the CSF/plasma ratios at every age for all markers. This is probably due to a different distribution space in the brain compared to CSF. Both inulin and sucrose are believed to be extracellular markers and will therefore have a much smaller distribution volume in brain compared to CSF.

Short-time course experiments

CSF/plasma and brain/plasma ratios measured in short-time course experiments (7-24 min) for both glycerol and L-glucose are shown in Figure 4.3. During this short initial period (7-24 min) the plasma concentrations were almost stable and therefore changes in CSF/plasma and brain/plasma concentration ratios with time were directly related to the rate of uptake into CSF and brain (see Figure 4.1). Analysis of the data points showed that uptake into CSF and brain was linear over this time period. This suggests a unidirectional uptake into the CNS compartments and the slope of fitted linear regression lines could be used to represent the initial uptake rate into either CSF or

brain (see Fenstermacher et al., 1981). The regression lines' intercept with the x-axis could estimate the initial distribution volume in the brain at P18 and P38. The radioactivity due to this volume was deducted from all brain samples in order to obtain true concentrations in brain tissue. Differences in the slope of the regression lines were compared using a student's t-test (unpaired). L-glucose showed a much faster initial rate of uptake into CSF and brain at P18 compared to P38 (Figure 4.3). The slope of the regression line for CSF uptake of L-glucose in P18 animals was significantly steeper than that of P38 (P=0.01). The difference in uptake into brain between the two ages, because of the greater scatter of the data, failed to reach statistical significance (P=0.07). The rate of uptake of glycerol into both CSF and brain appeared similar at both developmental ages (see Figure 4.3). The slopes of the regression lines for CSF uptake of glycerol, and for brain uptake of glycerol were not statistically different between the two ages (P=0.97 and P=0.33, respectively).

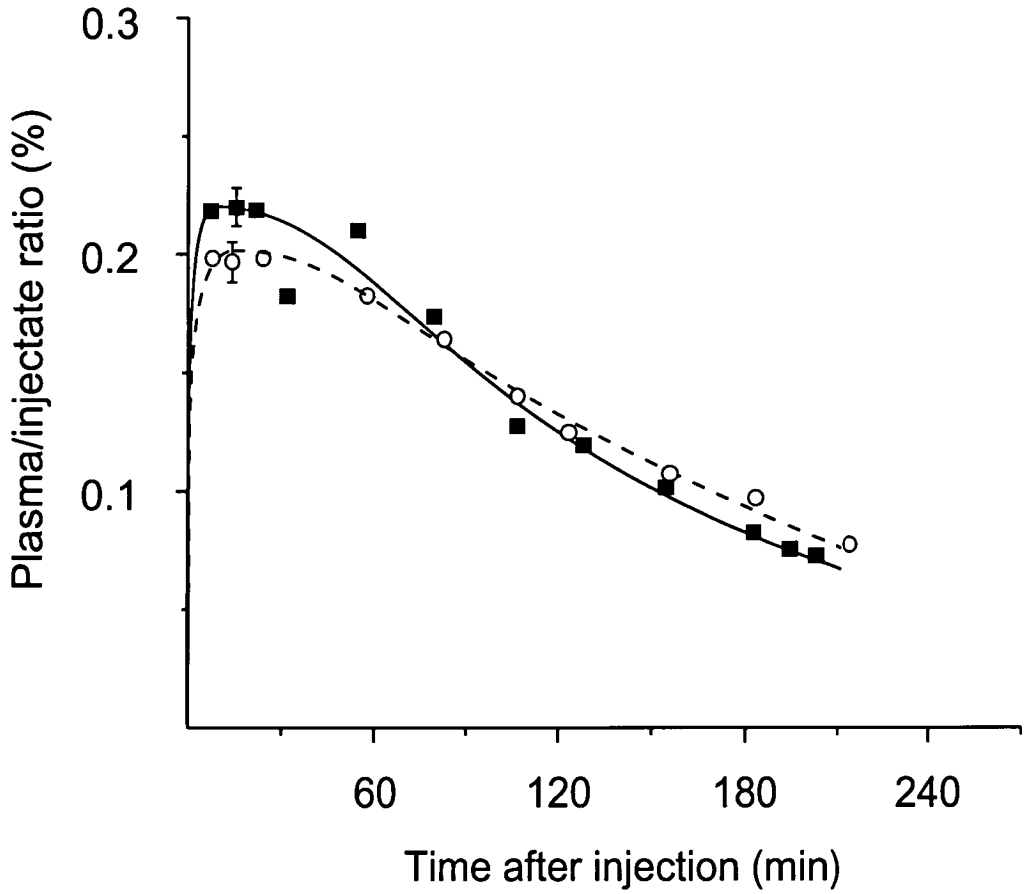

Figure 4.1

Plasma/injectate concentration ratios for ^{14}C-L-glucose in plasma after a single intraperitoneal injection in non-nephrectomised animals determined at P18 (○) and P38 (■). The x-axes show the time after the ip injection. The concentration in plasma, CSF and brain were divided by the original concentration in the injection solution in order to obtain normalised data that were comparable between different animals and experiments. The data points were averaged for 1-5 animals within the same 10-minute interval (0-10, 10-20, 20-30 minutes etc). The curves shown are bezier curves computer fitted to data points for each age and used to calculate mean plasma concentrations. The plasma/injectate concentration ratios reach a peak and then gradually decline over time. Note that the plasma concentration appeared to be almost stable between 7-25 minutes after the injection.

Figure 4.2

The y-axes show steady-state CSF/plasma (A) and brain/plasma (B) ratios (%) for ^{14}C-sucrose (■), ^{3}H-inulin (○), and ^{14}C-L-glucose (△) and the x-axes show the postnatal age in days. All ratios were measured in non-nephrectomised animals, except those at P65 which were measured in animals that had been nephrectomised. Both CSF/plasma and brain/plasma ratios declined markedly with increasing postnatal age. Brain/plasma ratios were also consistently lower than CSF/plasma ratios at all ages. Values shown are means (n=3-8) and the error bars indicate ± S.E.M. Where no error bars are visible, they are obscured by the symbols.

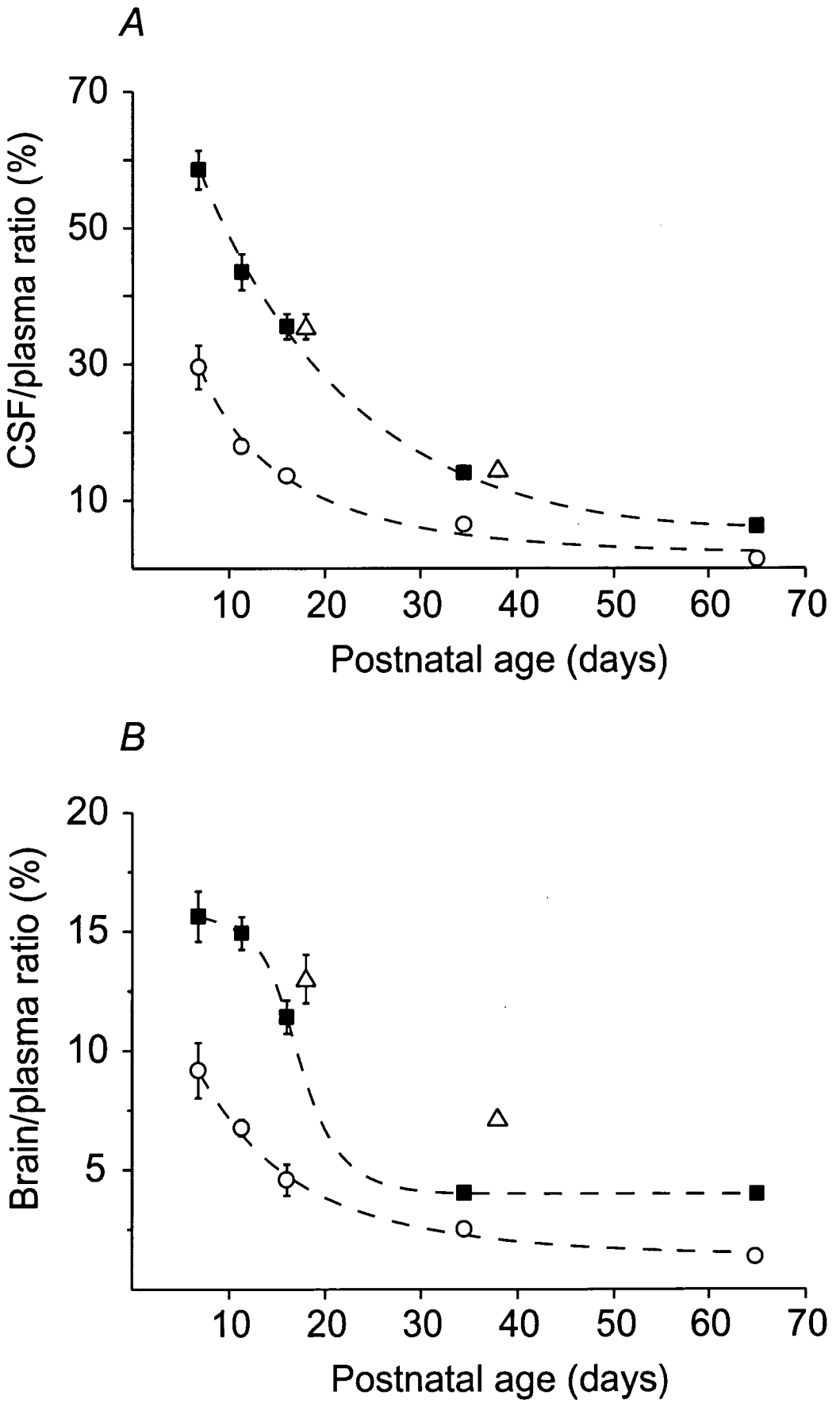
A
CSF/plasma ratio (%)
70
50
30
10
10
20
30
40
50
60
70
Postnatal age (days)
B
Brain/plasma ratio (%)
20
15
10
5
10
20
30
40
50
60
70
Postnatal age (days)

Figure 4.3

The y-axes show CSF/plasma and brain/plasma concentration ratios (%) for ^{14}C-L-glucose (A and C) and ^{3}H-glycerol (B and D) measured in short time course experiments after a single ip injection in P18 (■) and P38 (○) opossums. The x-axes show the time after injection at which samples were collected. Linear regression lines have been fitted to the data points. The slopes of the regression lines (the rate of uptake) between P18 and P38 animals were compared using a student's t-test. The rate of uptake of ^{14}C-L-glucose into CSF in P18 animals was significantly faster than in P38 animals (P=0.01). The rate of uptake of ^{14}C-L-glucose into brain at P18 appeared faster than at P38, but the difference was not statistically significant (P=0.07). The rate of uptake of 3H-glycerol into CSF and brain appeared similar both at P18 and P38 (P=0.33 and P=0.97,respectively).

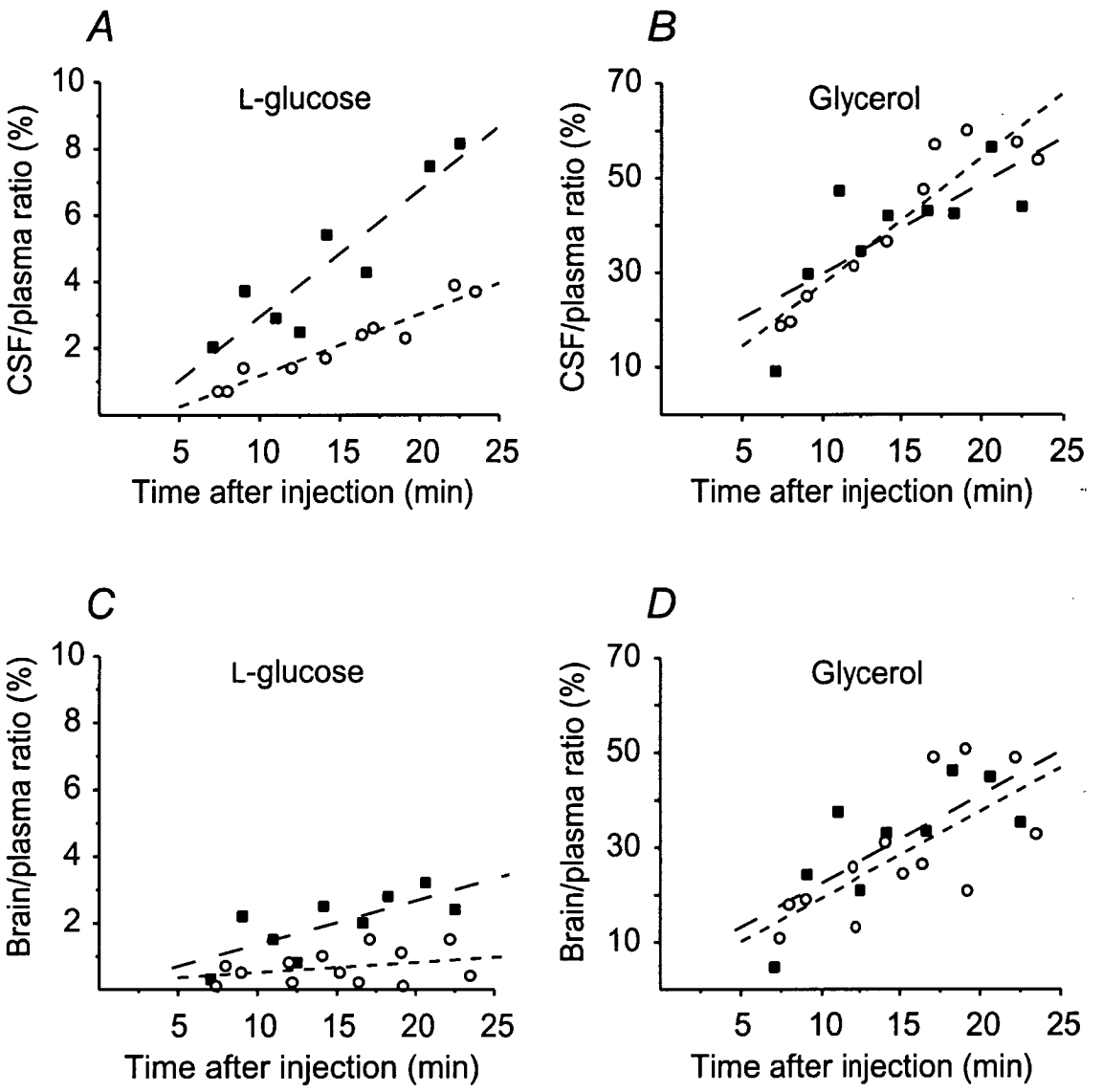
A
L-glucose
CSF/plasma ratio (%)
10
8
6
4
2
5
10
15
20
25
Time after injection (min)
B
Glycerol
CSF/plasma ratio (%)
70
50
30
10
5
10
15
20
25
Time after injection (min)
C
L-glucose
Brain/plasma ratio (%)
10
8
6
4
2
5
10
15
20
25
Time after injection (min)
D
Glycerol
Brain/plasma ratio (%)
70
50
30
10
5
10
15
20
25
Time after injection (min)

Discussion

Previous studies in rats and sheep have shown that the penetration of lipid insoluble molecules into brain and CSF is higher in early development and decreases with age (Ferguson and Woodbury, 1969; Dziegielewska et al., 1979; Habgood et al., 1993). The present study confirms earlier results, and shows that sucrose and inulin CSF/plasma ratios fell approximately tenfold from P6 to P65, and brain/plasma ratios about fivefold over the same time span. Ferguson and Woodbury (1969) reported much higher steady-state ratios in rat embryos than those presented in this study (CSF/plasma ratio for sucrose and inulin was 88% and 76% at E17, compared with 59% and 29% at P6 in this study). In similar experiments during postnatal development in the rat by Habgood et al. (1993), much lower ratios were reported. In both these studies neonates or pregnant females were nephrectomised and given an ip injection of markers in order to achieve a stable plasma concentration. Ferguson and Woodbury (1969) found that CSF/plasma and brain/plasma ratios did not reach a plateau until 16-24 hours after the injection or in some cases the ratios were still increasing at 24 hours. Steady-state was defined by little change in the ratio and no effort was made to investigate whether the plasma or CSF concentrations were stable throughout the whole 24 hours. Habgood et al. (1993) showed in neonatal rats that a plateau in plasma concentration was obtained after 2-3 hours, thereafter the plasma level gradually declined. This gradual decrease in plasma concentration probably explains the high steady-state ratios and also the long time until steady-state was achieved in the study by Ferguson and Woodbury (1969). The steady-state experiments for sucrose and inulin showed a large decrease in steady-state ratios during development (see Figure 4.2). This has been shown before in other species (Ferguson and Woodbury, 1969; Dziegielewska et al., 1979; Habgood et al., 1993) but the explanation for this is still debatable. As has been discussed before in Chapter 3, the

most likely explanations are:

a) a decrease in the permeability of exchange surface areas

b) an increase in CSF turnover rate

c) a decrease in area of exchange surfaces

d) a decrease in blood flow to exchange surfaces

These are discussed separately below.

Decrease in permeability of the brain barriers

One possible explanation for falling ratios with age could be a reduced rate of entry across the brain barriers during development. One of the distinct structural features of the mature brain barriers is the presence of complex tight-junctions in endothelia of the brain blood vessels and epithelia of the choroid plexus (Brightman and Reese, 1969). To what degree there are changes in the structure of the tight-junctions during development is still debatable (for more detailed discussion see Chapter 1). Reports showing complex tight-junctions from the first blood vessels that invade the brain (Møllgård and Saunders, 1975; Bauer et al., 1993) have been published as well as papers showing a more gradual change in the structure of the junctions (Stewart and Hayakawa, 1987). Nevertheless, as has been discussed before, there is a clear reduction in the penetration of lipid insoluble compounds after birth in the rat (Ferguson and Woodbury, 1969; Habgood et al., 1993) when the endothelial tight-junctions already show a mature form (Kniesel et al., 1996). This suggests that the development of tight-junctions is not the determinant of the changes in penetration of markers with age. Other explanations for the decline in permeability with age have been proposed to be due to a decrease in transcellular transport in vesicles (Xu and Ling, 1994) or different tubulo-canicular

structures (Lossinsky et al., 1986; Balslev et al., 1997a). Several authors have proposed that the penetration of lipid insoluble molecules into CSF is by unrestricted diffusion (Felgenhauer, 1974; Dziegielewska et al., 1979; Habgood et al., 1993). This means that larger molecules are not more restricted than smaller ones; instead it is the diffusion capacity of the molecule which is the deciding factor. A smaller molecule will penetrate faster because of its higher diffusion capacity. Habgood et al. (1993) found a parallel decrease in CSF/plasma ratios with age for inulin and sucrose and an absence of any increase in the slope of curves between diffusion coefficient (D_{37}) and steady-state CSF/plasma ratios. It was therefore suggested that there is change in 'pore' numbers rather than 'pore' size during development (Habgood et al., 1993). These 'pores' are morphologically uncharacterised structures that form an aqueous pathway between blood and CSF for water soluble molecules. In contrast, lipid soluble solutes will cross the blood-CSF interface rapidly in a non-selective way and newly formed CSF will therefore have the same concentration as in the plasma.

Increase in CSF turnover

A decrease in CSF/plasma steady-state levels of markers could also be a reflection of an increase in CSF sink, which is the process whereby CSF solutes are diluted by the continuous production of CSF (Davson and Segal, 1969). CSF is produced mainly by the choroid plexus, which is situated in the roof of each ventricle (Johanson, 1988). The detailed process of CSF production will not be discussed here but it involves Na^+ and HCO_3^- being actively transported by the epithelial cells from blood to CSF (Speake et al., 2001). This creates an osmotic force for water molecules to rapidly pass from plasma to CSF, whereby CSF is approximately isoosmolal to plasma (Johanson, 1995). The CSF production generates a flow through the ventricles, spinal canal and subarachnoid space, which results in drainage of CSF through the arachnoid villi in the arachnoids (see Figure 1.1). The arachnoid villi are believed to work like pressure

valves whereby ventricular pressure is not augmented even if CSF production increases (Johanson, 1995). The fluid is formed across a selective choroidal epithelial layer and drained out of the system by bulk flow across the non-selective arachnoid villi (Johanson, 1989). The newly formed fluid will dilute any substance in the CSF and the effect is often referred to as the CSF sink (Saunders and Dziegielewska, 1997).

Reproducible measurements of the CSF production rate have proven difficult. Most methods are quite invasive and have given different estimates of CSF production (Cserr, 1965; Dudzinski and Cutler, 1974; Nakamura and Hochwald, 1983). The most accurate estimations involve determining CSF production by dilution rate of a substance from the CSF. The marker substance needs to be as inert as possible without escaping from the CSF, therefore molecules such as inulin and larger dextrans have been used (Rothman et al., 1961; Johanson and Woodbury, 1974). The production rate is measured in µl/minutes, however, when comparing different animal species it is more useful to express it as the rate of newly formed fluid to the whole volume of CSF. This is called the CSF turnover and in adult humans has been estimated to be around 0.25 % per minute (Johanson, 1995).

Even more of a technical challenge is to estimate the CSF production during development due to the small size of the brain. This might be the reason why it has only been attempted in neonatal rats and fetal sheep with discrepancies between the reported results (Bass and Lundborg, 1973; Evans et al., 1974; Johanson and Woodbury, 1974; Fossan et al., 1985). There are, however, similar trends in the results of those papers: The CSF volume production clearly does increase during development in both species. When this is related to CSF volume and expressed as CSF turnover, there is no significant increase during development in sheep (Evans et al., 1974). Studies in neonatal rats by Bass and Lundborg (1973) and Johanson and Woodbury (1974)

reported an increase in the CSF turnover with age, however, the exact numerical value was quite different between the two studies. An increase in the CSF turnover should also reduce the time for substances to reach a steady level in the CSF. Habgood et al. (1993) noticed no change in the time to reach steady-state in rats between P2 and P20, when there was a marked decrease in steady-state ratios for both inulin and sucrose.

In the adult, brain/plasma ratios will also be affected by an increase in CSF sink since there is a free exchange of solutes between the extra cellular fluid (ECF) and CSF, however, the situation is more complicated than in the CSF. The brain ECF volume has been estimated to be 15-20% of the adult brain, which makes the ECF volume approximately the same or slightly larger than the CSF volume (Johanson, 1993). Considering this, it is more likely that brain composition influences CSF more than the other way round in the adult. Therefore the CSF turnover is only effective in removing solutes from the brain when they enter the brain via the blood-brain barrier at a slow rate. The effect has been demonstrated by experiments where the CSF production has been reduced showing increased steady-state levels in brain (Davson and Segal, 1969). The relative importance of CSF turnover on CSF and ECF has been shown using dilution rates of protein from CSF and ECF. The clearance rate from CSF is faster than from ECF (Johanson, 1993). This might show a physiological role of the CSF turnover whereby it constitutes a way for polar substances produced in the brain to be transported out from the CNS (Johanson, 1993). The relative importance between CSF and ECF may be quite different in the developing compared to the adult brain. In younger animals the choroid plexus and CSF volume are proportionally larger to the size of the brain (Johanson, 1995). Interestingly, when the CSF turnover is related to brain size there is a clear reduction in the CSF 'sink' effect on the brain with age (Saunders, 1992). If the turnover rate of CSF compared to brain size is lower in older animals this should, in contrast to the results of this study, increase the brain ratios during development. It therefore seem unlikely that an increase in the CSF sink is responsible

for the age related decline in steady-state ratios.

Decrease in exchange surfaces and blood flow

As mentioned before it has been suggested that the greater penetration of lipid insoluble compounds during development could be a result of a larger number of 'pores' available for penetration across the blood-CNS interface. This could be brought about by an increased surface area for exchange such as an augmented capillary bed. Morphological studies of brain capillaries have shown that capillary density increases during development (Caley and Maxwell, 1970; Dambska, 1995). These studies suggest that it is unlikely that an increase in exchange surface area could explain higher steady-state ratios of lipid insoluble molecules in the developing CNS. One of the factors influencing uptake rate is blood flow. The entry of a substance, which has high permeability across the brain barriers, is mostly restricted by the delivery (blood flow) to the exchange surfaces. However, sucrose and inulin, being lipid insoluble molecules (see Table 2.2), enter the CSF and brain at a slow rate and will therefore be affected very little by changes in the blood flow.

Nature of the decrease in steady-state ratios

The short-term uptake experiments were undertaken in order to more precisely examine the factors that could explain changes in steady-state ratios for markers with age. As mentioned before, the factors affecting steady-state ratios of small lipid insoluble molecules are permeability, CSF turnover rate, blood flow, and vascular surface area. The influence of CSF turnover was considered negligible in short-term experiments since the uptake rate was measured during a short time space in which the CSF production must have been very small. It was necessary to use a marker (L-glucose) that behaves passively and which is small enough to penetrate into the brain and CSF to a

measurable extent during the short time of the experiments. In addition to L-glucose, the uptake was measured of the moderately lipid soluble molecule glycerol (see Table 2.2). The radioactive labelling of glycerol in plasma and CSF was checked in samples 30 min after injection (see Table 2.3). This showed that 71% in blood and 80% in CSF of labelling was still on glycerol. Almost all the rest was on more water soluble compounds. Any label on water would have been rapidly and widely distributed throughout the whole body water and would therefore influence the CSF/plasma and brain/plasma ratios very little. That the proportion of radioactive label still on glycerol was higher in CSF than blood indicates that there was little label on compounds that penetrate from blood to brain at a higher rate than glycerol. Because glycerol is relatively lipid soluble, it could be expected to readily penetrate the cell membranes of endothelial and epithelial cells. The uptake rate should therefore not be affected by any possible tightening of the brain barriers such as a change in tight-junctional structure. It could, however, be expected to be influenced by a change in blood flow or exchange surface area. The initial uptake rate into brain and CSF for glycerol did not change significantly between P18 and P38. This indicates that there is little change in either blood flow or surface area for exchange between P18 and P38. In contrast to glycerol, the uptake rate for L-glucose decreased both into the CSF and brain. It can therefore be concluded that there is a significant decrease in the permeability of the brain barriers to L-glucose with age. This can to a large extent, if not all, explain the decrease in steady-state ratios between P18 and P38 for L-glucose and probably also the striking decline in ratios for inulin and sucrose with age (see Figure 4.2).

Chapter 5

*

Morphological and Tracer Studies

Introduction

There has been a lack of low molecular weight tracers available that can be visualised both for light and electron microscopy. Markers that have been previously used such as HRP, ferritin, and cytochrome *c* are large proteins that are difficult to quantitate in low concentrations. The only small molecular sized tracer that has been used in the past is lanthanum, however, it is probably not suitable for *in vivo* experiments because of its toxicity (Milhorat et al., 1975). Molecules such as inulin and sucrose, which are easy to quantitate because they can be radiolabelled, are water soluble, and will therefore be washed out of the material when tissue is processed. The only way to localise these molecules would be to quick-freeze the material and visualise them using autoradiography. However, this technique does not give high enough resolution to determine the intracellular distribution. In order to prevent washing out of molecules from the tissue, tracers need to be immobilised. This is achieved by fixation in which proteins and lipids crosslink, thereby preserving cell structure. Suitable tracing molecules need to be able to react with the fixation agents (eg. aldehydes) and be immediately attached to their surroundings. For the present study an inert tracer was needed that could be expected to cross the brain barriers in a manner similar to inulin and sucrose and be of comparable size. Biotin-dextrans have been extensively used for axonal tracing (for review see Köbbert et al., 2000) but their properties also make them appropriate low molecular weight tracers across the brain barriers. Dextrans are hydrophilic polysaccharides and have favourable characteristics for usage as an external tracer such as high water-solubility, they are inert *in vivo* and can be manufactured in a variety of different molecular weights. Their unusual α-1,6-polyglucose linkages are resilient to cleavage by most enzymes and they will therefore remain structurally intact for a long time. Lysine residues can be incorporated into the dextran and this makes it aldehyde fixable, a characteristic that was essential for the present study. Moreover, biotin can be conjugated to dextrans and this will make the molecule visible using avidin reactions. Therefore, a 3000 molecular weight, lysine fixable, biotin-dextran

(BDA-3000, Molecular Probes) was chosen as a small, lipid insoluble tracer. However, the molecular weight of the dextran is not uniform, and each sample of BDA-3000 contains a range of different sized biotin-dextrans with an average molecular weight close to 3000 (technical information provided in the Molecular Probes handbook for product number D-7135).

Experiments described in this Chapter were undertaken in order to visualise the route for small lipid insoluble molecules across the brain barriers, using BDA-3000, in the course of development. It was first necessary to establish whether BDA-3000 was crossing the brain barriers in a similar way to other small lipid insoluble molecules of comparable sizes. This was achieved by comparing BDA-3000 uptake into CSF with that of sucrose, inulin and L-glucose. BDA-3000 seemed to behave in a similar passive manner to these compounds (see Figure 5.9) and it was therefore further used in tracer experiments where it was visualised both at the light and electron microscopic levels. Preliminary experiments suggested that BDA-3000 was transferred across the blood-CSF barrier (choroid plexus) and then into brain tissue and did not seem to escape out of blood vessels inside the brain. In order to compare morphological aspects of the choroid plexus with the transfer of radioactive markers and BDA-3000, the structure of the choroid plexus was examined during development using both the light and electron microscope. As has been described in Chapter 1 the choroid plexus is the site for blood-CSF barrier mechanisms (see Figure 1.1). The structural basis of this barrier is believed to be tight-junctions present between adjacent epithelial cells that have been shown to stop the paracellular movement of tracers from blood into the CSF in adult animals (Becker et al., 1967; Brightman, 1968; Milhorat et al., 1973; van Deurs, 1978). Several studies have proposed that structural changes of tight-junctions are responsible for the decrease in brain barrier permeability during development (Stewart and Hayakawa, 1987; Kniesel et al., 1996), however, there are also studies showing that tight-junctions with mature appearance are present both at the blood-brain and the blood-CSF barrier

early in development (Tennyson and Appas, 1968; Møllgård and Saunders, 1975; Møllgård et al., 1979; Bauer et al., 1993; Xu and Ling, 1994). Other studies have suggested that the permeability change is caused by a decrease of transfer in vesicular structures or other subcellular organelles (Møllgård and Saunders, 1977; Lossinsky et al., 1986; Xu and Ling, 1994). These studies have been reviewed in detail in Chapter 1 and possible explanations for the somewhat contradictory results of these investigations have also been given. The electron microscopic study in this thesis focused on investigating the presence and appearance of tight-junctions, vesicles and other subcellular structures that have been proposed to be of importance for the transfer of molecules from the blood into CSF in the choroid plexus. The more general ultrastructural development of the choroid plexus was also examined in order to assess the opossum as a model to study the mammalian choroid plexus. This was important to assess since the opossum has been reported to show a difference in choroid plexus development from other mammals in that it does not seem to have a stage when the choroid plexus epithelial cells store large amounts of glycogen (Dziegielewska et al., 2001).

Methods

Validation of BDA-3000 as a tracer for small lipid insoluble molecules

To confirm that BDA-3000 is a suitable marker for small lipid insoluble molecules, CSF/plasma ratios were measured for a structurally similar lysine fixable 3000 molecular weight rhodamine dextran (D-3308, Molecular Probes). D-3308 was used instead of BDA-3000 since it is fluorescent and can therefore be measured quantitatively. A group of opossums pups aged P16 (n=9) were injected ip with D-3308 (0.7 mg g^{-1} body weight in sterile 0.9% NaCl solution) and samples of plasma and CSF were collected after three hours. For more detailed description of methods such as the

collection of CSF and plasma see Chapter 2. The amount of fluorescence in each sample was measured with an Olympus BX50 fluorescence microscope attached with a PM30 photomicrograph unit. Samples of plasma and CSF were transferred to 5 µl glass capillaries and mounted on glass slides. At ×10 magnification the exposure time (ET) was recorded for the centre of the glass capillary. CSF/plasma ratios were calculated as ET_{plasma}/ET_{CSF} (the ET is inversely related to the concentration in the sample, see Figure 5.1). The accuracy of measuring ratios this way was confirmed by comparison with ratios obtained using absorbance spectrophotometry. The absorbance of serial dilutions of D-3308 in saline was determined by a spectrophotometer at 518 nm and ET was recorded for the same solutions. Ratios calculated using absorbance spectrophotometry between the different solutions were almost identical to ratios calculated from the ET readings (Table 5.1). The influence of media on ET readings was also examined; similar concentrations of D-3308 in saline, CSF or plasma all gave similar ET readings. That this was a reliable method for determining concentrations in samples was further confirmed by serial dilutions of D-3308 in saline; this showed a linear relationship (R=0.996) between ET^{-1} and the concentration of D-3308 (Figure 5.1). The major advantage of measuring ratios with a fluorescence microscope is that very small sample volumes can be measured (1-2 µl) undiluted in a glass capillary. This was critical in young pups where only small volumes of CSF could be obtained (<10 µl); this would have been undetectable using conventional absorbance spectrophotometry.

Table 5.1

Measurements of solutions			Concentration ratios		
Solution	Absorbance at 518 nm	Exposure time (sec)	Ratios	Absorbance Spectrophotometry	Exposure time
A	0.304	4.85	B:A	0.296	0.317
B	0.090	15.3	C:A	0.082	0.089
C	0.025	54.7	C:B	0.278	0.280

On the left are measurements of absorbance and ET on three dilutions of D-3308. On the right are concentration ratios calculated between these solutions. Note that the ET for a sample is inversely related to its concentration and the concentration ratio between sample B and A is calculated by dividing the ET of sample A by B. Both methods gave similar ratios, which shows that exposure time readings is an accurate way of determining the concentration of D-3308 in a sample.

In order to check that the brain uptake of D-3308 and BDA-3000 were similar, their distribution in brain sections was compared. A P7 opossum was injected simultaneously with both D-3308 and BDA-3000 at the same dose (0.7 mg g^{-1} body weight) into the intraperitoneal cavity, and the brain fixed in Bouin's fixative after 30 min. D-3308 was detected directly using filters for rhodamine and BDA-3000 was visualised with the diaminobenzidine tetrahydrochloride (DAB) reaction (see below and Appendix A and B for more detailed description of histochemical methods and reagents used).

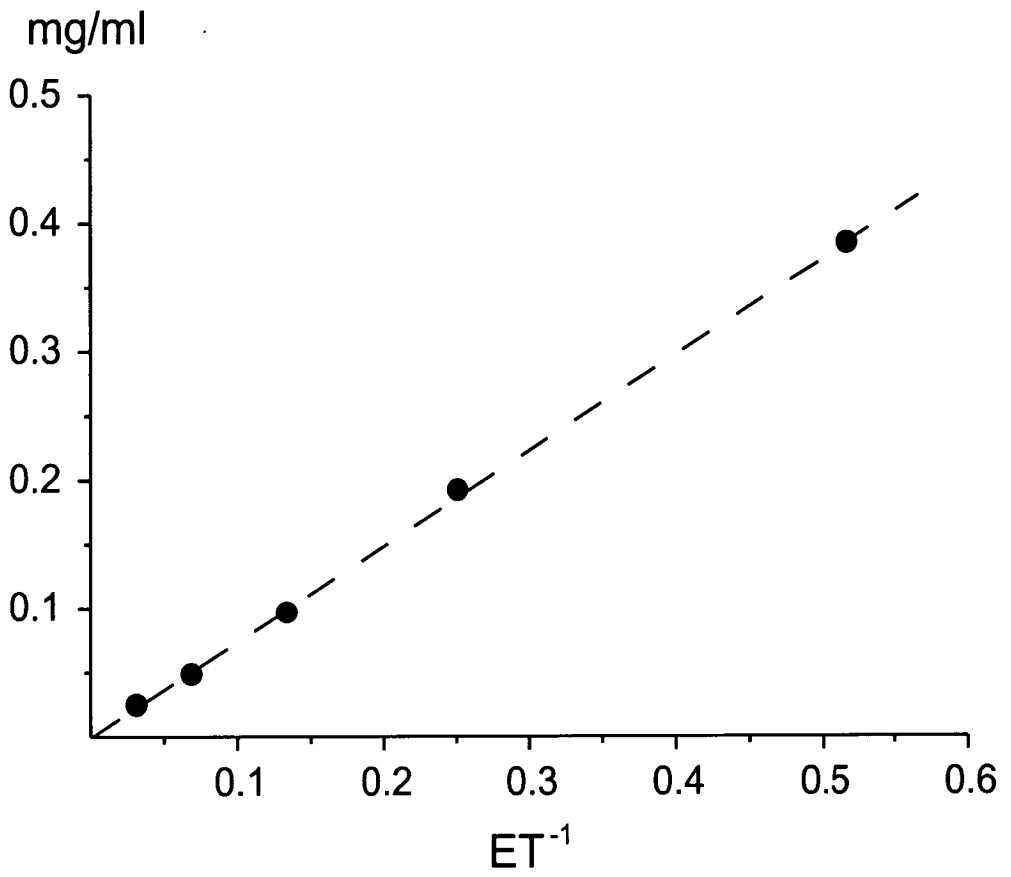

Figure 5.1

Standard curve for D-3308. The x-axis is the concentration (mg/ml) of D-3308 and the y-axis is ET^{-1} (note that the ET reading is inversely related to the concentration). A linear regression line was fitted to the data with a R-value of 0.996.

Light Microscopy

Tissue preparation

Litters of opossum pups at P0 (n=4), P5 (n=2), P8-P9 (n=6), P13 (n=2), and P30 (n=2) were detached from the mother and then injected ip with the BDA-3000 (0.7 mg g^{-1} body weight in a sterile 0.9% NaCl solution). Five to 90 minutes after the injection,

animals were killed with an overdose of inhaled halothane (Zeneca) and brains immediately fixed. For technical reasons it was not possible to fix all brains in the same manner. For animals aged between P0 and P13 brains were dissected out and submerged in Bouin's fixative. Animals at P30 were first perfuse-fixed with paraformaldehyde and then the brains were dissected out and submerged in Bouin's fixative. Paraformaldehyde was made up freshly as a 4 % solution in 0.15M phosphate buffered saline (PBS; pH 7.4) and kept at 4°C until just prior to perfusion. The right atrium was cut open and the fixative was delivered through propylene tubing into the left heart ventricle by a motor driven syringe pump. The delivery rate was set at half the animal's predicted total blood volume per minute and perfusion stopped after 10 minutes. The total blood volume was estimated as 10% of the weight of the animal. In order to clear blood from the vasculature, a PBS solution containing heparin (10 units/ml) was perfused for the first minute before switching to the fixative. After 24 hours in Bouin's fixative, brains were dehydrated in serial solutions of ethanol (70% to 100%) and cleared in chloroform. After embedding in paraffin wax, serial sagittal or coronal sections of brain tissue (5 μm) were cut and transferred to glass slides.

Detection of BDA-3000 in paraffin sections

Sections were dewaxed in xylene and rehydrated in serial ethanol solutions (100% to 70%). This was followed by incubation in peroxidase blocker (Dako) followed by protein blocker (Dako) for 30 min each at room temperature. An avidin-horseradish peroxidase complex was used to detect biotin using a Vectastain Elite ABC kit (Vector). Sections were then processed with the diaminobenzidine tetrahydrochloride (DAB Kit, Dako) reaction for about 5-10 min. After a 10 min rinse in tap water the sections were dehydrated in serial ethanol solutions (70% to 100%), cleared in xylene and mounted in DPX and left to dry overnight in a low heat oven (40°C). Control staining was performed on sections obtained from animals not given a BDA-3000 injection. For

detailed protocol see Appendix A and B.

Transmission electron microscopy

General morphology of choroid plexus

Choroid plexus tissue from opossums at P0-P1 (n=4), P13 (n=4) and P64 (n=2) was prepared for conventional electron microscopy in order to investigate its ultrastructure during development. Fresh 2.5 % glutaraldehyde solution in 0.1M sodium-cacodylate (Sigma) buffer adjusted to pH 7.3 was used as the primary fixative. Animals were killed by an overdose of halothane and the whole brain was carefully removed and submerged in fixative in a new dish for further dissection. Care was taken not to expose tissue to air. Holes through the cortex into the lateral ventricles were immediately cut in order to fix the choroid plexus as quickly as possible. The choroid plexuses in the 4th and lateral ventricles were removed with a small piece of brain tissue connected to it in order to facilitate the orientation and handling of the tissue. Larger pieces of the choroid plexus were sometimes cut into several smaller fragments so they would be of an appropriate size. Tissue was post-fixed in the same fixative for 2-3 hours at 4°C. Tissue was rinsed in cacodylate buffer for 30 min and postfixed in a 1:1 mixture of 4% osmium tetroxide solution and 0.05 M potassium ferrocyanide in cacodylate buffer for 45 minutes. After rinsing in cacodylate buffer for 30 minutes, tissue was stained *en bloc* in an aqueous 1% uranyl acetate solution for 30 minutes. Tissue was then dehydrated in serial ethanol solutions (50 to 100%), cleared in propylene oxide and embedded in Epon 812. Detailed procedure of protocol can be found in Appendix C.

BDA-3000 localisation in choroid plexus

Opossum pups at P1 (n=3) and P13 (n=3) were injected ip with BDA-3000 (0.7 mg/g body weight) and choroid plexus tissue was fixed 30-40 minutes after the injection for electron microscopy. A 2.5 % glutaraldehyde solution in phosphate buffered saline (0.1

M) adjusted to pH 7.3 was made up freshly and used as the primary fixative. Animals were killed by an overdose of halothane and choroid plexus tissue was dissected out in the same manner as described above. The tissue was post-fixed in the same fixative for 2-3 hours at 4°C. The tissue was washed in buffer for 30 min and permeabilised in a 50% Ethanol PBS solution for 30 min. After rinsing in buffer for 30 min, the tissue was incubated in an avidin-horseradish peroxidase complex (Vectastain Elite ABC kit, Vector) for 60 min. The tissue was washed in buffer and processed with the DAB reaction (DAB kit, Dako) for 2-3 min. The reaction time was kept as short as possible to minimise precipitation. Tissue was rinsed in PBS and postfixed in a 1:1 mixture of 4% osmium tetroxide solution and 0.05 M potassium ferrocyanide in PBS buffer for 45 minutes. After rinsing in PBS for 30 minutes, the tissue was stained *en bloc* in a 1% uranyl acetate solution for 30 minutes. The tissue was then dehydrated in serial ethanol solutions (50 to 100%), cleared in propylene oxide and embedded in Epon 812. Control tissue was obtained from animals not given an injection but otherwise treated in the same way. Detailed procedure of protocol can be found in Appendix D.

Sectioning

Semi-thin sections (0.5-1 μm) were cut and stained with toluidine blue and examined under the light microscope. Ultrathin sections were cut with an Ultratome LKB Nova and transferred to 200, 300 mesh grids, or butvar coated single slot grids. The interference colour of the thin-sections ranged from silver to pale gold. Thin-sections for general morphology were contrasted in 4-5% aqueous solution of uranyl acetate (30 min) followed by lead citrate (5-10 min), whereas thin-sections that were stained for BDA-3000 were not contrasted. Sections were examined with a CM100 Phillips electron microscope at 60 or 80 KV.

Results

Structural development of the choroid plexus

For the interpretation of BDA-3000 distribution, the morphological study of the choroid plexus is presented first. The light and electron microscope were used to study the structure of the lateral and 4th ventricular choroid plexuses at P1 and P13, and in young adults at P64. The main aim of the investigation was to study structures that may be relevant for the permeability of the blood-CSF barrier that is situated in the choroid plexus. Structures such as junctional complexes between cells that are believed to be determinants of the paracellular movement of molecules, and vesicles that may be significant for trancytosis of exogenous material were therefore studied in detail.

A general description of the choroid plexus structure in the opossum will be presented first. The choroid plexus can be divided into the stroma, which is the core of the choroid plexus and the epithelial cells that form a single layer of cells outside the stroma. The electron microscopic study showed that the stroma contained blood vessels that were fenestrated and that outside of these, between the blood vessels and the epithelial cells, connective tissue and few interspersed fibroblast cells were present. The fenestrations had a width of about 50 nm which is similar to what has been reported in other species (Brightman and Kaya, 2000). The fibroblast cells formed finger-like projections within the extracellular matrix. The epithelial cells, which rested on a basement membrane, had a centrally located nucleus and a brush border at the ventricular surface with microvilli and also with occasional tufts of cilia. The microvilli had the appearance of club-like or clavate projections, and the cilia had 9 peripheral doublets and 2 centrally located microtubules (Figure 5.5), which is consistent with what has been described in other mammals (Dohrmann and Bucy, 1970; Dohrmann and Herdson, 1970; Davis et al., 1973). Resting on the microvilli were occasional cells resembling the so-called epiplexus cells (also referred to as Kolmer cells) that have been reported in other

species (Sturrock, 1979; Zaki, 1981; Peters et al., 1991; Lu et al., 1993 and others). These cells had abundant projections, mostly in close contact with the microvilli and numerous vacuoles. The cytoplasm of the epithelial cells contained mitochondria, vesicles, rough and smooth endoplasmic reticulum, Golgi apparatus and a few dense bodies, which presumably contained lipids that stained dark because of osmium. A minority of the epithelial cells appeared to have darker cytoplasm, however, the shape and organelle organisation of these darker cells appeared similar compared to other cells. Similar "dark and light cells" have been reported in other mammalian species (see Discussion for references)

The choroid plexuses appear in the ventricles in the following order: 4th ventricular choroid plexus appears first, followed by that in the lateral ventricles; both these choroid plexuses are present at birth in the opossum, although the lateral ventricular plexuses are only rudimentary. The 3rd ventricular choroid plexus appears around P3-P4. In all the ventricles, the epithelial cells of the choroid plexuses show a similar morphological development that can be divided into three stages. The choroid plexus cells first have an elongated shape forming a pseudostratified layer. In the second stage they have a columnar form and in the third stage a more cuboidal shape. Under the light microscope the epithelial cells of the 4th and lateral ventricular choroid plexus appeared to be in different stages of development even in the same animal (see Figure 5.2). This was confirmed in the electron microscope which showed that a majority of the epithelial cells in the lateral ventricle had a pseudostratified appearance whereas the epithelial cells in the outer most parts of the choroid plexus villi had a columnar shape at birth (see Figure 5.4). In the 4th ventricle most of the epithelial cells had a columnar shape except for those closer to the root of the choroid plexus. However, the cell organelle structures were similar in all cells with few interspersed organelles throughout the cytoplasma and many nuclear invaginations. Figure 5.4 shows the comparison of a pseudostratified epithelium from the root of the 4th ventricular choroid plexus with a

columnar-shaped epithelia from the outer parts of the same choroid plexus. At P13 the epithelial cell at the root of the choroid plexuses in both ventricles still had a somewhat pseudostratified appearance. At P13 and P64, the epithelia appeared very similar in both the lateral and 4th ventricular choroid plexus (see Figure 5.4).

There were several ultrastructural changes of the choroid plexus during development. In the stroma, the endothelial wall consisted of wider segments with numerous vesicles and other cell organelles, and thinner sections with fenestrations. In animals at P0, normally only a small part of the endothelial wall contained thin segments exhibiting fenestrations whereas at P64 most of the endothelial wall was thin with a more uniform diameter exhibiting numerous fenestrations (see Figure 5.6). The individual fenestrations had a similar length (around 50 nm) and thickness in all animals (see Figure 5.6). In the endothelial wall many vesicles were present at all ages. At the luminal side of the intercellular cleft of the endothelial cells, *zonulae occludentes*-like junctions were present at all ages studied. Outside the blood vessels, the extracellular matrix became richer in connective tissue with age. As has been described above, the epithelial cells in the choroid plexus change in shape during development. As seen in Figure 5.3 the epithelial cells at P0 formed a pseudostratified layer with elongated epithelial cells, sometimes with bulbous structures. The pseudostratified epithelium at P0 formed a very uneven surface at the ventricular side, which changed into a layer with more uniform columnar cells with convex ventricular surface at P13, and changed further into a layer of almost cuboidal cells with flat or somewhat curved apical cell surface at P64. A prominent characteristic of the epithelial cells at P0 was the deep invaginations of the nuclei. In some sections this gave the appearance that the nuclei consisted of several lobes. At P13 the nuclei still had numerous invaginations, although each individual invagination was smaller than at P0, and at P64 the nuclei appeared spherical with only occasional invaginations. At P0 most epithelial cells had thin microvilli that formed short projections into the ventricle and a minority of cells lacked

microvilli and had a smooth ventricular cell surface. The microvilli progressively formed longer and more uniform projections between P13 and P64 so that the microvilli had a length of 2-3 μm at P64 (see Figure 5.5). Interspersed tufts of cilia were common at the epithelial surface at all ages. It was difficult to conclude whether the number of cilia changed during development in thin-sections since it is not easy to know from which epithelial cell individual cilia originated. It would require a very large amount of serial sectioning in order to estimate the true number of cilia. It is also difficult to judge whether the length of cilia changed with age, however, the cilia exhibited the normal 9+2 microtubular arrangement at all ages (see Figure 5.5). During development, the cytoplasma became more packed with different cell organelles, which also became more polarised mainly to the apical side. The most noticeable change was the increase in mitochondrial content of the cytoplasm; this increase was less prominent between birth and P13 than between P13 and P64. The mitochondria were distributed throughout the cell but were more common in the apical part (see Figures 5.3-5.5). Not only did the number of mitochondria increase with age but also the size of individual mitochondria became bigger (see Figure 5.5). The shape of the mitochondria changed from small, with a round or oval shape at P0, to large with an elongated or crescent shape in the young adults (P64). As cells became more polarised there was also an increase in other organelles such as rough endoplasmic reticulum, which tended to be mostly numerous towards the apical side of the cells. Small and large vesicles were present in the epithelial cells at all ages. The larger vesicles were especially abundant in the region towards the apical and intercellular surfaces. No apparent difference in the number of vesicles was found between the three ages. Large clear vacuole like structures (up to 2 μm) could be found in a minority the epithelial cells at P0 (see Figure 5.4). These structures were large enough to be visible under the light microscope in semi-thin sections. In the electron microscope it was revealed that a single membrane encapsulated the structures and it can therefore be assumed that they are intracellular structures. These structures were more abundant in the epithelial cells in the 4th

ventricle compared with those of the lateral ventricle. Similar structures could be found at P13, however, they were less frequent and with a smaller diameter. The large size of these vacuoles is probably an artefact.

In all sections studied, a junctional complex was always present towards the apical side between epithelial cells. Within the junctional complex, the cell membranes of neighbouring cells were in close contact with each other at certain points. Using the goniometric tilting device (up to 20° tilting) it appeared that these contact points were similar to tight-junctions described in the choroidal epithelium of other species (Tennyson and Appas, 1968). The tilting device helps to orientate the membranes in parallel to the electron beam resulting in a sharper view of the apposing membranes. The interepithelial cleft was often convoluted and it was therefore not always possible to view the junctional complex along its whole length in one section (see Figure 5.7). In sections where the cell membranes were visible below the apical surface it was found that several tight-junctions were present within the junctional complex. There was no noticeable difference in the appearance of the tight-junctions or the number of tight-junctions within the junctional complex between the three ages studied. Below the junctional complex, cisternal structures could often be seen that were in close contact with the cell membranes in adjacent cells. These cisterns were positioned in parallel to the cell membranes. At P0 several cisterns often formed a row below the apical junctional complex whereas only single cisterns were found interspersed along the cell membranes at older ages (see Figure 5.8).

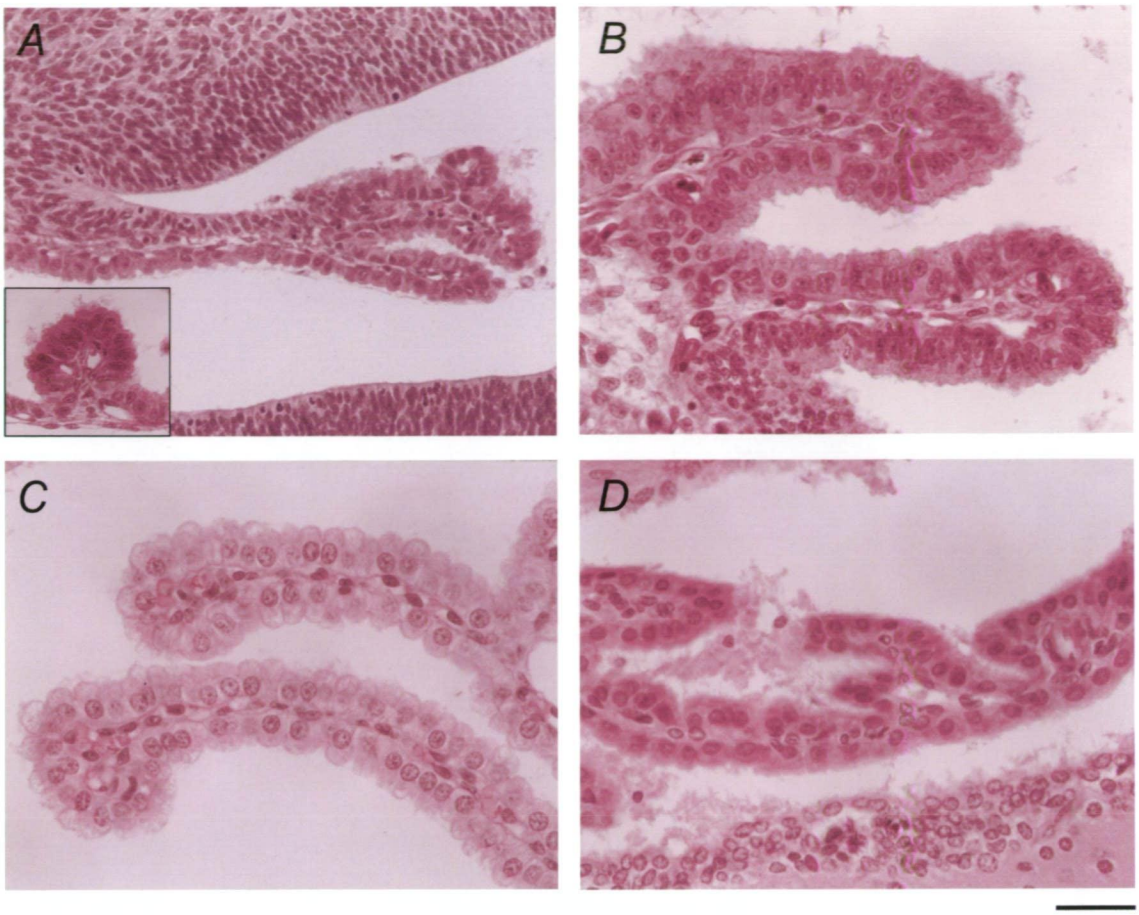

Figure 5.2

H&E stained paraffin sections of the fourth ventricular choroid plexus at P0 (A), and lateral ventricular choroid plexus at P0 (B), P13 (C) and P65 (D) in the opossum. Note the difference in the morphology of the epithelial layer in the lateral and fourth choroid plexus at birth (A and B). Most of the epithelium in the lateral ventricles forms a pseudostratified epithelium at birth whereas most of the epithelial cells in the fourth ventricle have a columnar form except for those close to the root of the choroid plexus (insert in A). At P13 the epithelial cells are simple columnar and at P65 the epithelial cells have a more cuboidal shape which is characteristic of the mature choroid plexus.

Scale bar is 50 μm in A, and 30 μm in B-C and insert in A.

Figure 5.3

Electron micrographs of the epithelial layer in the lateral ventricular choroid plexus at P0 (A), P13 (B) and P64 (C). The epithelial cells change in shape during development from being elongated (cell height 15-20 µm) at birth to short (cell height 8-12 µm) and wide in the mature choroid plexus. The epithelial cells at P1 formed great protrusions into the ventricles whereas the apical surface of the cells was round at P13 and more or less flat at P64. Note that at birth and at P13 there were few organelles in the cytoplasm. In contrast, the cytoplasm at P64 was very rich in organelles, especially abundant were mitochondria, which were concentrated towards the apical side of the cells. The nucleus shape also changed from being very lobulated at P0 (arrowheads in A), to having small invaginations at P13 (arrowhead in B) and changed further to almost spherical at P64.

Scale bar is 5 µm.

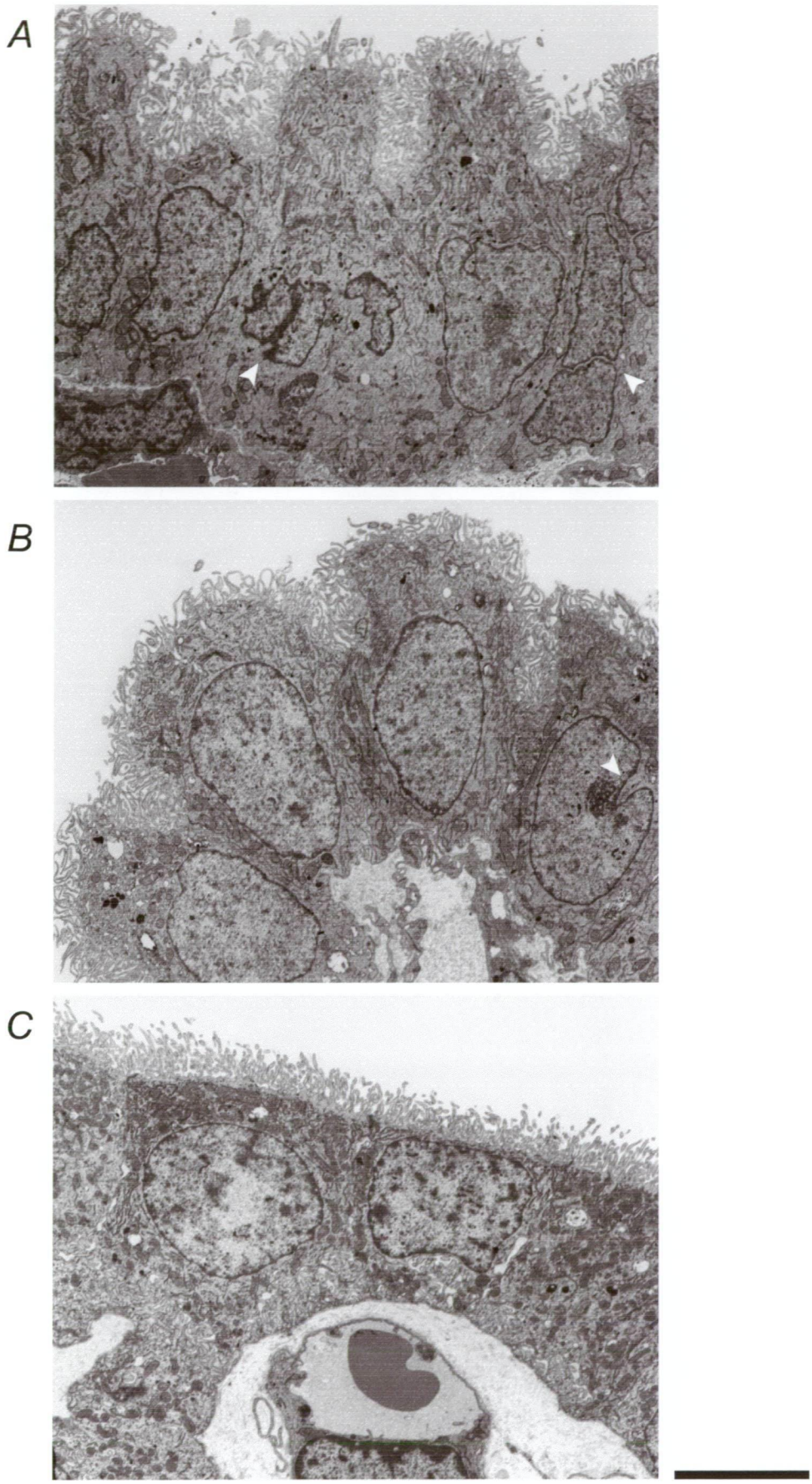
A
B
C

Figure 5.4

Electron micrographs of the choroidal epithelium in different parts of the choroid plexus at birth (A and B) and at P13 (C and D). A and B show the fourth ventricular choroid plexus from the root (A) and from the outer parts of the plexus villi (B). A and B highlights the heterogeneity of this tissue at birth when some parts formed a pseudostratified layer and others already have formed a simple columnar layer. Also compare B with the choroid plexus in the lateral ventricle at birth in Figure 5.3. Arrow in A points to an epiplexus cell; these cells were commonly observed at all ages. Note the numerous lysosomes in the epiplexus cell which suggests it has a phagocytic function. Arrowhead in A points to a large vacuole (between 1-3 µm); these were infrequently observed in animals at P1 and seemed to be more common in the 4th than the lateral ventricular choroid plexus. The enormous size of these vacuoles is possibly an artefact. The vacuoles always appeared empty, however, this may be a result of tissue processing. C and D show the choroid plexuses from the lateral (C) and 4th (D) ventricle at P13. These two choroid plexuses appeared similar at this age.

Scale bar is 7 µm in A and B, and 5 µm in C and D.

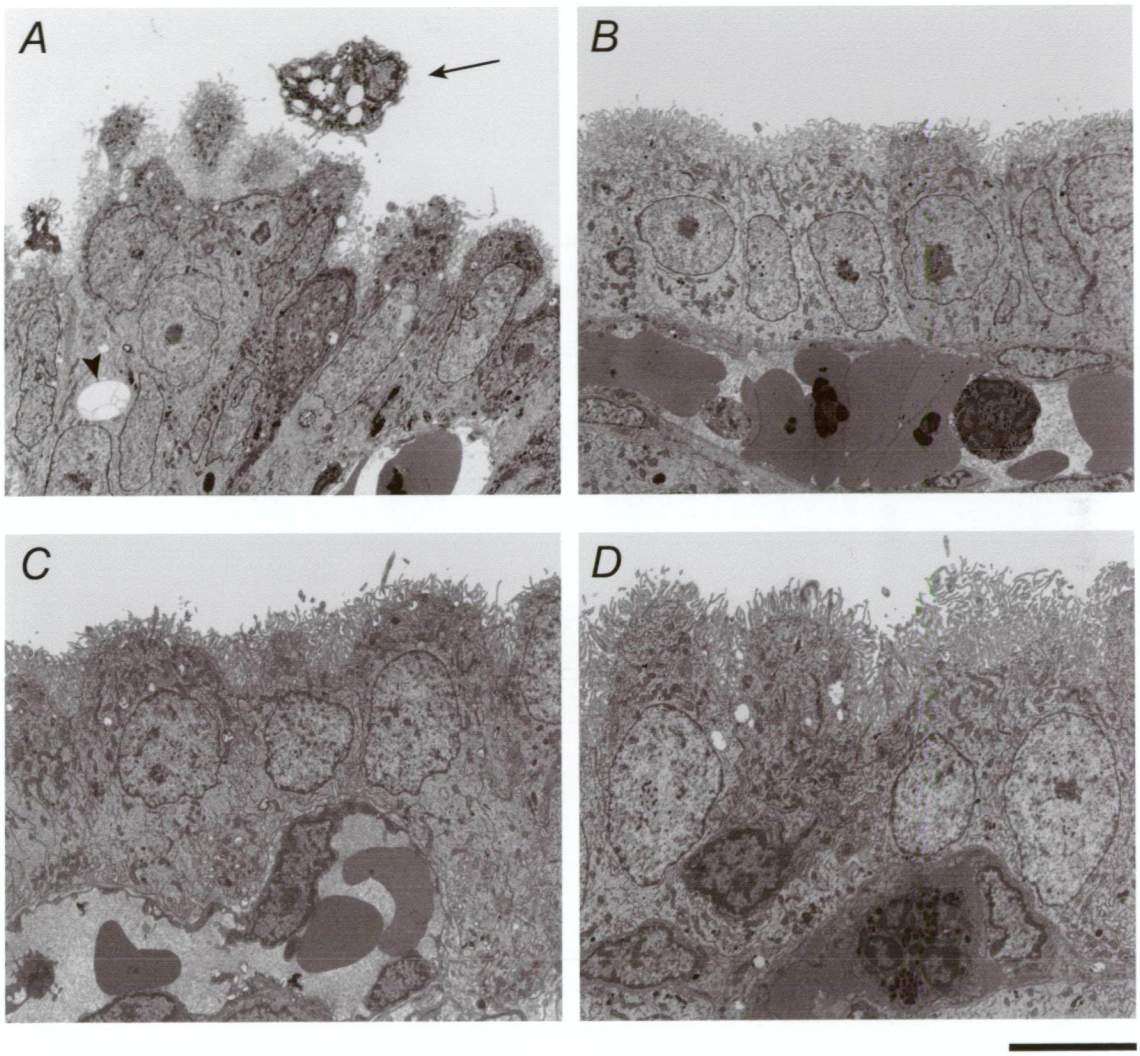
A
B
C
D

Figure 5.5

Electron micrographs of the apical side of epithelial cells at P0 (A), P13 (B) and P64 (C). Several changes in the cell organelles were seen during development. The most noticeable difference was the increase in microvilli and mitochondrial content with age. The microvilli became longer and more abundant, and the mitochondria became more numerous and increased in size during development. The endoplasmic reticulum was mostly smooth at P0 whereas ribosomes were often associated with the ER in the more mature epithelial cells. Note also the difference in nuclear shape at different ages. Tufts of cilia were situated interspersed on the surface of the epithelia at all ages. To the right hand side in B one such tuft can be seen that has been sectioned perpendicular to the tuft so that the cilia appear in cross section. Insert in A and B show high magnification of cross sections of cilia. At all ages the cilia showed the normal 9+2 microtubular organisation. Arrowheads point to vacuole-like structures (100-500 nm) that were common at all ages. As seen in B these structures sometimes contained vesicles and they therefore have some phagocytic function.

Scale bar is 2 μm in A-C, and 350 nm in insert in A, and 300 nm in insert in B.

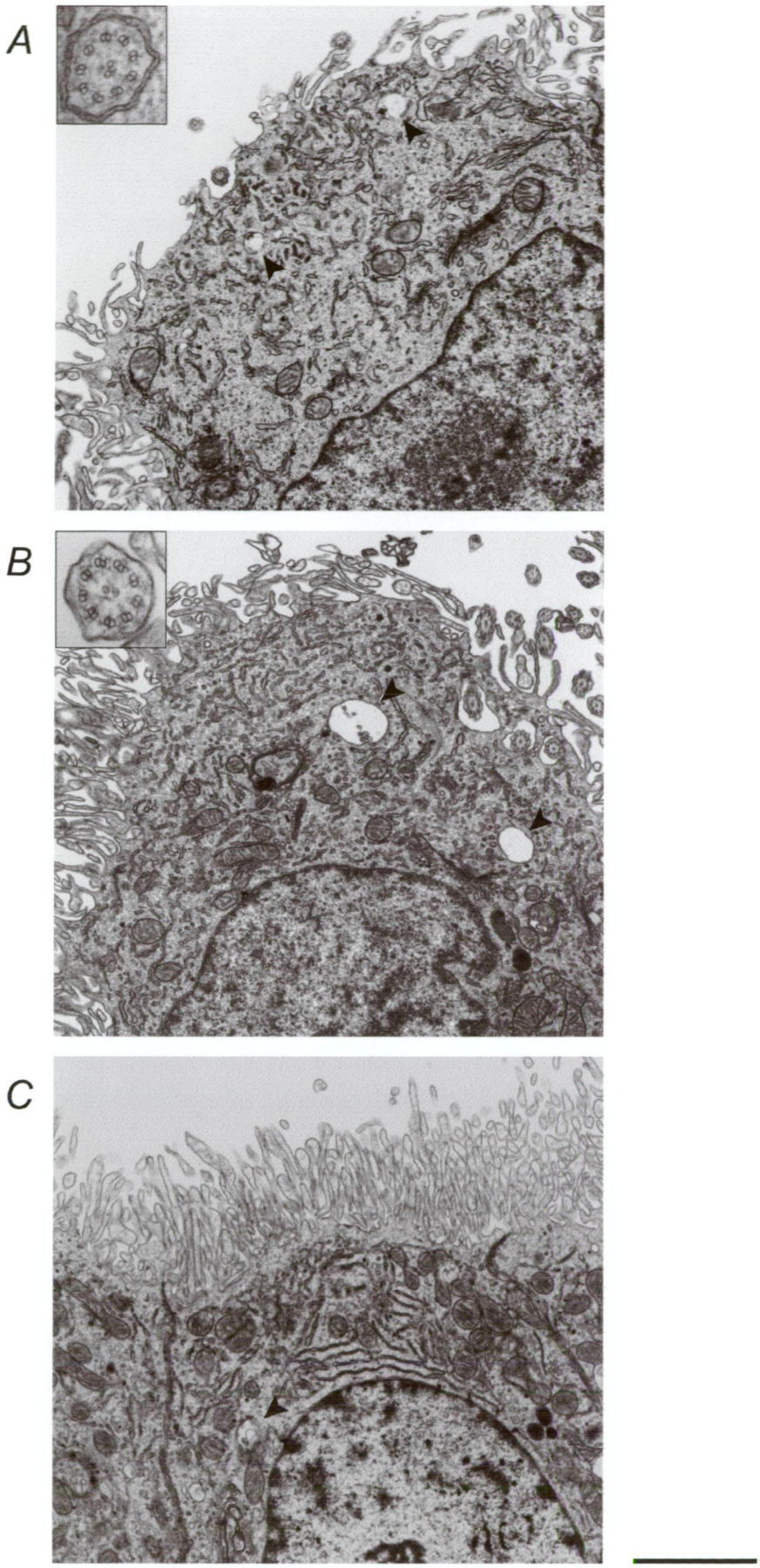
A
B
C

Figure 5.6

Electron micrographs of different parts of blood vessels in the choroid plexus at P1 (A, C and E) and P64 (B, D and F). The wall of the blood vessels was composed of thicker segments with numerous cell organelles, such as mitochondria, vesicles and endoplasmic reticulum, and thinner segments with numerous fenestrations. The fenestrations appeared as segments of the wall without cytoplasm but only thin membrane. At birth, the endothelial cell only had a small part of the wall exhibiting fenestrations whereas at P64 almost the whole wall was thin with numerous fenestrations. A and B shows the difference in the thickness of the blood vessel wall between P1 and P64. The appearance of individual fenestrations was similar at all ages with a width of about 50 nm (C and D). At the luminal side of the interendothelial cleft a single tight-junctional structure was present (arrows in E and F).

Scale bar is 2 μm in A and B, 250 nm in C and D, 125 nm in E, and 80 nm in F.

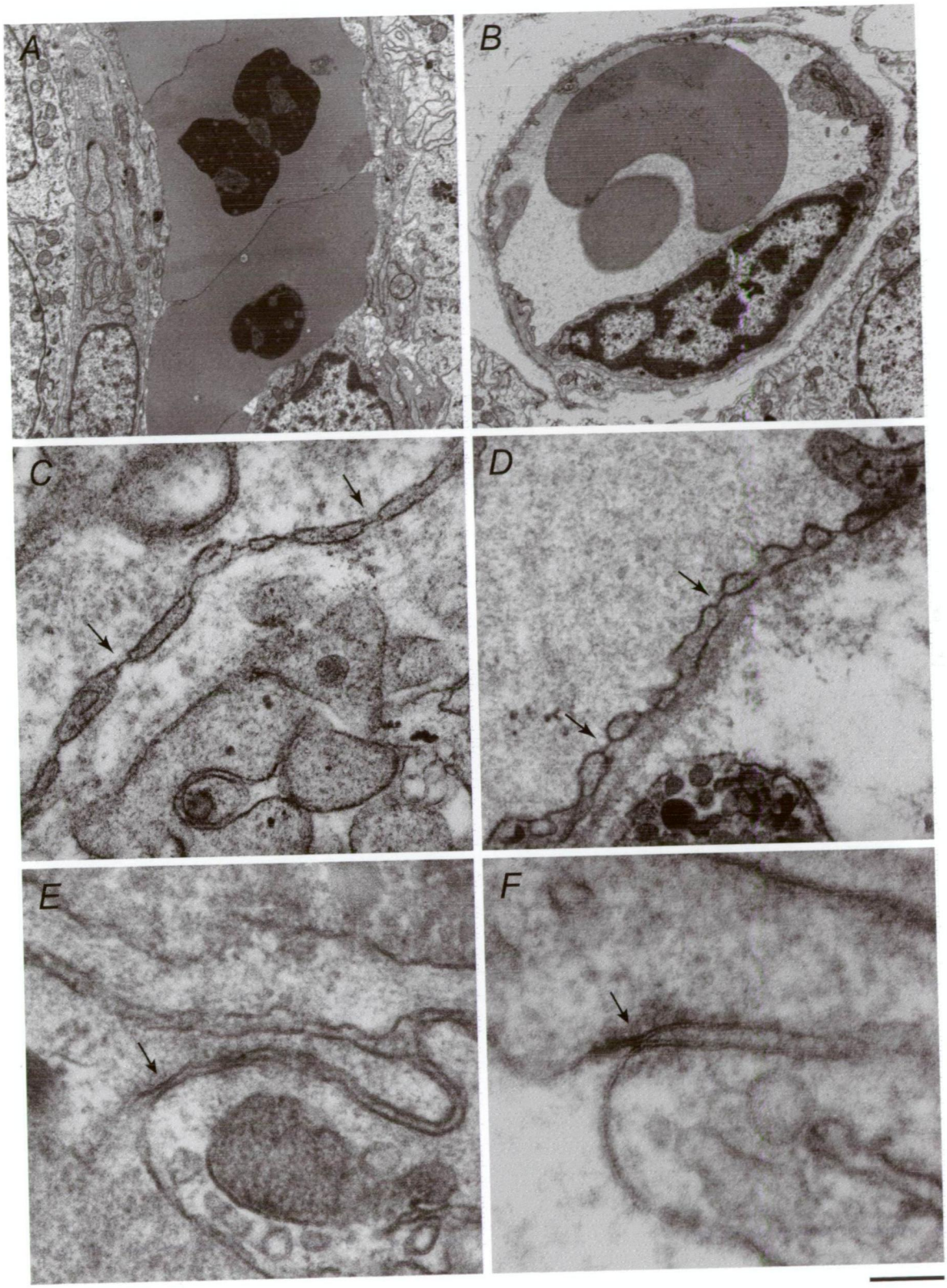
A
B
C
D
E
F

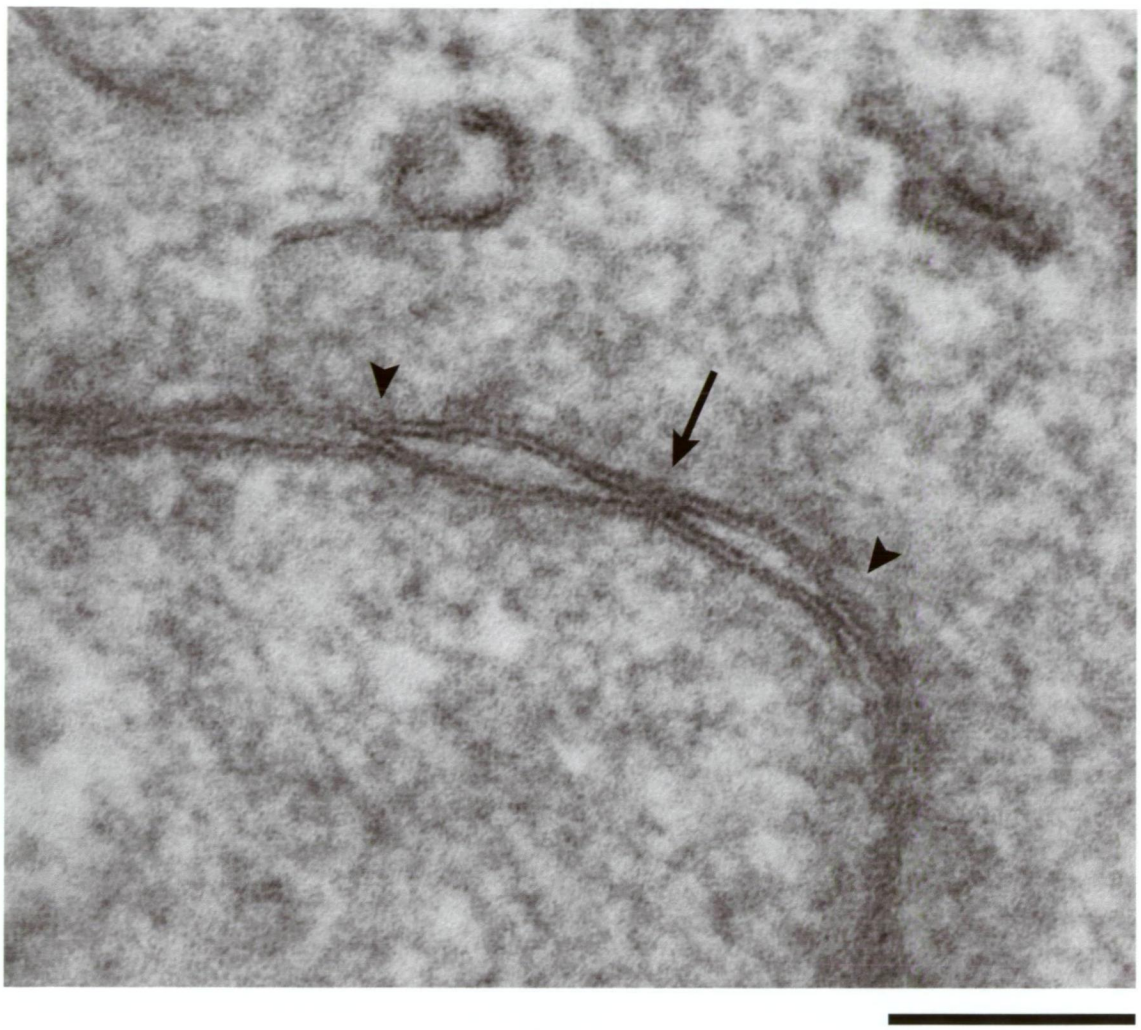

Figure 5.7

High-power electron micrograph showing the structural identification of a tight-junctional strand (arrow). The membranes of adjacent epithelial cells in the choroid plexus came together at certain point to form these junctions. The arrowheads show two other possible strands. The goniometric tilting device was used to obtain a sharper view of the cell membranes and improve the identification of such junctional structures. Compare also with Figures 5.6E-F which show tight-junctions in endothelial cells of the choroid plexus.

Scale bar is 100 nm.

Figure 5.8

Electron micrographs showing the interepithelial cleft at P1 (A) and P64 (B), and high power electron micrographs of the junctional complexes at P1 (C-D), P13 (E) and P64 (F). All electron micrographs are from the lateral ventricular choroid plexus except for A and C that are from the 4th choroid plexus. A junctional complex (zo) was always present at the apical side of the interepithelial cleft at all ages studied. Below this complex cisternal structures were often seen in close association with the intercellular cleft. These cisternal structures often formed a whole row at P1 whereas they were less frequent at P64. The structural significance of this difference is unknown. The *zonulae occludentes* in A is shown in high power in D. No noticeable difference could be seen between the junctional complexes at different ages (compare C-F). Up to five tight-junctions were often identified within the junctional complex (arrows).

Scale bar is 500 nm in A and B, and 125 nm in C-F.

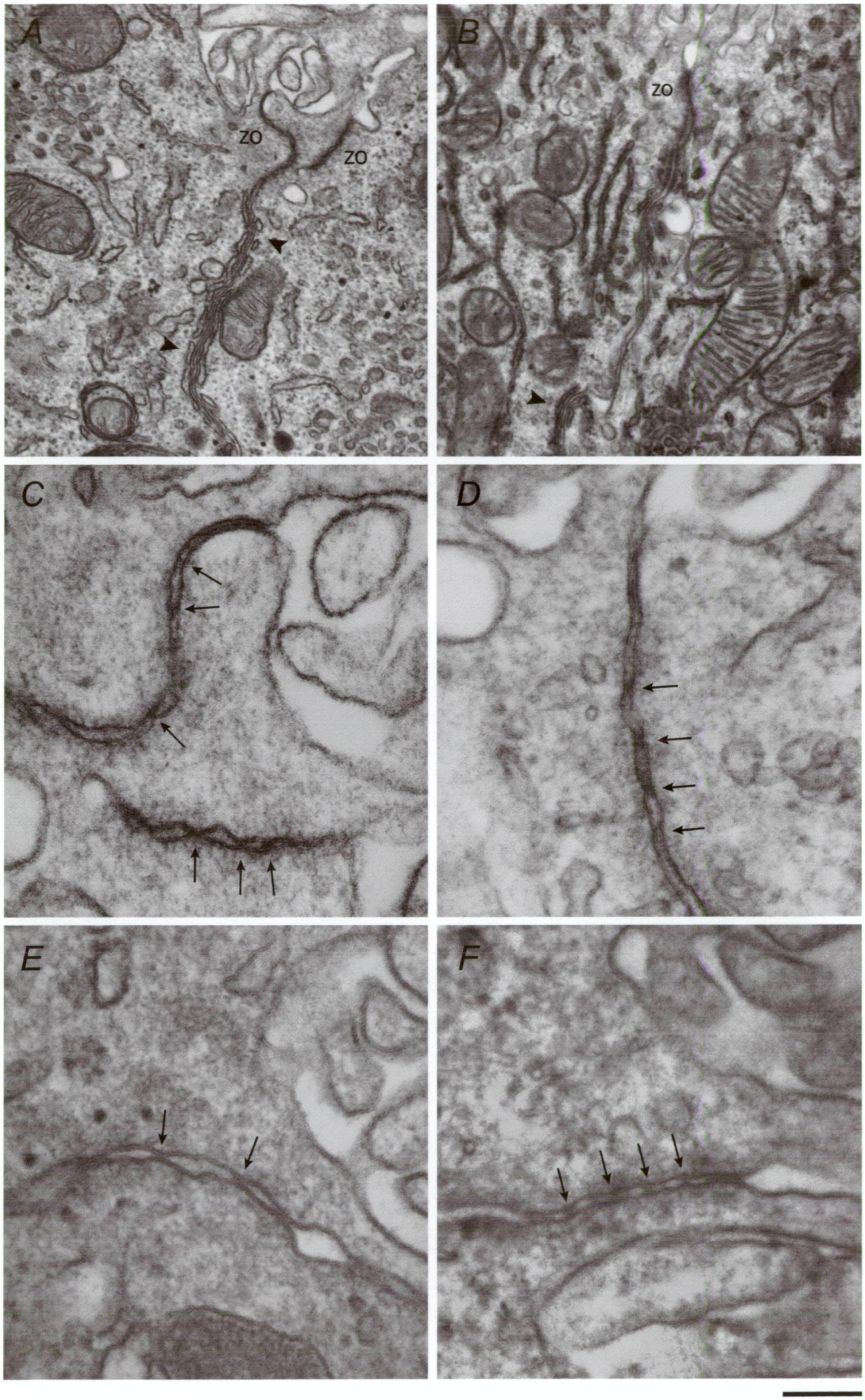
A
ZO
ZO
B
ZO
C
D
E
F

Uptake of D-3308 into the CSF and localisation in brain tissue

The CSF/plasma ratios for D-3308 were compared to ratios obtained for inulin, sucrose and L-glucose in order to assess whether D-3308 behaved in a similar passive manner across the brain barriers to other lipid insoluble markers. As has been mentioned before, several authors have proposed that the penetration of lipid insoluble molecules is by unrestricted diffusion (Felgenhauer, 1974; Dziegielewska et al., 1979; Habgood et al., 1993). Dziegielewska et al. (1979) showed that the concentration in CSF of several lipid insoluble markers was related to their diffusion coefficient (D), which can be calculated from the Einstein-Stokes radii. Values of D for inulin, sucrose and L-glucose were taken from Normand et al. (1971) and were multiplied by a factor of 1.1924 in order to transform values from 25°C to 32°C (D_{32}), which is the body temperature in the *Monodelphis* (Saunders et al., 1992). The D value for D-3308 was estimated from its molecular weight. The D_{25} values for a range of molecules given by Normand et al. (1971) were plotted against $MW^{-1/2}$ and a linear regression line fitted to the data ($r=0.997$, least squares regression). From this regression line, the D_{25} value could be estimated for D-3308 and corrected to 32°C as described above. Figure 5.9 shows the three-hour CSF/plasma ratios for D-3308 and other markers plotted against D_{32} obtained from experimental data in animals of similar ages (P15-P16 for inulin and sucrose, P16 for D-3308, and P17-P18 for L-glucose). The D-3308 reaches a ratio of approximately 16% which is similar to the ratio for inulin (15%), but substantially less than those for the smaller molecules sucrose (51%) and L-glucose (60%). Details of inulin, sucrose and L-glucose can be found in Chapter 4.

In order to validate D-3308 as a quantifiable replacement for BDA-3000, the distribution of both markers was compared in brain sections from a P7 opossum. The markers showed matching distribution patterns with staining in a small proportion of the choroidal epithelial cells and intracellular staining in some cells in the ventricular zone

and in the hippocampal area of the brain (Figure 5.10). The rest of the brain seemed to lack any staining except for the blood vessels, which were strongly stained.

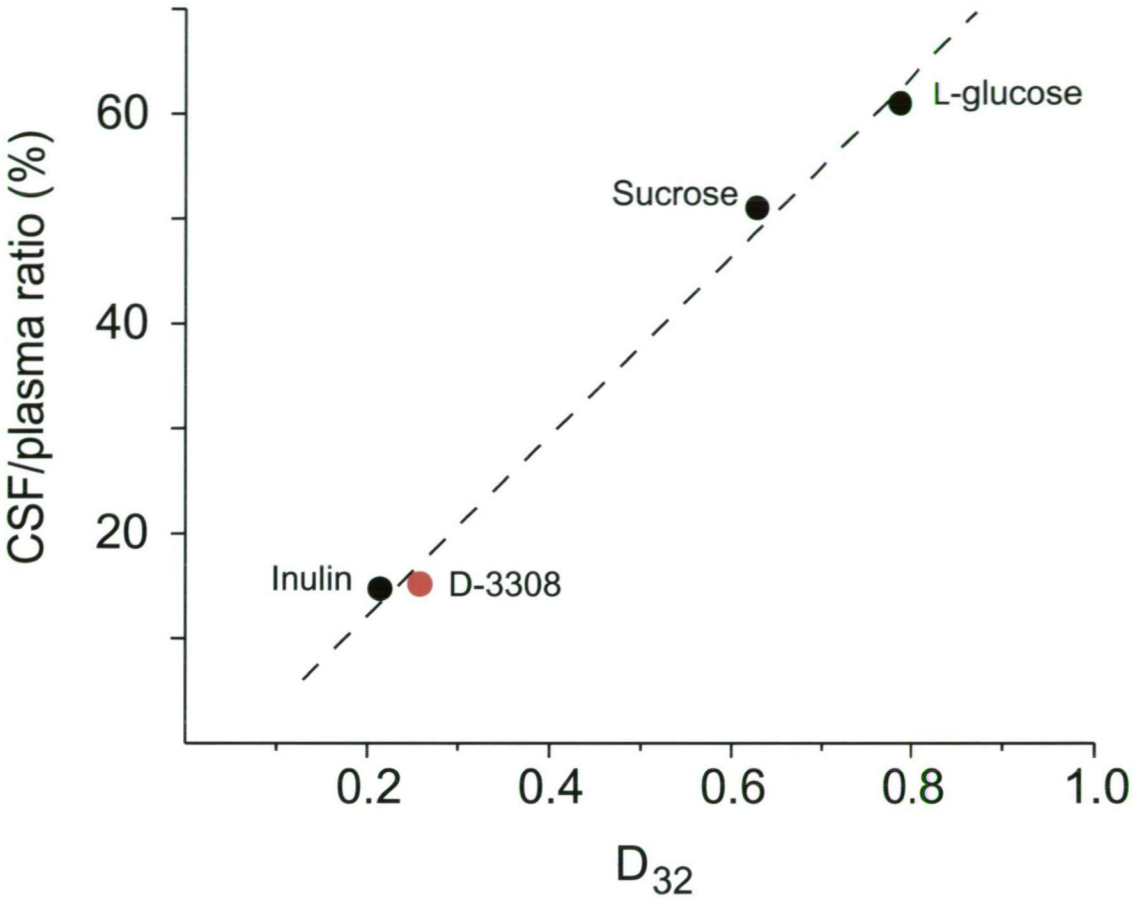

Figure 5.9

CSF/plasma ratios (y-axis), three hours after an intraperitoneal injection of markers against the diffusion coefficients D_{32} (x-axis) in opossums at P15-P16 for inulin and sucrose, P16 for D-3308, and P17-P18 for L-glucose. Data for inulin, sucrose and L-glucose are taken from experiments presented in Chapter 4. A linear regression line was fitted to the data points. This plot should be a straight line if the penetration of molecules is by unrestricted diffusion. D-3308 falls close to the regression line, confirming that its entry into CSF is consistent with diffusion.

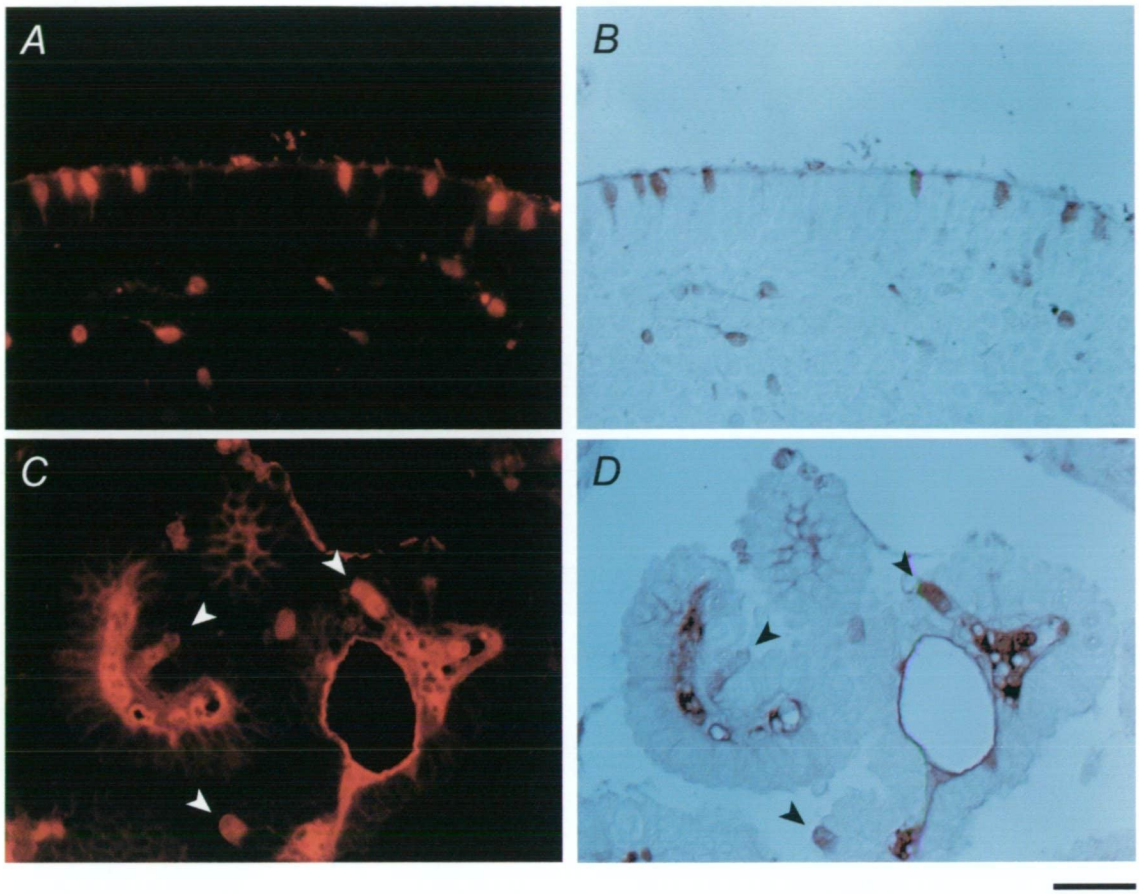

Figure 5.10

Localisation of D-3308 (A and C) and BDA-3000 (B and D) in brain sections 30 minutes after an ip injection of both tracers into a P7 opossum. D-3308 was viewed directly using filter for rhodamine and BDA-3000 detected using a Vectastain Elite ABC kit followed by the diaminobenzidine tetrahydrochloride (DAB) reaction. D-3308 and BDA-3000 showed identical intracellular staining in a small proportion of the ependymal cells in the ventricular zone (compare A and B) and in epithelial cells of the choroids plexus (compare C and D).

Scale bar is 30 μm.

BDA-3000 in the opossum brain at the light microscopic level

Examination of brain sections processed for BDA-3000 revealed that in the brain at all ages most of the reaction product was within the lumen of the blood vessels (see Figure 5.11). The endothelial cells also appeared positive for BDA-3000. This was most prominent in P30 animals in which the lumen was empty with no reaction product since the contents of the blood vessels had been washed out when animals were perfuse-fixed (see Figure 5.11). Many cells in the ventricular zone of the lateral ventricle showed intracellular staining in animals between P0 and P9. The number of cells with intracellular staining in the ependymal or subependymal layer in the ventricles decreased with development so that at P30 none of these cells appeared to be positive for BDA-3000. Occasional cells in the hippocampal area showed intracellular staining at all ages. Little or no staining was detectable outside the blood vessel wall or in the brain parenchyma. The surfaces of both the ventricular neuroependyma and of the choroid plexuses were positive where CSF had precipitated on the surface (see Figures 5.12 and 5.13). In general, the staining was more prominent in the brains of younger animals where intracellular staining in the basal forebrain and diencephalon was also found. At P30 the whole brain appeared devoid of reaction product except for endothelial cells in the brain and the perivascular space of the choroid plexus. Control sections showed no staining.

Uptake of BDA-3000 in choroid plexus

Light microscope

The uptake of BDA-3000 in the choroid plexus was studied under the light microscope at various ages between P0 and P30, and under the electron microscope at P1 and P13 after single intraperitoneal injection. In the light microscope the choroid plexuses blood vessels and surrounding connective tissue were strongly stained along with a small number of the epithelial cells. Staining was visible on the surface of the choroid plexus

and inside the ventricular system (see Figures 5.11-5.13). The staining was particularly abundant within the ventricular system at younger ages. In paraffin sections, the reaction product had a granular appearance and seemed to be absent from the nuclei of stained epithelial cells. The number of BDA-3000 positive cells in the choroid plexuses from all four ventricles decreased progressively with age. At the time of birth (P0) a proportionally higher number of epithelial cells was positive in the choroid plexuses in the lateral ventricles (Figure 5.12 and Table 5.2), whereas the 4th ventricular plexus contained only occasional stained epithelial cells. At this age the choroid plexus cells in the lateral ventricles have an elongated shape, whereas the 4th ventricular choroid plexus cells have a more mature columnar form (see Figure 5.2). At P8 and later only very occasional stained epithelial cells were found in the 4th ventricular choroid plexus and the proportion of stained epithelial cells in the lateral ventricles was substantially less than at P0 (Figure 5.12). In contrast, at P8 the choroid plexus in the 3rd ventricle had a high proportion of stained epithelial cells (Figure 5.13). At P30 all choroid plexuses showed only very occasional stained epithelial cells with rather faint intracellular staining (Figure 5.12). The choroidal epithelial cells at this age have a cuboidal shape which is characteristic of the adult choroid plexus. In paraffin sections, from P8-P9 and in older animals, there appeared to be no staining in the upper most apical parts in between epithelial cells. This is the region where the tight-junctions are present (see Figure 5.8). At earlier ages it was difficult to determine the extent of intercellular staining since the epithelium at these ages have a tightly packed pseudostratified appearance.

In order to quantitate the number of stained epithelial cells at different ages and in each separate choroid plexus, the proportion of epithelial cells with intracellular reaction product was determined at P0, P8 and at P30. In random coronal or sagittal sections, which contained choroid plexus tissue from one or all the ventricles, all epithelial cells were counted and the proportion of BDA-3000 positive epithelial cells was calculated.

A minimum of ten sections containing choroid plexus tissue from each ventricle was counted. The results are presented below in Table 5.2.

Table 5.2

	n	Lateral	3rd	4th
P0	10	15.1 ± 1.0		5.5 ± 0.2
P8	12	4.3 ± 0.6	11.4 ± 3.1	4.8 ± 1.1
P30	11	1.4 ± 0.3	1.9 ± 0.1	1.9 ± 0.1

Proportion (%) of epithelial cells with intercellular staining of BDA-3000 in the lateral, 3rd and 4th ventricular choroid plexus at P0, P8 and P30. The number for the 3rd ventricular choroid plexus at birth is missing because this choroid plexus has not formed yet at this age. The proportion of BDA-3000 positive cells dropped in all three different choroid plexuses during development. Values as means ± SEM

Figure 5.11

Localisation of BDA-3000 in the developing opossum brain 30-45 min after an intraperitoneal injection. Figures show coronal sections of the opossum forebrain at P0 (A, D and E), P8 (B and F) and P30 (C and G). Because of the increase in the size of the brain with age, C only shows half the brain at P30 in order to illustrate the brains at different ages at comparable sizes. BDA-3000 was detected using a Vectastain Elite ABC kit followed by the diaminobenzidine tetrahydrochloride (DAB) reaction. D shows a magnified area of the developing cortex (boxed area in A) and E is a high power micrograph of a blood vessel (arrow in D) from a P0 animal. Note that at P30 (C) only blood vessels stained positive and there was no staining in the rest of the brain. Strong staining could be seen in precipitated CSF at P0 (A and D). As shown in D it appeared that some cells in the ventricular zone had taken up BDA-3000 from the CSF. The low power view of a P8 opossum brain (B) showed strong staining in the stroma of the choroid plexus and in blood vessels throughout the brain. A few cells in the hippocampal area also seemed to have taken up BDA-3000. Note the larger number of blood vessels in the brain compared to P0 (A). F is a high power micrograph of a blood vessel at P8. At all ages no noticeable difference could be seen in the staining around the blood vessels compared to other areas of brain tissue (see E, F and G). In the younger animals, brains were immersed fixed and thus the lumen of the blood vessels were positively stained (E and F). At P30 the brains were perfuse fixed resulting in the lumen of blood vessels appearing empty, but the endothelial cells of the blood vessels contained reaction product (G). At this age no staining could be seen in the brain except for the endothelial cells.

Scale bar is 400 µm in A and B, 500 µm in C, 60 µm in D, 12 µm in E and F, and 60 µm in G.

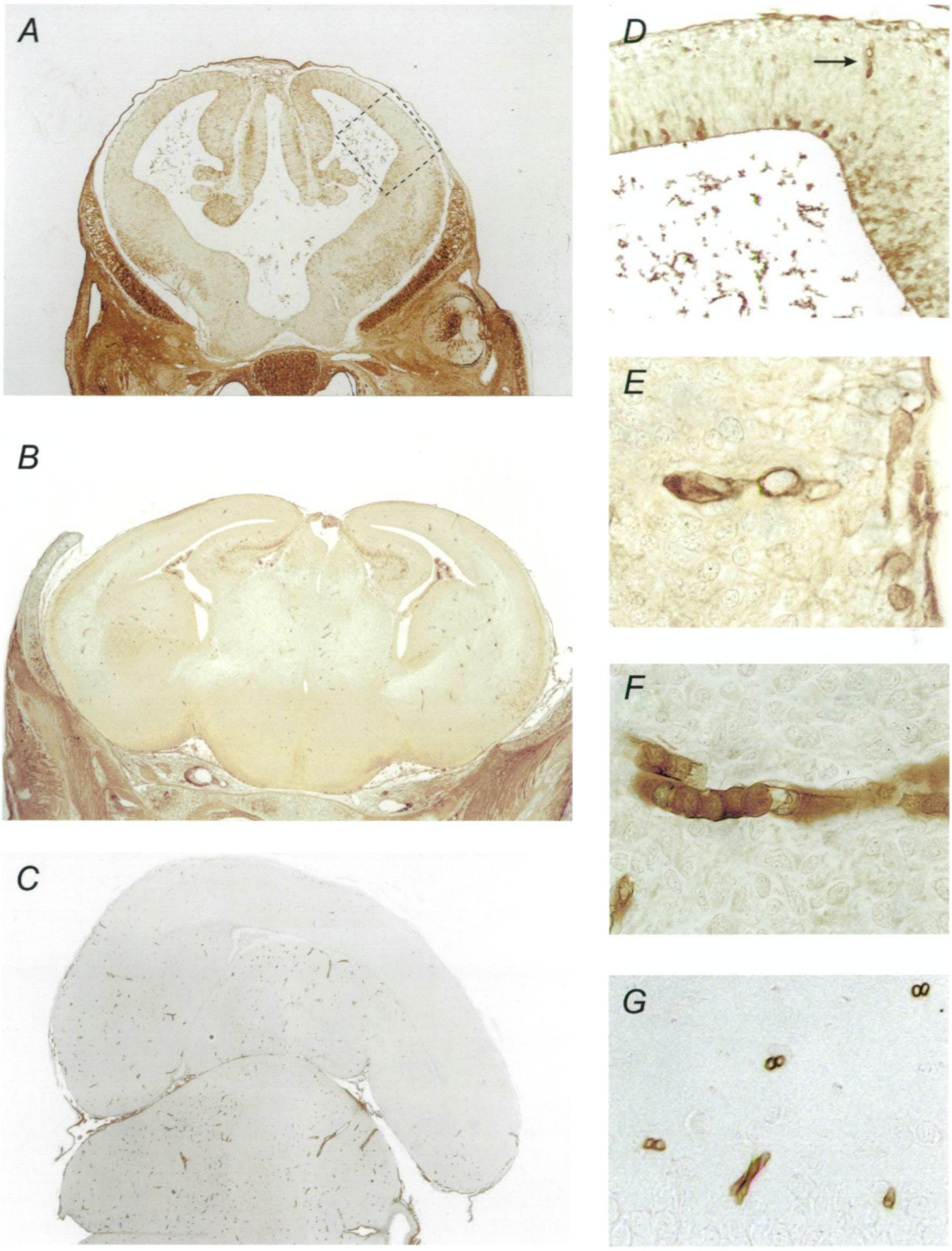
A
B
C
D
E
F
G

Figure 5.12

Localisation of BDA-3000 in the developing choroid plexus of the lateral ventricles approximately 45 min after intraperitoneal injection at P0 (A), P8 (B) and P30 (C). BDA-3000 was detected using a Vectastain Elite ABC kit followed by the diaminobenzidine tetrahydrochloride (DAB) reaction. The proportion of choroidal epithelial cells positive for BDA-3000 in the lateral ventricle decreased with age (A-C). Note the developmental change in choroid plexus morphology from a pseudostratified layer of epithelial cells (A) to the mature stage with cuboidal plexus cells exhibiting large apical surface area (C). In the younger animals brains were immersed fixed and thus the stroma of the choroid plexus was positively stained (A and B). At P30 the brains were perfuse fixed resulting in the lumen of blood vessels appearing empty (C).

Scale bar is 25 μm.

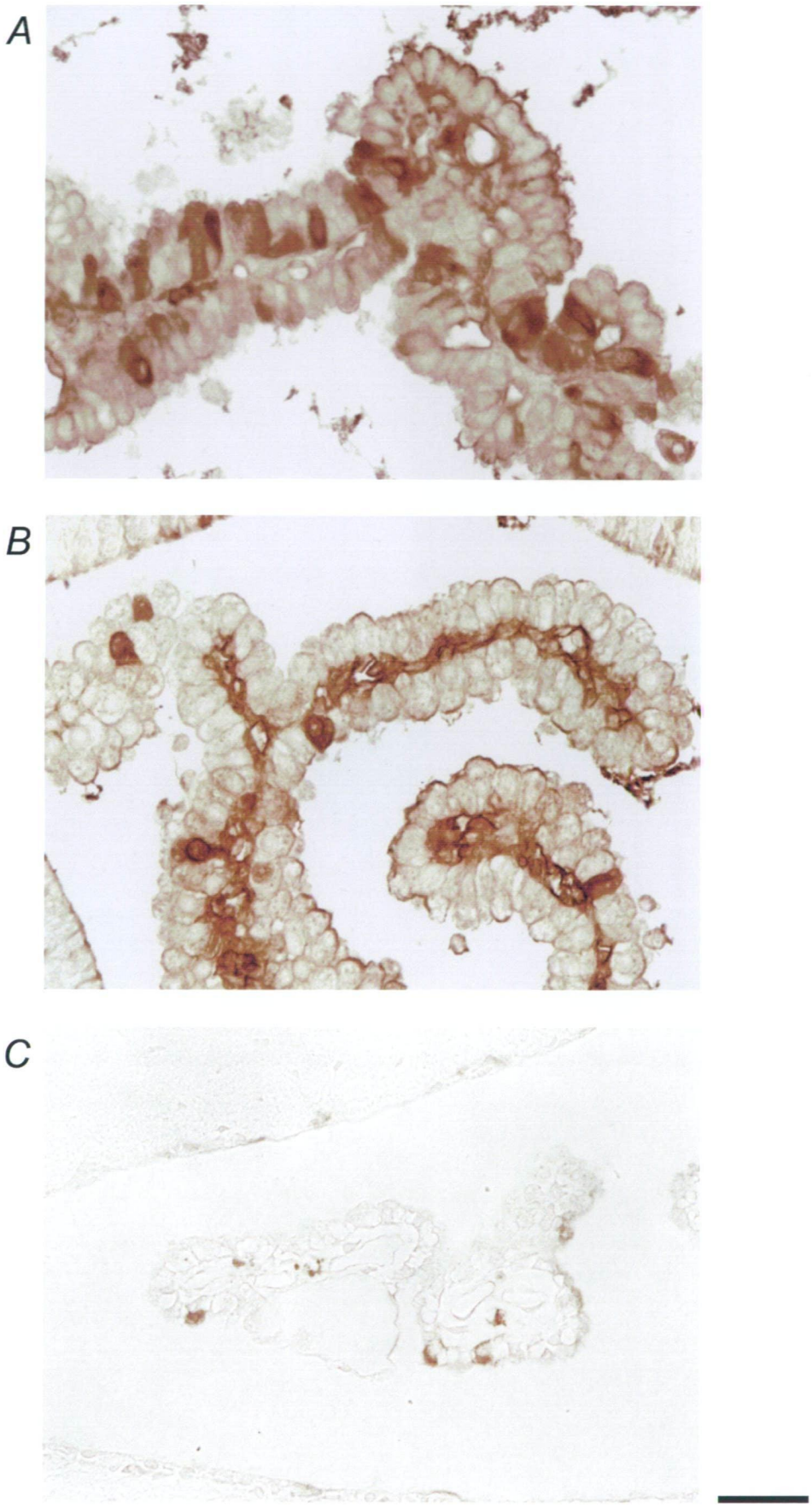
A
B
C

Figure 5.13

Localisation of BDA-3000 in the lateral (A and B), 3rd (C and D) and 4th (E and F) ventricular choroid plexuses at P8 30-40 min after intraperitoneal injection. On the right are higher power micrographs of the same choroid plexus which is shown on the left. BDA-3000 was detected using a Vectastain Elite ABC kit followed by the diaminobenzidine tetrahydrochloride (DAB) reaction. The proportion of epithelial cells with intracellular staining of BDA-3000 was higher in the 3rd ventricular choroid plexus (C and D) than in the other choroid plexuses at this age.

Scale bar is 60 μm in A and C and E, and 30 μm in B, D and F.

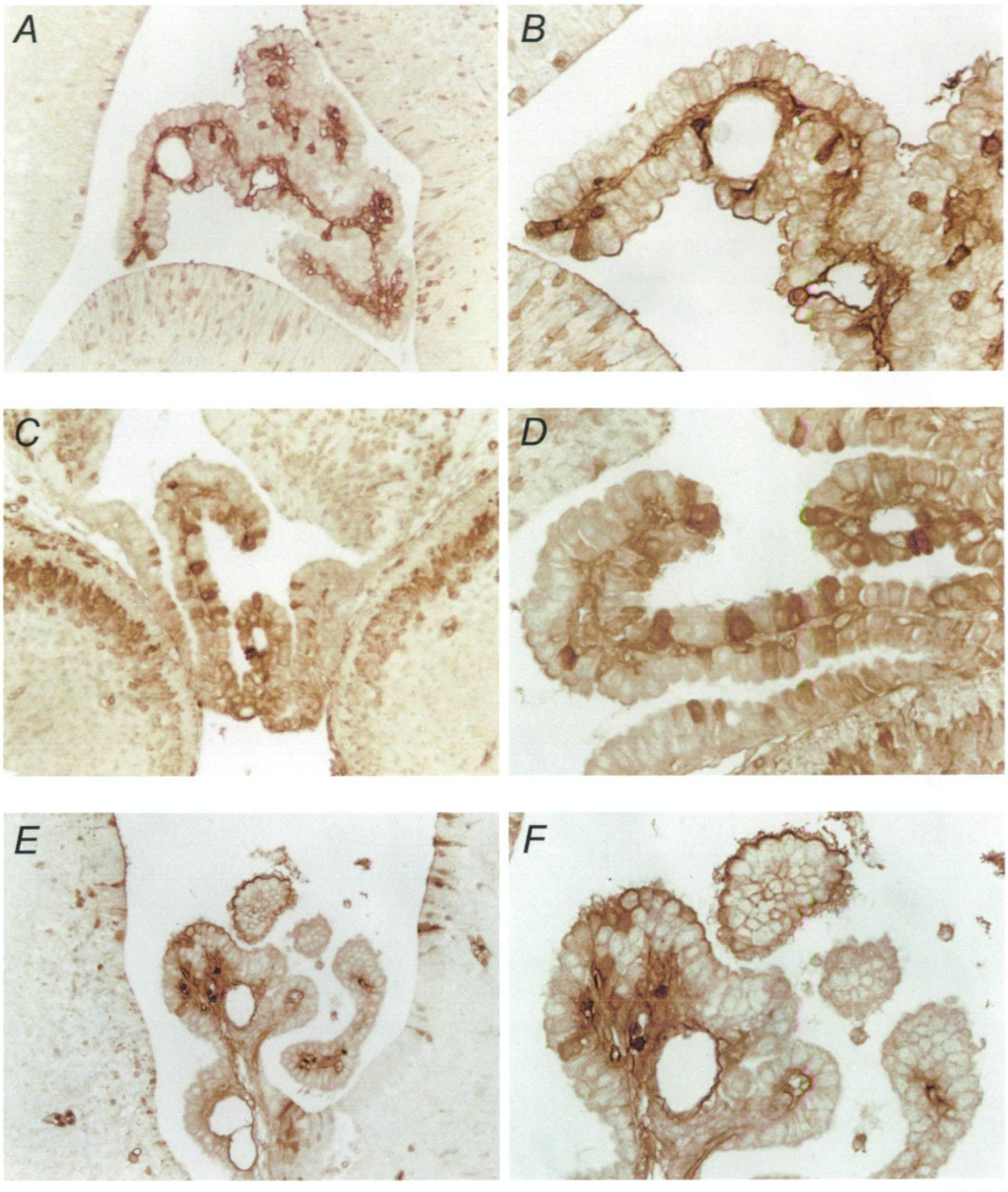
A
B
C
D
E
F

Transmission electron microscope

BDA-3000 was visualised in choroid plexus tissue from the lateral and 4th ventricle at P1 and P13. The uptake of BDA-3000 was visualised with avidin reactions followed by the DAB reaction, which gives an electron dense granular reaction product visible both under the light and electron microscope. The staining of BDA-3000 in this section is referred to as the reaction product. Only selected areas of semi-thin Epon sections of the choroid plexus, in which reaction product was visible either in the lumen of blood vessels or the perivascular space when examined under the light microscope, were further processed for thin-section electron microscopy.

A similar distribution of the reaction product in the choroid plexus was observed in ultrathin sections as in paraffin sections. Different parts of the choroid plexus exhibited similar staining patterns. As can be seen in Figure 5.14 the reaction product was abundant in the lumen of blood vessels but appeared to be most plentiful in the perivascular space between the blood vessels and the epithelial cells. The electron micrograph in Figure 5.14 is of the lateral choroid plexus at P13, however, a similar distribution of reaction product was seen in the lateral and 4th ventricular choroid plexuses at both P1 and P13. The reaction product was also abundant around the fenestrations of the endothelial wall. The intercellular cleft between the epithelial cells was often filled with the reaction product except for the most apical part. Reaction product was, especially at P1, abundant on the surface of the epithelial cells, between and around the apical microvilli. Many vesicles in the endothelial cells often filled with the reaction product at both ages. The reaction product was sometimes seen in small vesicles, multivesicular bodies or associated to cisternal structures in the epithelial cells at both ages (see Figure 5.15). Large vesicular structures in the epithelial cells were common and were often heavily labelled with reaction product at both P1 and P13 (see Figures 5.14 and 5.15). These vesicles were common throughout the epithelial cells, however, none were found to fuse with either the apical or basolateral cell membrane.

There was no noticeable difference in the number of these large vesicles containing the reaction product between the two ages. Both at P1 and P13, the outer most apical part of the interepithelial cleft lacked the reaction product in the area where the junctional complex was present. Sections of the apical side of the intercellular cleft showed that the reaction product was only present on the basal side of certain points of the intercellular cleft where the cell membranes of adjacent cells seemed to be fused (see Figure 5.17). Similar to the staining in paraffin sections, some of the epithelial cells contained large amounts of the reaction product. The proportion of these epithelial cells was much higher at P1 than at P13 in both choroid plexuses. Under the light microscope it appeared as these epithelial cells did not contain the reaction product in the nucleus. In contrast, under the electron microscope it was revealed that reaction product was present in the nucleus of these cells but in lesser quantities than in other parts of the cells (see Figure 5.16). The large amount of reaction product and rather diffuse intracellular staining of these epithelial cells made it difficult to resolve which organelles contained the reaction product (see Figure 5.16). The reaction product was especially plentiful in small vesicles and it also appeared to be associated with cell membranes of some cisternal-like structures (see Figure 5.16). These cisternal structures could be part of the endoplasmic reticulum. The mitochondria in these cells did not seem to contain the reaction product. Apart from having large amounts of intracellular reaction product the intracellular organisation of these cells was not different from other epithelial cells.

Figure 5.14

Electron micrograph showing the localisation of BDA-3000 in the lateral ventricular choroid plexus at P13. Large amounts of tracer have leaked out of the blood vessels and accumulated in the perivascular space. Similar localisation of reaction product was seen at P1. Large arrows point to large vacuolar structures that contained the reaction product (see also Figure 5.15). Note that there is reaction product in the intercellular space between adjacent epithelial cells but it does not appear to penetrate the *zonulae occludentes* at the most apical side of the intercellular cleft (small arrows).

Scale bar is 10 µm.

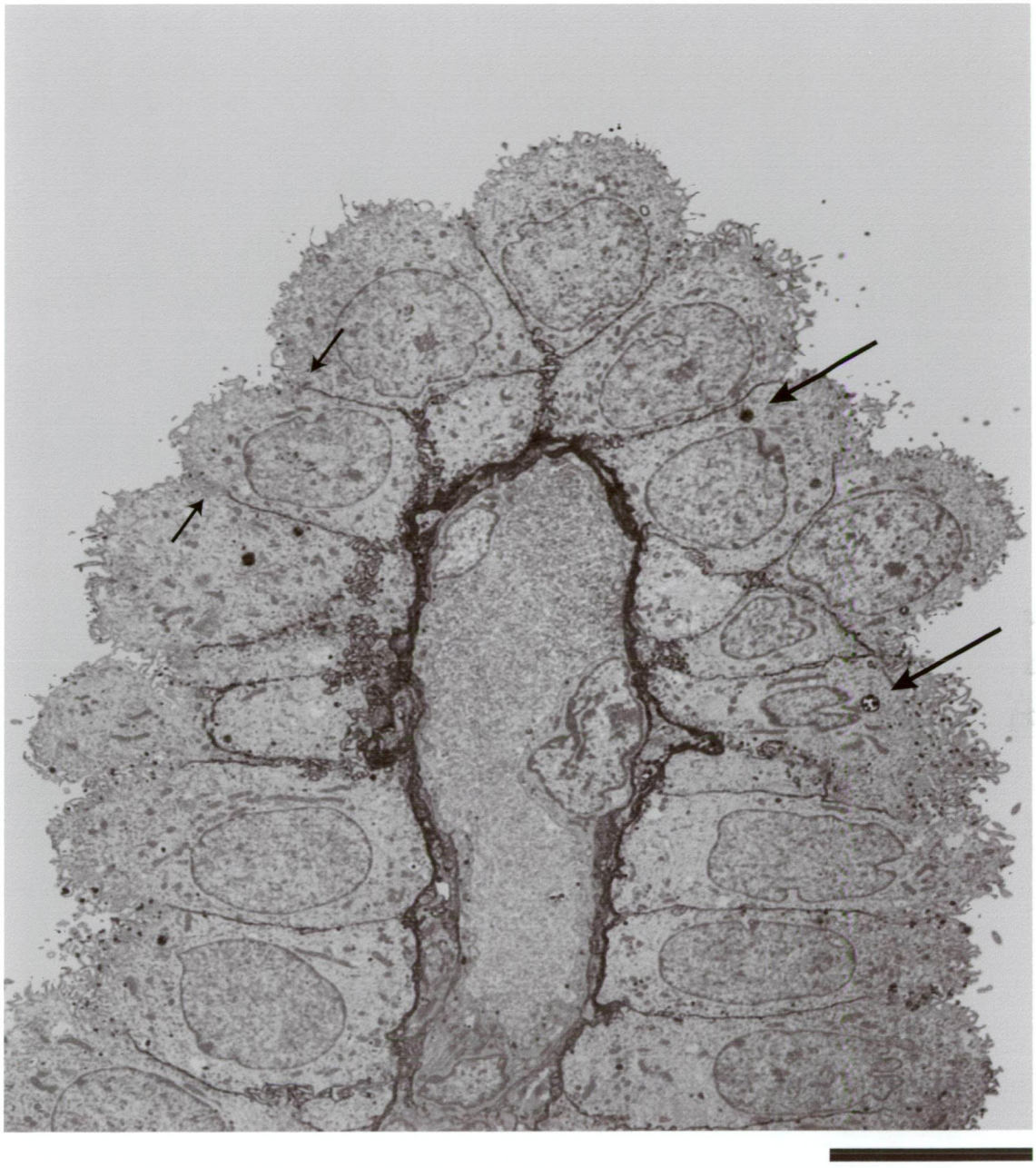

Figure 5.15

Electron micrograph showing the staining of BDA-3000 in epithelial cells of the lateral ventricular choroid plexus at P13. Note that the large amounts of tracer escaped the blood vessels and accumulated in the interstitial space between the blood vessels and the epithelial cells and in the intraepithelial cleft. The dextran could also be seen in some small and large vesicular structures (see arrows in A). The dark structures around the microvilli may be artefacts of the staining technique or a result of precipitation of CSF during fixation. Arrowhead in A points to a vacuolar structure that often contained large amounts of the reaction product. One of these vacuoles is shown in higher power in B (large arrow). Small arrow in B points to the upper most apical part of the intercellular cleft that lacked the reaction product (see also Figure 5.17).

Scale bar is 2 µm in A and 500 nm in B.

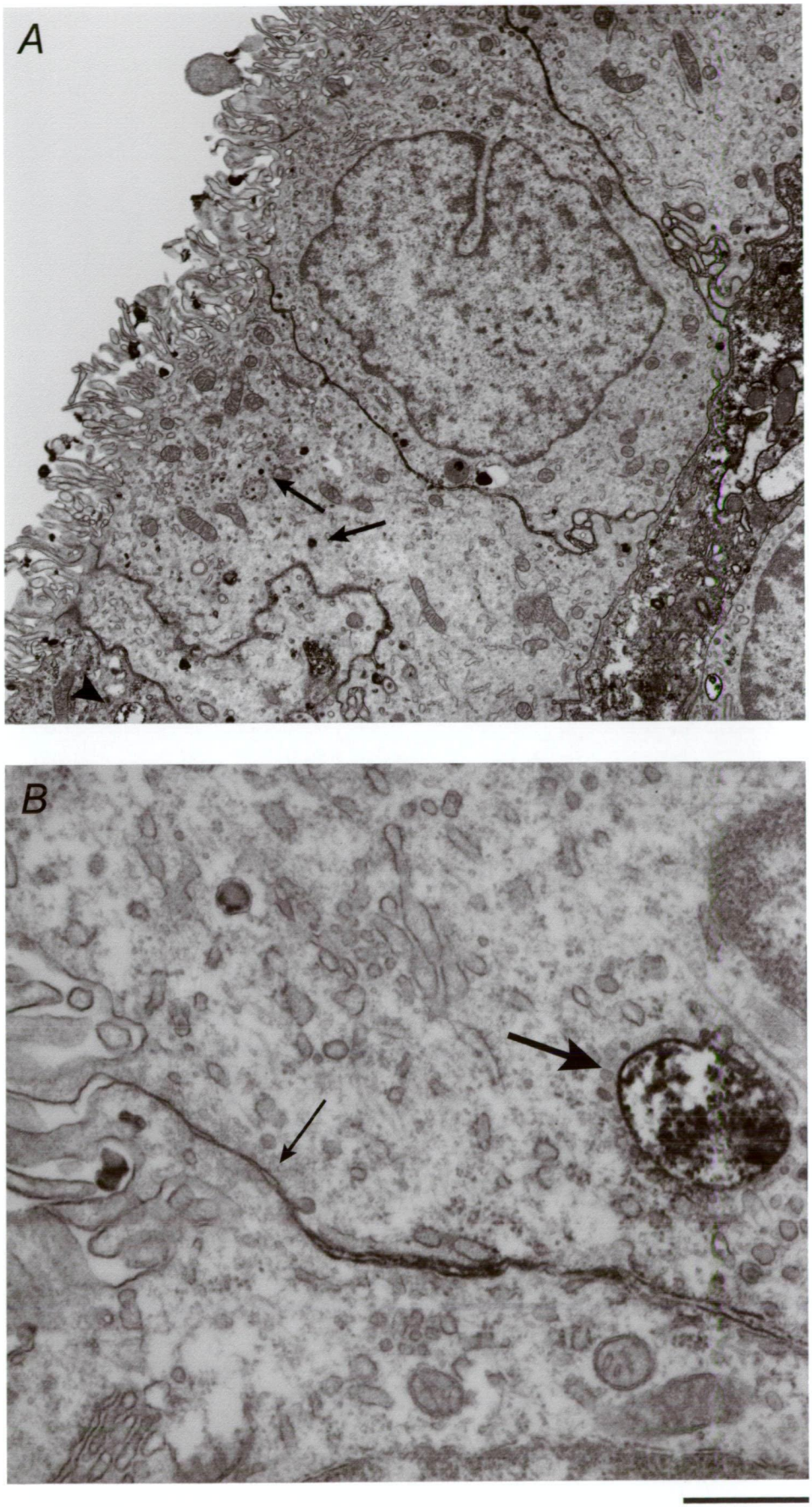
A
B

Figure 5.16

Electron micrograph showing intracellular staining of BDA-3000 in the lateral ventricular choroid plexus at P1. Some epithelial cells contained large amounts of reaction product, similar to what was observed in paraffin sections (see Figure 5.12). The reaction product was visible interspersed throughout the whole cytoplasm and also in the nucleus although less than in the cytoplasm. The reaction product was especially abundant in association with cisternal structures which may be part of the endoplasmic reticulum (arrows in B). The mitochondria in these cells seemed to lack the reaction product (arrowhead). Scale bar is 2 µm in A and 500 nm in B.

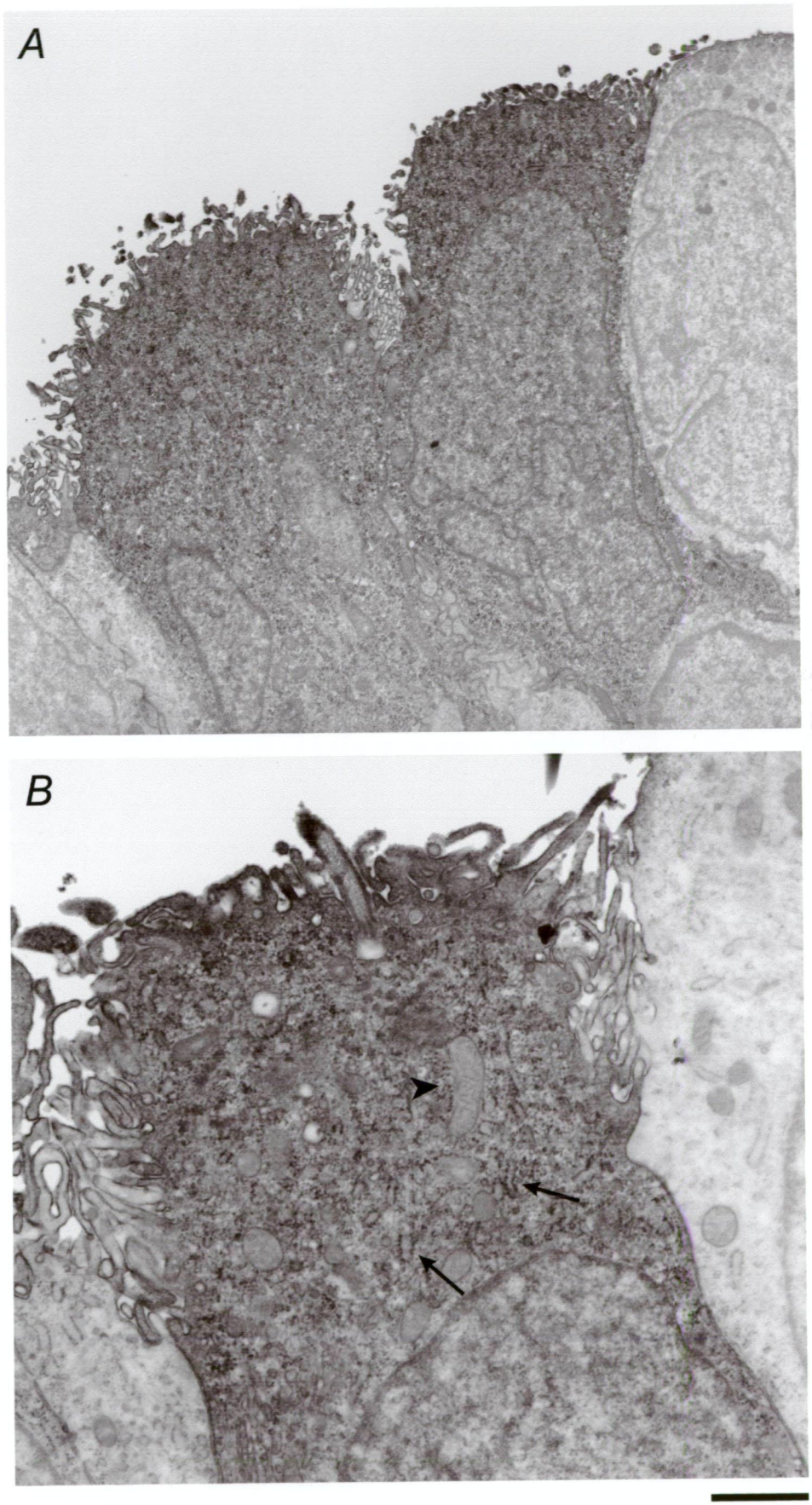
A
B

Figure 5.17

Electron micrographs showing the localisation of reaction product in the interepithelial cleft towards the ventricular surface (on the right side of the micrographs) at P1 (A and B) and P13 (C and D). The reaction product was absent from the most apical part of the interepithelial cleft. It seems that the *zonulae occludentes* restricts the paracellular movement of BDA-3000 at both ages. Arrows point to possible tight-junctions that appear to impede the penetration of BDA-3000, however, the contrast and resolution in these sections did not allow for definite identification.

Scale bar is 100 nm in A and 200 nm in B-D.

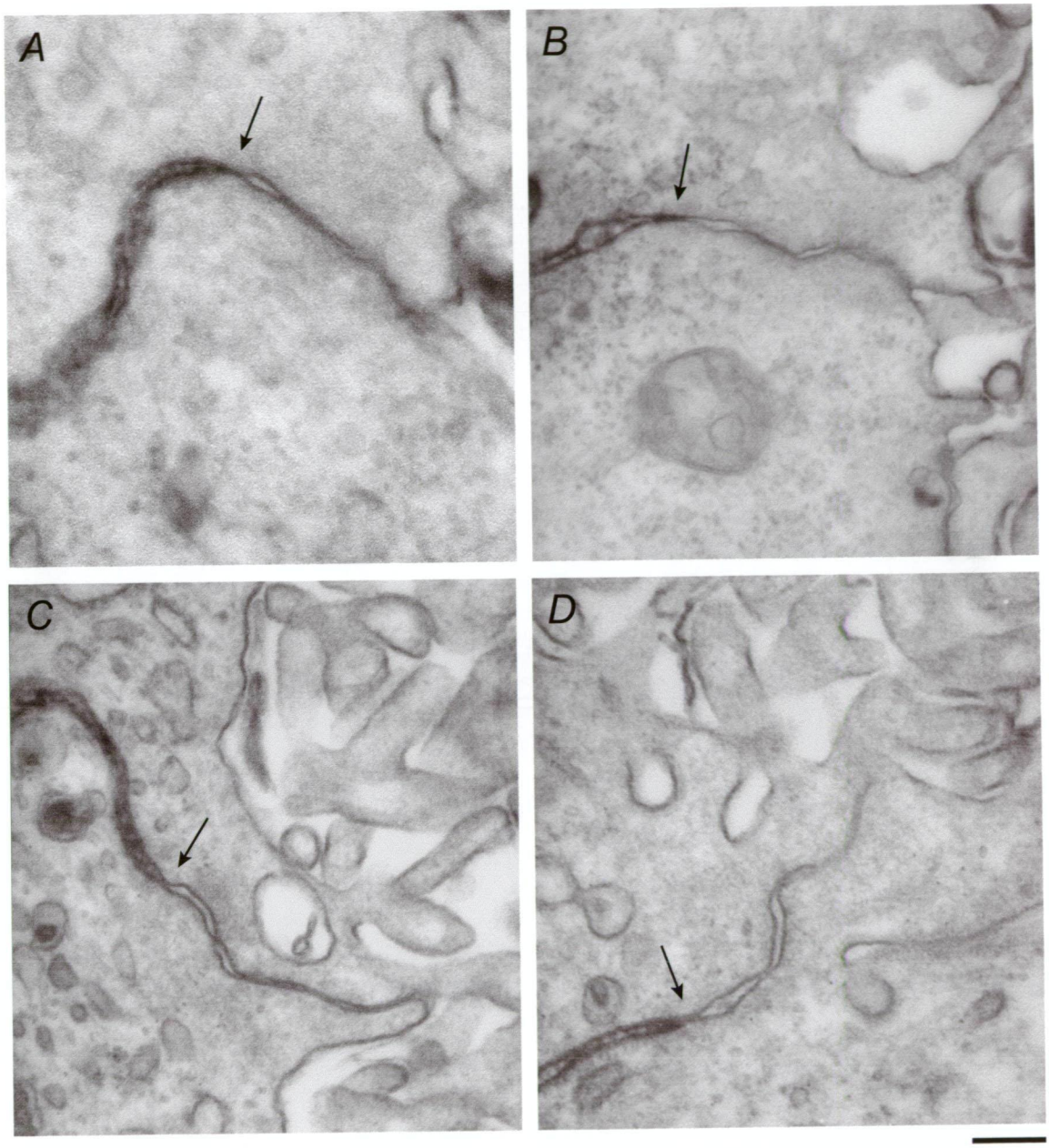
A
B
C
D

Discussion

The current study was undertaken in order to examine the route of penetration across the blood-brain barrier and blood-CSF barrier for small molecular size, lipid insoluble molecules. This was made in the opossum in parallel with uptake studies using radiolabelled markers such as inulin and sucrose, which were presented in Chapter 4. Ideally, the same marker that is used for permeability studies should also be used for tracer studies. However, this is not possible since molecules such as inulin and sucrose are water soluble, difficult to fix in tissue and cannot be readily visualised in the electron microscope. Instead, a lysine fixable biotin-dextran was used that had a molecular weight of 3000 Daltons which is slightly smaller than inulin but larger than sucrose (see Table 2.1). In order to assess the suitability of BDA-3000 as a lipid insoluble tracer molecule, CSF/plasma ratio was measured at three hours for a fluorescent dextran (D-3308) that is structurally similar to BDA-3000 and compared to ratios for inulin, sucrose and L-glucose at the same time points. The dextran reached a ratio similar to that of inulin, but much lower than sucrose and L-glucose as would be expected from its molecular size (Figure 5.9). Under the light microscope, D-3308 and BDA-3000 co-localised in the brain indicating that both markers behave in a similar manner across the brain barriers and also inside the brain (see Figure 5.10). It was necessary to use the fluorescently labelled dextran in order to be able to quantify CSF and plasma concentrations in very small samples and to calculate CSF/plasma ratios. BDA-3000 was preferred for morphological studies because histochemical methods give much better resolution and it can also be made visible for ultrastructural studies. Thus BDA-3000 appeared to be a suitable tracer in order to visualise the pathways from blood to CSF and brain for small lipid insoluble molecules.

Previous studies using electron dense markers have generally been restricted to morphology and lacked parallel physiological experiments, which are essential for

proper understanding of the functional mechanisms involved in brain barriers. These studies have used markers such as HRP (van Deurs et al., 1978; Tauc et al., 1984) and MP (van Deurs, 1978), but the physiological interpretation of these studies is difficult because it is not known whether the cerebral endothelial and choroid plexus epithelial cells handle these tracers similarly to quantitative markers such as inulin and sucrose used in physiological experiments (Ferguson and Woodbury, 1969; Habgood et al., 1993).

Route of penetration of BDA-3000 from plasma into the brain

BDA-3000 was visualised under the light microscope in the brain after intraperitoneal injection in opossums aged between P0 and P30.This showed that BDA-3000 appeared to penetrate into the brain to a lesser extent in older brains compared to younger brains (see Figure 5.11) suggesting a change in brain barrier permeability with age. At all ages cerebral endothelial cells appeared to contain BDA-3000, but there was little staining visible in the extracellular space surrounding blood vessels. This indicates that even as early as birth in the neocortex of the opossum, when blood vessels are only just beginning to appear, the blood-brain barrier to small molecular compounds is already present. It could be argued that the lack of staining around the extracellular space of the blood vessels could be due to dilution of the tracer to an extent that it could not be visualised with the present staining techniques although present. However, this seems unlikely since the staining techniques are very sensitive and would have been able to detect at least a 100-fold dilution of levels in CSF which were clearly visible. Many cells in close association of the ventricular system, in the ventricular zone and sub-ventricular zone, and on the outer surface of the brain were stained in young pups. There was also strong staining of precipitated CSF in the ventricles on the surfaces of the choroid plexus and the neuropendyma. In paraffin sections it was also noted that the strong staining was found in the choroid plexus tissue including a small proportion of

choroid plexus epithelial cells. Furthermore, the proportion of choroid plexus epithelial cells that was positive for BDA-3000 also declined during development. The highest proportion of BDA-3000 positive cells in the lateral ventricular choroid plexus was in the newborn animal and in the 3rd ventricular choroid plexus shortly after it appears at around P5 (see Table 5.2). The proportion of positive cells fell subsequently (earlier in the lateral ventricular choroid plexus) corresponding to the decline in permeability to small lipid insoluble markers (compare Figures 4.2, 5.12 and Table 5.2). The light microscopic study of BDA-3000 localisation in the brain therefore suggests that the route of penetration for lipid insoluble molecules into the early developing brain is across the blood-CSF interface in the choroid plexus and not directly across the blood vessels inside the brain. The intracellular staining of some of the epithelial cells in the choroid plexus suggested that there was an intracellular pathway in the epithelium of the choroid plexus.

The intracellular staining pattern for BDA-3000, that showed a small proportion of stained choroidal epithelial cells was similar to that reported for endogenous albumin by Balslev et al. (1997a) and Knott et al. (1997), in the same species. Balslev et al. (1997a) and Knott et al. (1997) suggested that these albumin positive cells may transfer albumin from the blood into the CSF in early development. The localisation of BDA-3000 and albumin was therefore compared using double labelling immunocytochemistry (see Appendix B for methods). Similar to DAB staining, localisation for BDA-3000 using streptavidin Texas-Red showed that the highest proportion of positive epithelial cells was found in the youngest animals. In all sections studied, choroidal epithelial cells were either double labelled for both BDA-3000 and albumin, or single labelled for BDA-3000 only. Even at P8 when the highest proportion of epithelial cells were found to be positive for albumin in the lateral and 4th ventricular choroid plexus by Knott et al. (1997), the number of BDA-3000 positive cells was higher than albumin positive cells in these choroid plexuses. In no sections were there any epithelial cells single

labelled for albumin (see Figure 5.18). The transfer of native albumin into the CSF during early development is by a specific mechanism that can distinguish between native albumin and other species of albumin (Dziegielewska et al., 1991; Habgood et al., 1992; Knott et al., 1997). The uptake of native albumin into the CSF seems to be the result of a contribution of specific transport and diffusion. Knott et al. (1997) suggested that both the specific transfer of native proteins such as albumin and the passive transfer of other proteins into the brain, are intracellular through a subset of the choroidal epithelial cells. Similar to the study of Knott et al. (1997) the transfer of BDA-3000 also seems to be intracellular since there was a good correlation between BDA-3000 positive choroidal epithelial cells and the decline in steady-state ratios of markers such as inulin and sucrose. In order to resolve in more detail possible routes of entry across the blood-CSF barrier of small lipid insoluble molecules, both the ultrastructure of the choroid plexus and the localisation of BDA-3000 in the choroid plexus were studied during development using the electron microscope.

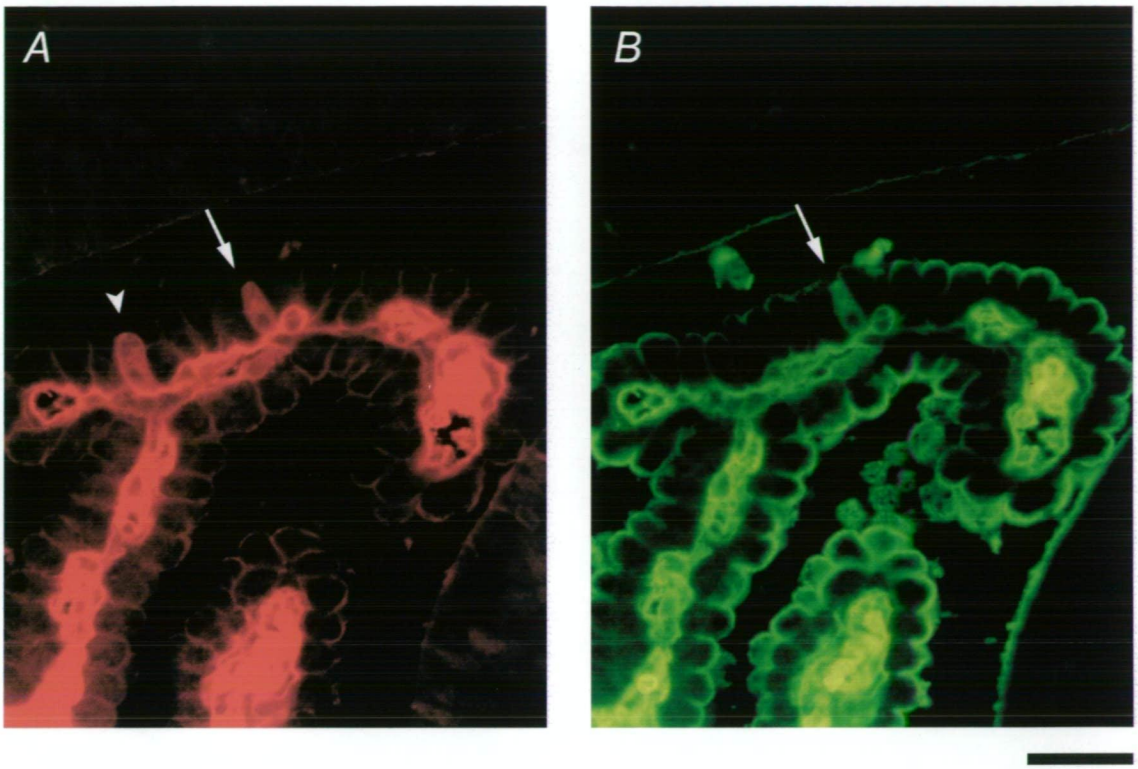

Figure 5.18

Double labelling of BDA-3000 (A) and albumin (B) in the lateral ventricular choroid plexus of a P8 opossum. Albumin was detected using antibodies to human albumin and FITC coupled secondary antibodies, and BDA-3000 was detected using streptavidin conjugated with Texas-red. Arrows indicate a double-labelled cell and the arrowhead indicate a single labelled cell for BDA-3000. The number of cells positive for BDA-3000 was higher than for albumin. No cells were found to be labelled only for albumin.

Scale bar is 30 μm.

Transfer of BDA-3000 across the choroid plexus

BDA-3000 was visualised under the electron microscope after intraperitoneal injection in opossums aged P1 and P13. Ultrathin sections of the choroid plexus revealed that large amounts of reaction product were present within the perivascular space. This shows that there is little or no barrier function of the blood vessels in the choroid plexus since the dextran easily leaked out of them (see Figure 5.14). This is in agreement with previous studies using other tracers such as HRP (Balin and Broadwell, 1988), MP (van Deurs, 1978), and cytochrome c (Milhorat et al., 1973), which all easily leaked out of the blood vessels in the choroid plexus. The dextran may have crossed the endothelial cells in several ways: firstly, the dextran may have passed through the intercellular cleft. Conventional electron microscopy showed that at least a single tight-junctional structure always seemed to be present at the luminal side of the intercellular cleft (see Figure 5.6), which might seem to render this pathway unlikely. However, in thin sections it is difficult to judge whether these junctions are continuous and freeze-etch studies have shown that the tight-junctions in the choroidal endothelial cells are discontinuous (Dermietzel, 1975a). Even if the intercellular clefts were filled with reaction product it is difficult to evaluate whether these tight-junctions were penetrated by the dextran since it was possible that the dextran may have reached the upper part of the intercellular cleft through some other pathway, circumventing the junctions. Secondly, it was noted that endothelial vesicles often contained the dextran and these may have transferred substantial amounts of dextran from the lumen to the perivascular space. Thirdly, the dextran may have crossed directly through the endothelial fenestrations (see Figure 5.6). It is not possible to resolve whether the fenestrations were leaky to the dextran, however, fenestrations have been related to higher permeability in vessels (Dermietzel, 1975a; Brightman and Kaya, 2000). Cells in the extracellular matrix, between the endothelial and epithelial cells, also seem to have little barrier functions since large amounts of reaction product were present in the interepithelial cleft. Under the light microscope it appeared that the dextran was not present in the upper most

apical part of the interepithelial cleft from around P8 and in older animals, however, in the resolution of the light microscope it was not possible to reveal whether this was the case for younger animals as well, because of the pseudostratified appearance of the epithelium. That dextran was not present in the apical intercellular cleft was confirmed by electron microscopy as it seemed to be stopped by junctional structures between epithelial cells at P1 and also in pups at P13 (see Figure 5.17). The contrast and resolution of the thin-sections did not allow for definite identification of these junctional structures, however, the appearance and localisation of these structures strongly suggest that they are tight-junctions (compare Figures 5.8 and 5.17). With conventional electron microscopy it was found that at birth a junctional complex was always present at the most apical part of the interepithelial cleft and that several tight-junctions could be seen within the complex (see Figure 5.8). The tight-junctions in the pups at P0 were not noticeably different from junctions found in older opossums (see below for more discussion). Studies of the movement of other tracers across the blood-CSF barrier in developing animals have been reviewed in Chapter 1 and will therefore only briefly be discussed here. Whether the epithelial tight-junctions prevent the movement of HRP in early development has been a matter of some controversy. Wakai and Hirokawa (1978, 1981) and Bertossi et al. (1988) reported that in the chick the tight-junctions are leaky to HRP during early development (before incubation day 10-11). In contrast, Tauc et al. (1984) showed that the junctions stop HRP as early as E14 in the rat and Dziegielewska et al. (1988) reported that tight-junctions prevent the intercellular movement of HRP at birth in an Australian marsupial, the tamar wallaby. These differences may be species related, however, as has been discussed before in Chapter 1, all the studies in chicks used large amounts of HRP which may have affected the integrity of the brain barriers. Since this could have particularly affected younger fetuses it may have resulted in false appearances indicating that the barriers were not tight early in development. BDA-3000 has a molecular weight less than a tenth of HRP. The present experiments show that the structural barrier to a low molecular weight lipid insoluble tracer, that was shown to

behave in a similar manner to other lipid insoluble molecules across the barrier, appears to be present early in development. The opossum at birth can be compared to a E13-14 rat embryo or a 6-7 week human embryo in regard to brain development (Saunders et al., 1989).

Other structures that have been proposed to be responsible for the higher permeability during development have been vesicles (Tauc et al., 1984). Vesicles were occasionally found that contained the dextran (see Figure 5.15). However, there was no indication whether these vesicles transferred the dextran across the epithelium since none were found to fuse with the cell membranes. Even if these vesicles do transfer molecules from the blood into the CSF it is unlikely that they are responsible for the change in permeability for small lipid insoluble markers during development since there was no difference in the number of vesicles that were labelled with dextran at P1 and P13. Most epithelial cells also contained vacuole-like structures that were found at both P1 and P13 and these seemed to be filled with the dextran (see Figure 5.15). These structures were infrequently seen close to the cell membranes but were never found to fuse with the cell membrane. It is therefore unlikely that they have transporting functions but may have some phagocytic role. Furthermore, these vacuole-like structures were also identified with conventional electron microscopy, yet again, there was no noticeable difference in the number of vacuoles between birth and 64-day old opossums.

Similar to the light microscopic study, the electron microscopic investigation showed that a small proportion of the epithelial cells had large amounts of BDA-3000 intracellularly. The proportion of these cells was much higher at P1 than at P13. The subcellular staining in these cells appeared diffuse which made the interpretation of the results difficult. The diffuse staining may be a consequence of the staining methods. The labelling technique of BDA-3000 using an avidin-peroxidase complex followed by

the DAB reaction is based on an electron dense enzymatic reaction product. The deposition of the reaction product may extend to areas around where the peroxidase complex is present. That the reaction product tended to spread was apparent around heavily stained areas such as the intercellular cleft (see Figure 5.17B). This made it difficult to identify the subcellular presence of the dextran in these cells. Nevertheless, the reaction product was particularly associated with cisternal structures that may be part of the endoplasmic reticulum and was also present in small vesicles in these cells. As has been discussed before, the transfer of albumin has been suggested to be through certain epithelial cells in the choroid plexus (Knott et al., 1997). The double label experiments with albumin and BDA-3000 showed that these co-localised to a high degree (Figure 5.18). Balslev (1997a) studied the uptake of albumin in the choroid plexus using the electron microscope and found that it was present in a system of tubulo-cisternal endoplasmic reticulum. The authors suggested that this system is the route for albumin into the CSF. Whether stained cisternal structures in the present study are the same as the tubulo-cisternal endoplasmic reticulum described by Møllgård and Saunders (1977) and Balslev (1997a) is difficult to conclude because of the diffuse staining. In order to test whether the diffuse staining in the present study is an artefact, another technique has to be applied. Nano-gold labelling could possibly give more specific staining of BDA-3000, however, this technique is also associated with other problems such as penetration limitations of the gold particles.

It cannot be ruled out that the BDA-3000 positive cells may have taken up the dextran from the CSF and not from the blood. The dextran may have gained access to the CSF through some other route and then have been taken up by these cells. This could be tested by localising BDA-3000 in the choroid plexus after administering it directly into the CSF. However, such experiments would be technically very difficult because of the small size of the newborn opossum. The CSF volume of an opossum at birth is only a few microlitres.

Fine structure and function of the choroid plexus during development

The fine structure of the choroid plexus was examined at three developmental ages (P0, P13 and P64) corresponding to ages studied in permeability experiments (see Chapter 4). The different choroid plexuses from each separate ventricle have been reported to have almost matching light microscopic and ultrastructural appearances in late developing and adult animals (Davis et al., 1973; Gomez and Potts, 1981). This may be the reason why the choroid plexus is often referred to as one tissue and results from studies of one choroid plexus are often generalised for all choroid plexuses. As pointed out by Dziegielewska et al. (2001) some authors do not even mention which of the choroid plexuses is used in their studies. Ultrastructural studies of choroid plexus development have mostly used choroid plexus tissue from the lateral ventricles and some from the fourth ventricle, however, comparative studies of all the different choroid plexuses are lacking. To the author's knowledge only very few studies have made comparative investigations of the different choroid plexuses during development using the transmission electron microscope and none seem to have examined the diencephalic (3rd ventricular) choroid plexus. Keep et al. (1986) and Keep and Jones (1990) made quantitative measurements of some morphological features of the developing lateral and 4th ventricular choroid plexuses in the rat. They stated that the development of the two choroid plexuses appeared similar although the timing of morphogenesis was different. Tennyson (1971) studied the same two choroid plexuses of the rabbit, and at some stages of man during development. This study reported several ultrastructural differences of the two choroid plexuses with the most striking being that the epithelial cells of the lateral choroid plexus go through a glycogen rich stage which was much less prominent in the myelencephalic (4th ventricular) choroid plexus. The only other comparative studies of the developing choroid plexuses have

been presented by el-Gammal (1981, 1983) who studied the surface changes of the lateral and third ventricular choroid plexus in embryonic chicks using the scanning electron microscope. These studies showed that the morphogenesis of lateral choroid plexuses was distinct in regard to proximal to distal differentiation whereas the cells in the 3rd choroid plexus appeared to differentiate from several unrelated sites of the choroid plexus.

Kappers (1958) distinguished three stages in the development of the choroid plexus, however, later Shuangshoti and Netsky (1966) and Tennyson and Appas (1968) characterised four stages. The difference in classification is that Shuangshoti and Netsky (1966) and Tennyson and Appas (1968) divided the last stage (stage III) into two separate stages based on stages when the epithelium is poor or rich in glycogen and also on reposition of the nucleus. The opossum follows a similar development to eutherians with the exception that the choroid plexuses seem to be lacking the large amounts of glycogen stored in the epithelial cells as has been observed in eutherians (Dziegielewska et al., 2001). This observation was confirmed in the present study, which did not reveal any glycogen in the epithelial cells at any age. The glycogen has been postulated to be serving as an energy source for the developing brain (Shuangshoti and Netsky, 1966). The reason for the lack of glycogen in the opossum is not clear, however, Dziegielewska et al. (2001) suggested that the explanation may be related to the higher oxygen tension in a species developing outside the uterus compared to *in utero*. As the opossum seems to lack glycogen, its choroid plexus can be divided into three stages of development, starting with a single columnar pseudostratified layer of epithelial cells, changing into a columnar layer and then further flattens into a cuboidal layer (see Figures 5.2 and 5.3). In the course of development, the choroid plexuses in each ventricle seem to exhibit similar microscopic changes. At birth in the opossum, most parts of the fourth ventricular choroid plexus were in stage II and some in stage I, whereas most of the lateral ventricular choroid plexus was in stage I. At P13, almost all

of the choroid plexuses were in stage II, except for a small part in the root of the choroid plexus that still had a somewhat pseudostratified appearance. At P64 the choroid plexus epithelium formed a uniform layer in stage III. Not only does it seem that each individual choroid plexus goes through similar developmental changes but also within each choroid plexus the maturation process is repeated. The choroid plexus shows distal to proximal differentiation of cells. The cells at the root of the choroid plexus are less mature than the ones in the more distal parts of the choroid plexus villi. This is in agreement with the belief that the choroid plexus grows from the proximal parts where the cells show a pseudostratified appearance until later in development. At P64 when the choroid plexuses can be expected to have stopped growing, the whole choroid plexus appears to form a uniform layer.

The three stages of choroid plexus development were associated with several ultrastructural changes in both the core of the choroid plexus but more noticeably in the epithelial cells. The choroid plexus of the opossum showed similar ultrastructural changes during development that have been reported in other mammalian species such as rats (Cancilla et al., 1966; Keep et al., 1986; Keep and Jones, 1990), mice (Sturrock, 1979; Zaki, 1981) and rabbits (Tennyson and Appas, 1968) with one noticeable difference in that no glycogen was found in the developing opossum choroid plexus. Several of these changes are probably a reflection of progressive specialisation of the choroid plexus as a highly secreting epithelium during development. That the choroid plexus CSF production rate increases with development has been demonstrated by Bass and Lundborg (1973), Evans et al. (1974), and Johanson and Woodbury (1974). This is not just due to an increase in overall mass of the choroid plexus but also to an increase in production per weight of choroid plexus tissue (Johanson and Woodbury, 1974). That one of the main functions of the choroid plexus is to produce CSF is today unquestioned. During development there was an increase in mitochondrial content mainly as a result of an increase in the number of mitochondria but also due to an

increase in the size of individual mitochondria. The increase in mitochondrial content of the epithelial cells is probably a reflection of an increase in CSF production of the choroid plexus. The production of CSF is a secretory process and therefore is dependant on energy. The production of CSF is dependant on fluid transfer between the blood vessels and into the epithelial cells. The increase in fenestrations of the blood vessels and basal infolding of the epithelial cells may be a reflection of this increase in fluid transfer. As well as producing CSF, the choroid plexus is also responsible for a constant regulation of the composition of the CSF. Several studies have shown that the regulation and transfer of ions by the choroid plexus is greatly increased during development (Jones and Keep, 1987; Parmelee and Johanson, 1989; Parmelee et al., 1991; Preston et al., 1993). Structures such as microvilli and cilia on the apical surface, and numerous pinocytotic vesicles are probably an indication of an increase in exchange between the apical cell surface and the ventricular CSF. The opossum also showed a distinct change in the structure of the nucleus of the epithelial cells during development from being irregular in shape with great invaginations to almost spherical with a smooth membrane. Similar developmental changes in nuclear structure of the epithelial cells have been described before in mice by Dohrmann and Herdson (1969). These authors suggested that the lobulated nucleus along with a high abundance of rough endoplasmic reticulum and polyribosomes in the interlobulated cytoplasm were a reflection of greater interaction between the nucleus and cytoplasm in younger animals. More evidence that the changes in the ultrastructure of the choroid plexus presented in this study is a reflection of its functional development comes from studies of the aging choroid plexus. In rats, both morphological and functional changes during development appears to be reversed with aging; for instance, there is a decrease in the number of microvilli with age (Serot et al., 2001), while there is a reduction in the CSF secretion in older rats (Preston, 2001).

One of the main aims of the present ultrastructural study was to investigate the presence

of tight-junctions between adjacent epithelial cells. Using the goniometric tilting device, several tight-junctions were often found within the junctional complex. The tight-junctions appeared as points along the intercellular cleft where the two cell membranes of neighbouring epithelial cells were touching each other; this is similar to tight-junctions that have been described between epithelial and endothelial cells of other mammals (Tennyson and Appas, 1968; Bouchaud and Bouvier, 1978; Stewart and Hayakawa, 1987; Peters et al., 1991; Schulze and Firth, 1992; Sedlakova et al., 1999). These tight-junctional structures appeared similar at all ages showing that the structural basis for the brain barriers is formed early in development. Other studies have reported differences in endothelial tight-junctions using the goniometric tilting device (Stewart and Hayakawa, 1987). It therefore does not seem that structural changes in the tight-junctions can explain the changes in permeability to low molecular weight markers with age. The tight-junctions form a complex network at the apical part of the intercellular cleft. Serial sectioning can follow a junction a shorter distance but it has to be mentioned that establishing whether there are gaps in the junctional network is difficult using this technique. In order to determine whether there are openings in the tight-junctional network a freeze-fracture study is needed. In freeze-fracture, the cell membrane is cleaved and junctions appear as ridges or grooves depending which side of the fractured membrane is visualised. This technique enables visualisation of the whole network of junctions between two adjacent cells in one preparation and is therefore a more practical technique of determining whether there are gaps in the junctions. This technique can also determine the complexity of the overall junctional network. Thin-section electron microscopy and freeze-fracture studies of epithelial tight-junctions during development have been discussed in Chapter 1 and will therefore not be discussed in detail in this Chapter. Briefly, studies have not found any significant differences in either tight-junctional appearance in thin-sections or the complexity of the junctional network in freeze-fracture preparations of choroid plexus epithelial cells between developing and adults animals (Tennyson and Appas, 1968; Dermietzel et al.,

1977; Møllgård et al., 1979; Tauc et al., 1984).

Under the electron microscope the epithelial cells showed differences in their overall density, ranging from a light to dark appearance, but otherwise there was no difference in structure observed. These variations have also been reported in other species (Dohrmann, 1970; van Deurs et al., 1978; Sturrock, 1979). Dohrmann (1970) suggested that these differences in appearance of cells may represent different states of cell hydration but others have considered them as artefacts of fixation. Sturrock (1979) quantitated the dark and light cells in mice and found that the dark cells first appeared at E14, constituted around 12% of all the epithelial cells, and that this fraction remained almost constant up to 90 days after birth. Similar to Dohrmann (1970), the authors postulated that the dark cells may be dehydrated and reduced in size based on the fact that these cells had thinner microvilli than surrounding cells. In the present study, it seems unlikely that these differences can be explained by timing of fixation since the choroid plexus was dissected out and fixed by immersion immediately after animals were killed. The single layer of epithelial cells would have been exposed to the fixative instantly and was therefore presumably rapidly and uniformly fixed. There was no obvious pattern in the distribution of light and dark cells and dark cells were often found interspersed in the epithelium. It is still not known whether these morphological differences in cell density are of functional importance.

Summary

The uptake of a fluorescently labelled dextran (D-3308) showed that dextrans are suitable tracers for lipid insoluble molecules across the brain barriers. The lack of staining for BDA-3000 around blood vessels and in the extracellular space of the brain demonstrates that the blood-brain barrier is formed at birth in the opossum. The reaction product was particularly abundant in cells of the ventricular zone, precipitated CSF and

in the choroid plexus suggesting that the route for BDA-3000 into the brain could be via the choroid plexus and not across the brain blood vessels. Tight-junctional structures between adjacent epithelial cells seemed to impede the extracellular movement of BDA-3000. This suggests that the dextran reached the CSF through an intracellular pathway in the choroid plexus. This intracellular pathway may be through some of the epithelial cells of the choroid plexus since the proportion of epithelial cells with intracellular staining of BDA-3000 declined in a similar manner to the reduction in steady-state ratios for inulin and sucrose. The very few blood vessels found early in development supports the hypothesis that these do not constitute a major route of entry for lipid insoluble molecules into the brain at this early age. This study could only suggest that this possible intracellular route at the subcellular level is associated with the endoplasmic reticulum. Experiments using some other labelling technique may be able to answer this question.

Two main conclusions can be drawn from the ultrastructural study of the opossum choroid plexus. Firstly, at birth in the opossum, which can be compared to an E13-E14 rat embryo regarding general brain development, the ultrastructural basis for the blood-CSF barrier is already present in that tight-junctions with a mature appearance were visible between epithelial cells. Secondly, apart from the lack of glycogen, the morphogenesis of the choroid plexus in the opossum is similar to what has been described in other mammals both at immature and mature stages. This shows that the opossum choroid plexus seems to be a good model to study the functional development of the choroid plexus.

Chapter 6

*

Conclusions

The experiments presented in this thesis measured the uptake and visualised the route of entry for low molecular weight, lipid insoluble molecules from the blood into the CNS from early development stages until young adulthood. The main strength of these experiments was that permeability, tracer and morphological studies have been carried out in the same species over a similar developmental period. These experiments are therefore directly comparable with respect to developmental stages and also uncertainties about species variations are avoided. The present experiments together with previous studies (Dziegielewska et al., 1989; Knott et al., 1997; Li et al., 1997) mean that the grey short-tailed South-American opossum is now one of most studied mammalian models of transfer mechanisms into the developing brain.

Transfer of small lipid insoluble molecules into the developing brain

In order to study the uptake of radiolabelled markers into the brain and CSF of newborn opossums, a new experimental model had to be developed since previously used methods in other species were not suitable due to the small size of the animals. The model, which is described in Chapter 3, estimated steady-state concentration ratios between blood and CSF or brain in animals after a single ip injection without invasive surgery. The accuracy of determining steady-state ratios in this way was determined by comparing ratios obtained from intact animals with ratios from nephrectomised animals that had been shown to approach steady-states between plasma, CSF and brain. It was shown that the model could accurately estimate steady-state concentration ratios. The new model therefore can be used to study the uptake of molecules from blood to different body compartments with minimal manipulation of animals. It was further used to study the uptake of several radiolabelled markers of various sizes into the brain and CSF during development. These experiments, presented in Chapter 4 showed that the steady-state concentration ratios for low molecular weight, lipid insoluble molecules were high in early development and that they declined with age, particularly in youngest

animals. This is the earliest stage of brain development that such studies have been carried out. The decrease in steady-state ratios during development was shown to be due to a reduction in permeability of the interfaces between the blood-brain and blood-CSF. A plot of steady-state ratios and diffusion coefficient for radioactive markers in the opossum, and including data on succinylated albumin from Knott et al. (1997) is illustrated in Figure 6.1. This shows that in the opossum, at early stages of brain development, there is an inverse correlation between diffusion coefficient and steady-state CSF/plasma ratios. Furthermore, with increasing developmental age there is a parallel decline in these curves. This suggests that the penetration of lipid insoluble molecules into CSF is probably by unrestricted diffusion through some water filled 'pore' (see Dziegielewska et al., 1979). Moreover, it implies that there is a decrease in the number of such pores with age rather than a decrease in pore diameter, which would have been expected to alter the slope of curves between steady-state CSF/plasma ratios and diffusion coefficient (Dziegielewska et al., 1979; Habgood et al., 1993). However, the experiments in Chapter 4 could not determine which of the blood-CNS interfaces were avenues of entry for these molecules. With the use of a small dextran tracer the experiments presented in Chapter 5 showed that the major route into the brain for small lipid insoluble molecules appears to be from the blood vessels of the choroid plexus, across the choroidal epithelial cells, and then into brain tissue via the CSF. There was little evidence that the dextran crossed the endothelial cells of cerebral blood vessels directly into brain tissue. Although the cerebral endothelial cells stained for BDA-3000, none could be detected in the extracellular space around the blood vessels. This was in contrast to the strong staining for BDA-3000 in the CSF.

The possible routes of entry for lipid insoluble molecules through the cells of the brain barriers are shown in Figure 1.2. Several of these pathways can most certainly be ruled out as major contributors to the transfer of lipid insoluble molecules across the barriers such as receptor- and carrier-mediated trancytosis and absorptive-mediated transfer.

These transfer mechanisms can only be used by molecules of certain configuration and charge. Moreover, the quantitative permeability experiments showed that these molecules are transferred in a passive manner and not by a facilitated mechanism. Another possible route for small lipid insoluble molecules into the brain could be through the intercellular cleft including the *zonulae occludentes*. Structural changes of the tight-junctions producing increased restrictions on the movement of molecules through the intercellular cleft during development, could then explain the decrease in permeability with age. However, the present studies using BDA-3000 do not support this theory. The dextran seemed to be impeded by tight-junctional structures in the choroid plexus already at birth whereas there was a significant decrease in the brain barrier permeability of radiolabelled markers after birth. Furthermore, the ultrastructural investigation did not reveal any differences in the appearance of the tight-junctions in the CNS between newborn opossums and young adults. This would have been expected if structural changes of these junctions were responsible for the decline in permeability with age. The postulated pore could be a water-filled intracellular pathway through the cells as was suggested by Balslev et al. (1997a). Both the light and electron microscopic study demonstrated an intracellular distribution of BDA-3000 in the choroidal epithelial cells suggesting that the dextran may have an intracellular pathway through a small proportion of the epithelial cells of the choroid plexus. Moreover, this intracellular pathway appeared to diminish during brain maturation which would fit with the hypothesis that this pathway is responsible for the higher permeability in young animals. The particular electron microscopic method used did not localise this possible intracellular pathway precisely because of uncertainties about reaction product diffusion. This problem can be further studied by the use of immunogold labelling.

The present study demonstrated that brain barriers are certainly present at early stages of development, although their properties are different from those of the adult animal. The strength of the current studies is that physiological and morphological approaches

have been combined in the same preparation, so that it is possible to draw conclusions about the structural basis for the permeability changes observed. Without the morphological studies in these experiments, one could interpret the observed high permeability of the brain barriers in young animals to be due to the barriers simply not being properly developed at early stages of development. However, the morphological studies showed that the ultrastructural basis for the blood-CSF barrier (tight-junctions) is present very early in development. Subsequently, if the transfer of molecules into the CSF is higher in development because of a developmentally regulated intracellular pathway, this can be regarded as a specialisation of the transfer mechanism across the brain barriers in early development rather than a reflection of poorly developed barriers. It is difficult to hypothesise about the exact physiological importance for such transfer mechanisms. However, they may be important for the provision of a suitable environment for the growing brain. There is a high concentration of protein in the CSF in early development which at least for albumin has been shown to be due to specialised transporting mechanisms across choroid plexus cells that is only present in the developing brain (Habgood, 1990; Dziegielewska et al., 1991; Knott et al. 1997). The high levels of proteins in the CSF have been postulated to be a driving force for normal brain enlargement and also to provide nutrients for the growing brain (Dziegielewska et al., 2001). The transfer mechanisms at the choroid plexus for low molecular weight, lipid insoluble molecules in the CSF may have similar functions.

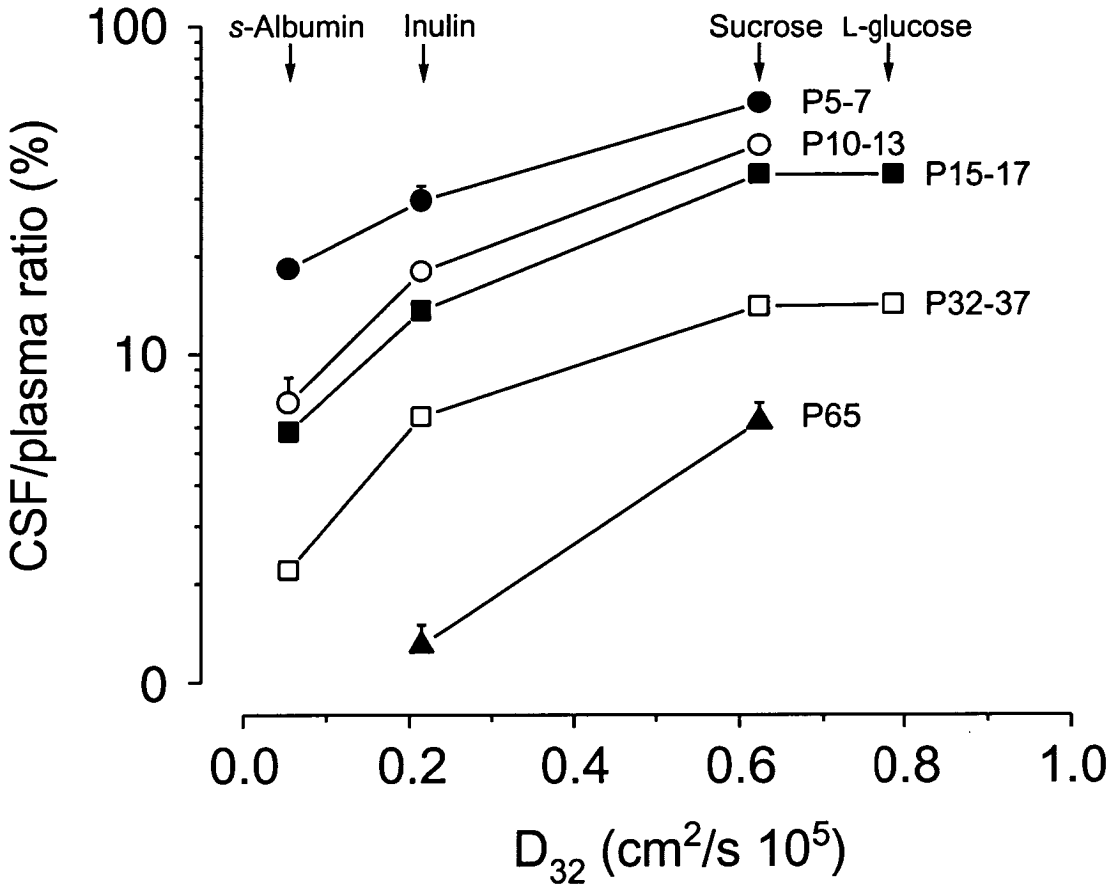

Figure 6.1

Steady-state CSF/plasma ratios (y-axis, note logarithmic scale) against the diffusion coefficients (D_{32}) for molecules of various molecular sizes (x-axis) in P5-P7 (●), P10-P13 (○), P15-P17 (■), P32-P37 (□), and P65 (▲) opossums. Diffusion coefficients were calculated for 32°C, as this is the normal body temperature for opossums. Data for succinylated albumin (*s*-Albumin) are from Knott et al. (1997). Values shown are means (n=3-10) and the error bars are ± SEM. Where no error bars are visible, they are obscured by the symbols. There was a parallel decrease in the curves between CSF/plasma ratios and diffusion coefficients with increasing postnatal age

Further studies

The model and techniques described in this thesis could be used for several further studies of transfer mechanisms into the brain. Under the light microscope it appeared that BDA-3000 was taken up by endothelial cells within the brain but did not appear to escape from these into the surrounding brain tissue. It would be interesting to determine the subcellular distribution of BDA-3000 in endothelial cells. This could also determine whether there is a paracellular pathway of the tracer in the developing blood vessels. Since BDA-3000 did not appear to escape the blood vessels in the brain it could be expected that intercellular movement of BDA-3000 between endothelial cells is already restricted by tight-junctions at early stages of brain development, as has been demonstrated in this thesis for the *zonulae occludentes* between choroidal epithelial cells. BDA-3000 could also be used to study the barriers situated within the meninges and the pial surface of the brain which are fluid interfaces of the brain have been almost forgotten in studies of exchange between blood, brain and CSF. Several species have been found to have developmentally regulated intercellular junctions (strap-junctions) of the ependymal lining of the brain ventricles. Whether such junctions exist in the opossum is not known but would be of interest to examine.

This thesis presents quantitative data on the uptake of several markers (L-glucose, sucrose and inulin) from blood to brain and CSF along with a visualisable tracer BDA-3000, that is of similar size to inulin. There are now several other small tracers that could be used to study transfer mechanisms into the brain. It will, however, be essential to check whether each tracer behaves in a comparable manner across the brain barriers to other small lipid insoluble molecules before they should be used as tracers. This has been overlooked in previous studies with other tracers. Biotin-dextrans are only available in sizes larger then BDA-3000. However, several other neuronal tracers are derivates of biotin and may be suitable as low molecular weight tracers. Biocytin,

neurobiotin and biotin cadaverine are all water soluble low molecular weight tracers (molecular weight range of about 250-800 Daltons) that all have amine residues and can therefore be fixed using aldehydes. They can be visualised with similar techniques to biotin-dextrans and are also available with flourophore conjugates. This means they could easily be quantitated using the same methods as in this thesis in order to test whether their transfer mechanisms into the brain can be expected to be similar to biotin-dextrans and other lipid insoluble compounds.

References

Adinolfi M. (1985). The development of the human blood-CSF-brain barrier. *Developmental Medicine and Child Neurology* **27**: 532-537.

Allt G and Lawrenson JG. (1997). Is the pial microvessel a good model for blood-brain barrier studies? *Brain Research. Brain Research Reviews* **24**: 67-76.

Angelov DN. (1990a). Ultrastructural characteristics of the cranial dura mater-arachnoid interface layer. *Zeitschrift für Mikroskopisch-Anatomische Forschung* **104**: 982-990.

Angelov DN. (1990b). Ultrastructural investigation of the meningeal compartment of the blood-cerebrospinal fluid-barrier in rats and cats. A horseradish peroxidase study. *Zeitschrift für Mikroskopisch-Anatomische Forschung* **104**: 1-16.

Angelov DN and Vasilev VA. (1988). Electron microscopic study of cat meninges. *Anatomischer Anzeiger* **166**: 1-8.

Angelov DN and Vasilev VA. (1989). Morphogenesis of rat cranial meninges. A light- and electron-microscopic study. *Cell and Tissue Research* **257**: 207-216.

Audus KL. (1999). Controlling drug delivery across the placenta. *European Journal of Pharmaceutical Sciences* **8**: 161-165.

Bain MD, Copas DK, Landon MJ and Stacey TE. (1988). In vivo permeability of the human placenta to inulin and mannitol. *Journal of Physiology* **399**: 313-319.

Balin BJ and Broadwell RD. (1988). Transcytosis of protein through the mammalian cerebral epithelium and endothelium. I. Choroid plexus and the blood-cerebrospinal fluid barrier. *Journal of Neurocytology* **17**: 809-826.

Balin BJ, Broadwell RD, Salcman M and el-Kalliny M. (1986). Avenues for entry of peripherally administered protein to the central nervous system in mouse, rat, and squirrel monkey. *Journal of Comparative Neurology* **251**: 260-280.

Balslev Y, Dziegielewska KM, Møllgård K and Saunders NR. (1997a). Intercellular barriers to and transcellular transfer of albumin in the fetal sheep brain. *Anatomy and Embryology* **195**: 229-236.

Balslev Y, Saunders NR and Møllgård K. (1997b). Ontogenetic development of diffusional restriction to protein at the pial surface of the rat brain: an electron microscopical study. *Journal of Neurocytology* **26**: 133-148.

Bamforth SD, Kniesel U, Wolburg H, Engelhardt B and Risau W. (1999). A dominant mutant of occludin disrupts tight junction structure and function. *Journal of Cell Science* **112**: 1879-1888.

Bass NH and Lundborg P. (1973). Postnatal development of bulk flow in the cerebrospinal fluid system of the albino rat: clearance of carboxyl-(^{14}C)inulin after intrathecal infusion. *Brain Research* **52**: 323-332.

Bauer H, Sonnleitner U, Lametschwandtner A, Steiner M, Adam H and Bauer HC. (1995). Ontogenic expression of the erythroid-type glucose transporter (Glut 1) in the telencephalon of the mouse: correlation to the tightening of the blood-brain barrier. *Brain Research. Developmental Brain Research* **86**: 317-325.

Bauer HC, Bauer H, Lametschwandtner A, Amberger A, Ruiz P and Steiner M. (1993). Neovascularization and the appearance of morphological characteristics of the blood-brain barrier in the embryonic mouse central nervous system. *Brain Research. Developmental Brain Research* **75**: 269-278.

Becker NH and Almazon R. (1968). Evidence for the functional polarization of micropinocytotic vesicles in the rat choroid plexus. *Journal of Histochemistry and Cytochemistry* **16**: 278-280.

Becker NH, Novikoff AB and Zimmerman HM. (1967). Fine structure observations of the uptake of intravenously injected peroxidase by the rat choroid plexus. *Journal of Histochemistry and Cytochemistry* **15**: 160-165.

Begley DJ. (1992). Peptides and the blood-brain barrier. In: *Handbook of Experimental Pharmacology. Physiology and Pharmacology of the Blood-Brain Barrier.* MWB Bradbury (ed). pp 151-203. Springer-Verlag, Berlin.

Behnsen G. (1927). Über die farbstoffspeicherung im zentralnervensystem der weissen maus in verschiedenen alterzusständen. *Zeitschrift für Zellforschung und Mikrosckopische Anatomie* **4**: 515-572.

Bertossi M, Ribatti D, Nico B, Mancini L, Lozupone E and Roncali L. (1988). The barrier systems in the choroidal plexuses of the chick embryo studied by means of horseradish peroxidase. *Journal of Submicroscopic Cytology and Pathology* **20**: 385-395.

Biedl A and Kraus R. (1898). Über einer bisher unbekannte toxische wirkung der gallensäuren auf das zentralnervensystem. *Zentralblatt für innere Medizin* **19**: 1185-1200.

Birge WJ,.Rose AD, Haywood JR and Doolin PF. (1974). Development of the blood-cerebrospinal fluid barrier to proteins and differentiation of cerebrospinal fluid in the chick embryo. *Developmental Biology* **41**: 245-254.

Bohr V and Møllgård K. (1974). Tight junctions in human fetal choroid plexus visualized by freeze-etching. *Brain Research* **81**: 314-318.

Bolton SJ, Anthony DC and Perry VH. (1998). Loss of the tight junction proteins occludin and zonula occludens-1 from cerebral vascular endothelium during neutrophil-induced blood-brain barrier breakdown in vivo. *Neuroscience* **86**: 1245-1257.

Borst P and Schinkel AH. (1998). P-glucoselycoprotein, a guardian of the brain. In: *Introduction to the blood-brain barrier: methodology, biology and pathology*. WM Pardridge (ed). pp 198-206. University Press, Cambridge.

Bouchaud C and Bouvier D. (1978). Fine structure of tight junctions between rat choroidal cells after osmotic opening induced by urea and sucrose. *Tissue and Cell* **10**: 331-342.

Bouldin TW and Krigman MR. (1975). Differential permeability of cerebral capillary and choroid plexus to lanthanum ion. *Brain Research* **99**: 444-448.

Brightman MW. (1968). The intracerebral movement of proteins injected into blood and cerebrospinal fluid of mice. *Progress in Brain Research* **29**: 19-40.

Brightman MW and Kaya M. (2000). Permeable endothelium and the interstitial space of brain. *Cellular and Molecular Neurobiology* **20**: 111-130.

Brightman MW and Reese TS. (1969). Junctions between intimately apposed cell membranes in the vertebrate brain. *Journal of Cell Biology* **40**: 648-677.

Broman T. (1941). The possibilities of the passage of substances from the blood to the central nervous system. *Acta Psychiatrica Scandinavica* **16**: 1-25.

Brunjes PC, Jazaeri A and Sutherland MJ. (1992). Olfactory bulb organization and development in Monodelphis domestica (grey short-tailed opossum). *Journal of Comparative Neurology* **320**: 544-554.

Butt AM, Jones HC and Abbott NJ. (1990). Electrical resistance across the blood-brain barrier in anaesthetized rats: a developmental study. *Journal of Physiology* **429**: 47-62.

Cabana T. (2000). The development of mammalian motor systems: the opossum Monodelphis domestica as a model. *Brain Research Bulletin* **53**: 615-626.

Caley DW and Maxwell DS. (1970). Development of the blood vessels and extracellular spaces during postnatal maturation of rat cerebral cortex. *Journal of Comparative Neurology* **138**: 31-47.

Cancilla PA, Zimmerman HM and Becker NH. (1966). A histochemical and fine structure study of the developing rat choroid plexus. *Acta Neuropathologica* **6**: 188-200.

Castel M, Sahar A and Erlij D. (1974). The movement of lanthanum across diffusion barriers in the choroid plexus of the cat. *Brain Research* **67**: 178-184.

Catala M. (1998). Embryonic and fetal development of structures associated with the cerebro-spinal fluid in man and other species. Part I: The ventricular system, meninges and choroid plexuses. *Archives D Anatomie et de Cytologie Pathologiques* **46**: 153-169.

Cavanagh ME, Cornelis ME, Dziegielewska KM, Evans CA, Lorscheider FL, Møllgård K, Reynolds ML and Saunders NR. (1983). Comparison of proteins in CSF of lateral and IVth ventricles during early development of fetal sheep. *Brain Research* **313**: 159-167.

Chamberlain JG. (1973). Analysis of developing ependymal and choroidal surfaces in rat brains using scanning electron microscopy. *Developmental Biology* **31**: 22-30.

Chen Yh, Lu Q, Schneeberger EE and Goodenough DA. (2000). Restoration of tight junction structure and barrier function by down-regulation of the mitogen-activated protein kinase pathway in ras-transformed Madin-Darby canine kidney cells. *Molecular Biology of the Cell* **11**: 849-862.

Claude P and Goodenough DA. (1973). Fracture faces of zonulae occludentes from "tight" and "leaky" epithelia. *Journal of Cell Biology* **58**: 390-400.

Clough G and Michel CC. (1981). The role of vesicles in the transport of ferritin through frog endothelium. *Journal of Physiology* **315**: 127-142.

Connell CJ and Mercer KL. (1974). Freeze-fracture appearance of the capillary endothelium in the cerebral cortex of mouse brain. *American Journal of Anatomy* **140**: 595-599.

Cornford EM. (1998). The carotid artery single injection technique. In: *Introduction to the blood-brain barrier: methodology, biology and pathology.* WM Pardridge (ed). pp 11-23. University Press, Cambridge.

Crone C. (1984). Lack of selectivity to small ions in paracellular pathways in cerebral and muscle capillaries of the frog. *Journal of Physiology* **353**: 317-337.

Crone C and Olesen SP. (1982). Electrical resistance of brain microvascular endothelium. *Brain Research* **241**: 49-55.

Cserr H. (1965). Potassium exchange between cerebrospinal fluid, plasma, and brain. *American Journal of Physiology* **209**: 1219-1226.

Cserr HF and Bundgaard M. (1984). Blood-brain interfaces in vertebrates: a comparative approach. *American Journal of Physiology* **246**: R277-288.

Dambska M. (1995). The vascularization of the developing human brain. *Folia Neuropathologica* **33**: 189-193.

Davis DA, Lloyd BJJ and Milhorat TH. (1973). A comparative ultrastructural study of the choroid plexuses of the immature pig. *Anatomical Record* **176**: 443-454.

Davis JE and Garrison NE. (1968). Mean weights of chick embryos correlated with the stages of Hamburger and Hamilton. *Journal of Morphology* **124**: 79-82.

Davson H. (1955). A comparative study of the aqueous humour and cerebrospinal fluid in the rat. *Journal of Physiology* **129**: 111-133.

Davson H and Segal MB. (1969). Effect of cerebrospinal fluid on volume of distribution of extracellular markers. *Brain* **92**: 131-136.

Delorme P. (1972). Différenciation ultrastructurale des jonctions intercellulaires de l'endothelium des capillaires telencephaliques chez l'embron de poulet. *Zeitschrift fur Zellforschung und Mikroskopische Anatomie* **133**: 571-582.

Delorme P, Gayet J and Grignon G. (1970). Ultrastructural study on transcapillary exchanges in the developing telencephalon of the chicken. *Brain Research* **22**: 269-283.

Dermietzel R. (1975a). Junctions in the central nervous system of the cat. IV. Interendothelial junctions of cerebral blood vessels from selected areas of the brain. *Cell and Tissue Research* **164**: 45-62.

Dermietzel R. (1975b). Junctions in the central nervous system of the cat. V. The junctional complex of the pia-arachnoid membrane. *Cell and Tissue Research* **164**: 309-329.

Dermietzel R, Meller K, Tetzlaff W and Waelsch M. (1977). In vivo and in vitro formation of the junctional complex in choroid epithelium. A freeze-etching study. *Cell and Tissue Research* **181**: 427-441.

Dermietzel R and Schunke D. (1975). A complex junctional system in endothelial and connective tissue cells of the choroid plexus. *American Journal of Anatomy* **143**: 131-136.

Derossi D, Chassaing G and Prochiantz A. (1998). Trojan peptides: the penetratin system for intracellular delivery. **8**: 84-87.

Desmond ME. (1985). Reduced number of brain cells in so-called neural overgrowth. *Anatomical Record* **212**: 195-198.

Desmond ME and Jacobson AG. (1977). Embryonic brain enlargement requires cerebrospinal fluid pressure. *Developmental Biology* **57**: 188-198.

Dohrmann GJ. (1970). Dark and light epithelial cells in the choroid plexus of mammals. *Journal of Ultrastructure Research* **32**: 268-273.

Dohrmann GJ and Bucy PC. (1970). Human choroid plexus: a light and electron microscopic study. *Journal of Neurosurgery* **33**: 506-516.

Dohrmann GJ and Herdson PB. (1969). Lobated nuclei in epithelial cells of the choroid plexus of young mice. *Journal of Ultrastructure Research* **29**: 218-223.

Dohrmann GJ and Herdson PB. (1970). The choroid plexus of the mouse: a macroscopic, microscopic and fine structural study. *Zeitschrift für Mikroskopisch-Anatomische Forschung* **82**: 508-522.

Doolin PF and Birge WJ. (1969). Ultrastructural differentiation of the junctional complex of the avian choroidal epithelium. *Journal of Comparative Neurology* **136**: 253-267.

Drewes LR. (1998). Biology of the blood-brain glucose transporter. In: *Introduction to the blood-brain barrier: methodology, biology and pathology*. WM Pardridge (ed). pp 165-174. University Press, Cambridge.

Dudzinski DS and Cutler RW. (1974). Spinal subarachnoid perfusion in the rat: glycine transport from spinal fluid. *Journal of Neurochemistry* **22**: 355-361.

Dziegielewska KM, Ek J, Habgood MD and Saunders NR. (2001). Development of the choroid plexus. *Microscopy Research and Technique* **52**: 5-20.

Dziegielewska KM, Evans CA, Malinowska DH, Møllgård K, Reynolds JM, Reynolds ML and Saunders NR. (1979). Studies of the development of brain barrier systems to lipid insoluble molecules in fetal sheep. *Journal of Physiology* **292**: 207-231.

Dziegielewska KM, Evans CA, Malinowska DH, Møllgård K, Reynolds ML and Saunders NR. (1980). Blood-cerebrospinal fluid transfer of plasma proteins during fetal development in the sheep. *Journal of Physiology* **300**: 457-465.

Dziegielewska KM, Habgood M, Jones SE, Reader M and Saunders NR. (1989). Proteins in cerebrospinal fluid and plasma of postnatal Monodelphis domestica (grey short-tailed opossum). *Comparative Biochemistry and Physiology. B: Comparative Biochemistry* **92**: 569-576.

Dziegielewska KM, Habgood MD, Møllgård K, Stagaard M and Saunders NR. (1991). Species-specific transfer of plasma albumin from blood into different cerebrospinal fluid compartments in the fetal sheep. *Journal of Physiology* **439**: 215-237.

Dziegielewska KM, Hinds LA, Møllgård K, Reynolds ML and Saunders NR. (1988). Blood-brain, blood-cerebrospinal fluid and cerebrospinal fluid-brain barriers in a marsupial (Macropus eugenii) during development. *Journal of Physiology* **403**: 367-388.

Egleton RD and Davis TP. (1997). Bioavailability and transport of peptides and peptide drugs into the brain. *Peptides* **18**: 1431-1439.

Ehrlich P. (1885). Das sauerstoff-bedurfnis des organismus. Eine farbenanalytische studie. Hirschwald, Berlin.

Ehrlich P. (1887). Zur therapeutischen bedutung der subslituirenden schwefelsauregruppe. *Therap. Monatsh.* **1**: 88-90.

Ehrlich P. (1904). Über die beziehungen von chemischer constitution, vertheilung, und pharmakologischer wirkung. Hirschwald, Berlin.

Ek CJ, Habgood MD, Dziegielewska KM, Potter A and Saunders NR. (2001). Permeability and route of entry for lipid insoluble molecules across brain barriers in developing Monodelphis domestica. *Journal of Physiology* **536**: 841-853.

el-Gammal S. (1981). The development of the diencephalic choroid plexus in the chick. A scanning electron-microscopic study. *Cell and Tissue Research* **219**: 297-311.

el-Gammal S. (1983). Regional surface changes during the development of the telencephalic choroid plexus in the chick. A scanning-electron microscopic study. *Cell and Tissue Research* **231**: 251-263.

Evans CA, Reynolds JM, Reynolds ML, Saunders NR and Segal MB. (1974). The development of a blood-brain barrier mechanism in foetal sheep. *Journal of Physiology* **238**: 371-386.

Feder N. (1971). Microperoxidase. An ultrastructural tracer of low molecular weight. *Journal of Cell Biology* **51**: 339-343.

Felgenhauer K. (1974). Protein size and cerebrospinal fluid composition. *Klinische Wochenschrift* **52**: 1158-1164.

Fenstermacher JD, Blasberg RD and Patlak CS. (1981). Methods for quantifying the transport of drugs across the brain barrier systems. *Pharmacology & Therapeutics* **14**: 217-248.

Ferguson RK and Woodbury DM. (1969). Penetration of ^{14}C-inulin and ^{14}C-sucrose into brain, cerebrospinal fluid, and skeletal muscle of developing rats. *Experimental Brain Research* **7**: 181-194.

Flexner LB. (1938). Changes in the chemistry and nature of the cerebrospinal fluid during foetal life in the pig. *American Journal of Physiology* **124**: 131-135.

Fossan G, Cavanagh ME, Evans CA, Malinowska DH, Møllgård K, Reynolds ML and Saunders NR. (1985). CSF-brain permeability in the immature sheep fetus: a CSF-brain barrier. *Brain Research* **350**: 113-124.

Frelin C and Vigne P. (1998). Ions channels in endothelial cells. In: *Introduction to the blood-brain barrier: methodology, biology and pathology*. WM Pardridge (ed). pp 214-220. University Press, Cambridge.

Gilstrap LC. (1997). Drugs in pregnancy. Introduction. *Seminars in Perinatology* **21**: 113.

Goldmann EE. (1909). Die äussere und innere Sekretion des gesunden und kranken Organismus im Lichte der 'vitalen Farbung'. *Beitr. Klin. Chirurg.* **64**: 192-265.

Goldmann EE. (1913). Vitalfarbung am Zentral-nervensystem. *Abh. Preuss. Akad. Wissensch., Physkol. Mathem Klasse. 1*: 1-60.

Gomez DG and Potts DG. (1981). The lateral, third, and fourth ventricle choroid plexus of the dog: a structural and ultrastructural study. *Annals of Neurology* **10**: 333-340.

Goodenough DA. (1999). Plugging the leaks. *Proceedings of the National Academy of Sciences of the United States of America* **96**: 319-321.

Graham RCJ and Karnovsky MJ. (1966). The early stages of absorption of injected horseradish peroxidase in the proximal tubules of mouse kidney: ultrastructural cytochemistry by a new technique. *Journal of Histochemistry and Cytochemistry* **14**: 291-302.

Habgood MD. (1990). Barriers in the developing brain. PhD thesis. University of Southampton.

Habgood MD, Begley DJ and Abbott NJ. (2000). Determinants of passive drug entry into the central nervous system. *Cellular and Molecular Neurobiology* **20**: 231-253.

Habgood MD, Knott GW, Dziegielewska KM and Saunders NR. (1993). The nature of the decrease in blood-cerebrospinal fluid barrier exchange during postnatal brain development in the rat. *Journal of Physiology* **468**: 73-83.

Habgood, MD, Liu ZD, Dehkordi LS, Khodr HH, Abbott J and Hider RC. (1999). Investigation into the correlation between the structure of hydroxypyridinones and blood-brain barrier permeability. *Biochemical Pharmacology* **57**: 1305-1310.

Habgood MD, Sedgwick JE, Dziegielewska KM and Saunders NR. (1992). A developmentally regulated blood-cerebrospinal fluid transfer mechanism for albumin in immature rats. *Journal of Physiology* **456**: 181-192.

Hirase T, Staddon JM, Saitou M, ando-Akatsuka Y, Itoh M, Furuse M, Fujimoto K, Tsukita S and Rubin LL. (1997). Occludin as a possible determinant of tight junction permeability in endothelial cells. *Journal of Cell Science* **110**: 1603-1613.

Jacobsen M, Møllgård K, Reynolds ML and Saunders NR. (1983). The choroid plexus in fetal sheep during development with special reference to intercellular plasma proteins. *Developmental Brain Research* **8**: 77-88.

Johanson CE. (1988). The choroid plexus-arachnoid memebrane-cerebrospinal fluid system. In: *Neuromethods. Neuronal microenvironment-electrolytes and water spaces*. A Boulton, G Baker and W Walz (ed). pp 33-104. Humana Press, Clifton, New Jersey.

Johanson CE. (1989). Ontogeny and phylogeny of the blood-brain barrier. In: *Basic Science Aspects. Implications of the blood-brain barrier and its manipulation.* EA Neuwelt (ed). pp 157-198. Plenum Publishing Corp., New York.

Johanson CE. (1993). Tissue barriers: diffusion, bulk flow, and volume transmission of proteins and peptides within the brain. In: *Biological barriers to protein delivery*. KL Audus and TJ Raub (ed). pp 467-486. Plenum Press, New York.

Johanson CE. (1995). Ventricles and cerebrospinal fluid. In: *Neuroscience in medicine.* PM Conn (ed). pp 171-196. J.B Lippincott Company, Philadelphia.

Johanson CE. (1998). Arachnoid membrane, subarachnoid CSF and pia-glia. In: *Introduction to the blood-brain barrier: methodology, biology and pathology.* WM Pardridge (ed). pp 259-269. University Press, Cambridge.

Johanson CE. (1999). Choroid plexus. In: *Elsevier's Encyclopedia of Neuroscience.* G Adelman and BH Smith (ed). pp 384-387. Elsevier Science, Amsterdam.

Johanson CE and Woodbury DM. (1974). Changes in CSF flow and extracellular space in the developing rat. In: *Drugs and the developing brain.* A Vernadikis and N Weiner (ed). pp 281-286. Plenum Press, New York.

Johansson BB. (1997). The blood-brain barrier as a protector against neurotoxic agents. In: *Principals of Medical Biology. Molecular and Cellular Pharmacology.* pp 1051-1063. JAI Press Inc., New York.

Jones HC and Keep RF. (1987). The control of potassium concentration in the cerebrospinal fluid and brain interstitial fluid of developing rats. *Journal of Physiology* **383**: 441-453.

Kappers JA. (1958). Structural and functional changes in the telenchephalon choroid plexus during human ontogenesis. In: *Ciba foundationsymposium on the Cerebrospinal fluid.* GEW Wolstenholem, CM O'Connor (ed). pp 3-31. Boston.

Karnovsky MJ. (1967). The ultrastructural basis of capillary permeability studied with peroxidase as a tracer. *Journal of Cell Biology* **35**: 213-236.

Keep RF and Jones HC. (1990). A morphometric study on the development of the lateral ventricle choroid plexus, choroid plexus capillaries and ventricular ependyma in the rat. *Brain Research. Developmental Brain Research* **56**: 47-53.

Keep RF, Jones HC and Cawkwell RD. (1986). A morphometric analysis of the development of the fourth ventricle choroid plexus in the rat. *Brain Research* **392**: 77-85.

King LS. (1939). The hematoencephalic barrier. *Archives for Neurology Psychiatry* **41**: 51-72.

Kniesel U, Risau W and Wolburg H. (1996). Development of blood-brain barrier tight junctions in the rat cortex. *Brain Research. Developmental Brain Research* **96**: 229-240.

Kniesel U and Wolburg H. (2000). Tight junctions of the blood-brain barrier. *Cellular and Molecular Neurobiology* **20**: 57-76.

Knott GW, Dziegielewska KM, Habgood MD, Li ZS and Saunders NR. (1997). Albumin transfer across the choroid plexus of South American opossum (Monodelphis domestica). *Journal of Physiology* **499**: 179-194.

Knott GW, Kitchener PD and Saunders NR. (1999). Development of motoneurons and primary sensory afferents in the thoracic and lumbar spinal cord of the South American opossum Monodelphis domestica. *Journal of Comparative Neurology* **414**: 423-436.

Köbbert C, Apps R, Bechmann I, Lanciego JL, Mey J and Thanos S. (2000). Current concepts in neuroanatomical tracing. *Progress in Neurobiology* **62**: 327-351.

Kraus DB and Fadem BH. (1987). Reproduction, development and physiology of the gray short-tailed opossum (Monodelphis domestica). *Laboratory Animal Science* **37**: 478-482.

Krisch B. (1986). The functional and structural borders between the CSF- and blood-dominated milieus in the choroid plexuses and the area postrema of the rat. *Cell and Tissue Research* **245**: 101-115.

Krisch B, Leonhardt H and Oksche A. (1984). Compartments and perivascular arrangement of the meninges covering the cerebral cortex of the rat. *Cell and Tissue Research* **238**: 459-474.

Krogh A. (1946). The active and passive exchanges of inorganic ions through the surfaces of living cells and through living membranes generally. *Proceedings of the Royal Society of London. Series B* **133**: 140-200.

Lautier D, Canitrot Y, Deeley RG and Cole SP. (1996). Multidrug resistance mediated by the multidrug resistance protein (MRP) gene. *Biochemical Pharmacology* **52**: 967-977.

Levin VA. (1980). Relationship of octanol/water partition coefficient and molecular weight to rat brain capillary permeability. *Journal of Medicinal Chemistry* **23**: 682-684.

Lewandowsky M. (1900). Zur lehre der cerebrospinal flüssigkeit. *Z. Klinische. Medizin.* **40**: 480-494.

Li ZS, Dziegielewska KM and Saunders NR. (1997). Transthyretin distribution in the developing choroid plexus of the South American opossum (Monodelphis domestica). *Cell and Tissue Research* **287**: 621-624.

Lossinsky AS, Vorbrodt AW and Wisniewski HM. (1983). Ultracytochemical studies of vesicular and canalicular transport structures in the injured mammalian blood-brain barrier. *Acta Neuropathologica* **61**: 239-245.

Lossinsky AS, Vorbrodt AW and Wisniewski HM. (1986). Characterization of endothelial cell transport in the developing mouse blood-brain barrier. *Developmental Neuroscience* **8**: 61-75.

Lu J, Kaur C and Ling EA. (1993). Uptake of tracer by the epiplexus cells via the choroid plexus epithelium following an intravenous or intraperitoneal injection of horseradish peroxidase in rats. *Journal of Anatomy* **183**: 609-617.

Madsen JK and Møllgård K. (1979). The tight epithelium of the Mongolian gerbil subcommissural organ as revealed by freeze-fracturing. *Journal of Neurocytology* **8**: 481-491.

Martinez-Palomo A and Erlij D. (1975). Structure of tight junctions in epithelia with different permeability. *Proceedings of the National Academy of Sciences of the United States of America* **72**: 4487-4491.

Mayer SE, Maickel RP and Brodie BB. (1959). Kinetics of penetration of drugs and foreign compounds into cerebrospinal fluid and brain. *Journal of Pharmacology* **127**: 205-211.

Milhorat TH, Davis DA and Hammock MK. (1975). Experimental intracerebral movement of electron microscopic tracers of various molecular sizes. *Journal of Neurosurgery* **42**: 315-329.

Milhorat TH, Davis DA and Lloyd BJJ. (1973). Two morphologically distinct blood-brain barriers preventing entry of cytochrome c into cerebrospinal fluid. *Science* **180**: 76-78.

Møllgård K, Balslev Y, Lauritzen B and Saunders NR. (1987). Cell junctions and membrane specializations in the ventricular zone (germinal matrix) of the developing sheep brain: a CSF-brain barrier. *Journal of Neurocytology* **16**: 433-444.

Møllgård K, Lauritzen B and Saunders NR. (1979). Double replica technique applied to choroid plexus from early foetal sheep: completeness and complexity of tight junctions. *Journal of Neurocytology* **8**: 139-149.

Møllgård K, Malinowska DH and Saunders NR. (1976). Lack of correlation between tight junction morphology and permeability properties in developing choroid plexus. *Nature* **264**: 293-294.

Møllgård K and Saunders NR. (1975). Complex tight junctions of epithelial and of endothelial cells in early foetal brain. *Journal of Neurocytology* **4**: 453-468.

Møllgård K and Saunders NR. (1977). A possible transepithelial pathway via endoplasmic reticulum in foetal sheep choroid plexus. *Proceedings of the Royal Society of London. Series B: Biological Sciences* **199**: 321-326.

Møllgård K and Saunders NR. (1986). The development of the human blood-brain and blood-CSF barriers. *Neuropathology and Applied Neurobiology* **12**: 337-358.

Molnár Z, Knott GW, Blakemore C and Saunders NR. (1998). Development of thalamocortical projections in the South American gray short-tailed opossum (Monodelphis domestica). *Journal of Comparative Neurology* **398**: 491-514.

Nabeshima S, Reese TS, Landis DM and Brightman MW. (1975). Junctions in the meninges and marginal glia. *Journal of Comparative Neurology* **164**: 127-169.

Nag S. (1998). Blood-brain barrier permeability measured with histochemistry. In: *Introduction to the blood-brain barrier: methodology, biology and pathology*. WM Pardridge (ed). pp 113-121. University Press, Cambridge.

Nag S, Robertson DM and Dinsdale HB. (1982). Intracerebral arteriolar permeability to lanthanum. *American Journal of Pathology* **107**: 336-341.

Nakamura S and Hochwald GM. (1983). Spinal fluid formation and glucose influx in normal and experimental hydrocephalic rats. *Experimental Neurology* **82**: 108-117.

Normand IC, Olver RE, Reynolds EO and Strang LB. (1971). Permeability of lung capillaries and alveoli to non-electrolytes in the foetal lamb. *Journal of Physiology* **219**: 303-330.

Oldendorf WH. (1974). Lipid solubility and drug penetration of the blood brain barrier. *Proceedings of the Society For Experimental Biology and Medicine* **147**: 813-815.

Oldendorf WH and Davson H. (1967). Brain extracellular space and the sink action of cerebrospinal fluid. Measurement of rabbit brain extracellular space using sucrose labeled with carbon 14. *Archives of Neurology* **17**: 196-205.

Pardridge WM. (1999). Non-invasive drug delivery to the human brain using endogenous blood-brain barrier transport systems. *Pharmaceutical Science and Technology Today* **2**: 49-59.

Parmelee JT, Bairamian D and Johanson CE. (1991). Response of infant and adult rat choroid plexus potassium transporters to increased extracellular potassium. *Brain Research. Developmental Brain Research* **60**: 229-233.

Parmelee JT and Johanson CE. (1989). Development of potassium transport capability by choroid plexus of infant rats. *American Journal of Physiology* **256**: R786-791.

Penta P. (1932). Sulla colorazione vitale del sistema nervosa negli centrale animali neonati. *Rivista di Neurologia* **5**: 62-80.

Peters A, Palay SL and Webster H. (1991). The fine structure of the nervous system. Neurons and their supporting cells. Oxford University Press, New York.

Prescott L and Brightman MW. (1998). Circumventricular organs of the brain. In: *Introduction to the blood-brain barrier: methodology, biology and pathology.* WM Pardridge (ed). pp 270-276. University Press, Cambridge.

Preston JE. (2001). Ageing choroid plexus-cerebrospinal fluid system. *Microscopy Research and Technique* **52**: 31-37.

Preston JE, Dyas M and Johanson CE. (1993). Development of chloride transport by the rat choroid plexus, in vitro. *Brain Research* **624**: 181-187.

Rapoport SI and Levitan H. (1974). Neurotoxicity of X-ray contrast media. Relation to lipid solubility and blood-brain barrier permeability. *American Journal of Roentgenology, Radium Therapy and Nuclear Medicine* **122**: 186-193.

Rascher G and Wolburg H. (1997). The tight junctions of the leptomeningeal blood-cerebrospinal fluid barrier during development. *Journal für Hirnforschung* **38**: 525-540.

Rayburn WF and Lavin JP. (1986). Drug prescribing for chronic medical disorders during pregnancy: an overview. *American Journal of Obstetrics & Gynecology* **155**: 565-569.

Reese TS, Feder N and Brightman MW. (1971). Electron microscopic study of the blood-brain and blood-cerebrospinal fluid barriers with microperoxidase. *Journal of Neuropathology and Experimental Neurology* **30**: 137-138.

Reese TS and Karnovsky KM. (1967). Fine structural localization of a blood-brain barrier to exogenous peroxidase. *Journal of Cell Biology* **34**: 207-217.

Rippe B and Haraldsson B. (1987). On the steady-state relationship between the microvascular hydrostatic pressure and the transvascular filtration rate. Effects of heteroporosity. *Acta Physiologica Scandinavica* **129**: 441-442.

Risau W, Esser S and Engelhardt B. (1998). Differentiation of blood-brain barrier endothelial cells. *Pathologie Biologie* **46**: 171-175.

Roncali L, Nico B, Ribatti D, Bertossi M and Mancini L. (1986). Microscopical and ultrastructural investigations on the development of the blood-brain barrier in the chick embryo optic tectum. *Acta Neuropathologica* **70**: 193-201.

Rothman AR, Freireich EJ, Gaskins JR, Patlak CS and Rall DP. (1961). Exchange of inulin and dextran between blood and cerebrospinal fluid. *American Journal of Physiology* **201**: 1145-1148.

Rousselle C, Clair P, Lefauconnier JM, Kaczorek M, Scherrmann JM and Temsamani J. (2000). New advances in the transport of doxorubicin through the blood-brain barrier by a peptide vector-mediated strategy. *Molecular Pharmacology* **57**: 679-686.

Rubin LL and Staddon JM. (1999). The cell biology of the blood-brain barrier. *Annual Review of Neuroscience* **22**: 11-28.

Saitou M, Fujimoto K, Doi Y, Itoh M, Fujimoto T, Furuse M, Takano H, Noda T and Tsukita S. (1998). Occludin-deficient embryonic stem cells can differentiate into polarized epithelial cells bearing tight junctions. *Journal of Cell Biology* **141**: 397-408.

Saitou M, Furuse M, Sasaki H, Schulzke JD, Fromm M, Takano H, Noda T and Tsukita S. (2000). Complex phenotype of mice lacking occludin, a component of tight junction strands. *Molecular Biology of the Cell* **11**: 4131-4142.

Saunders NR. (1992). Ontogenic development of brain barrier mechanism. In: *Handbook of Experimental Pharmacology: Physiology and Pharmacology of the Blood-Brain Barrier*. MWB Bradbury (ed). pp 327-369. Springer-Verlag, Berlin.

Saunders NR, Adam E, Reader M and Møllgård K. (1989). Monodelphis domestica (grey short-tailed opossum): an accessible model for studies of early neocortical development. *Anatomy and Embryology* **180**: 227-236.

Saunders NR, Balkwill P, Knott G, Habgood MD, Møllgård K, Treherne JM and Nicholls JG. (1992). Growth of axons through a lesion in the intact CNS of fetal rat maintained in long-term culture. *Proceedings of The Royal Society of London. Series B: Biological Sciences* **250**: 171-180.

Saunders NR and Dziegielewska KM. (1997). Barriers in the developing brain. *News in Physiological Sciences* **12**: 21-31.

Saunders NR, Dziegielewska KM, Ek J, Møllgård K. (1999c). Morphology and physiological aspects of the developing brain. In: *Alfred Benzon Symposium* 45, *Brain Barrier Systems*. O Paulson, GM Knudsen, T Moos (ed). pp 191-203. Munksgaard, Copenhagen.

Saunders NR, Habgood MD and Dziegielewska KM. (1999a). Barrier mechanisms in the brain, I. Adult brain. *Clinical and Experimental Pharmacology and Physiology* **26**: 11-19.

Saunders NR, Habgood MD and Dziegielewska KM. (1999b). Barrier mechanisms in the brain, II. Immature brain. *Clinical and Experimental Pharmacology and Physiology* **26**: 85-91.

Saunders NR, Kitchener P, Knott GW, Nicholls JG, Potter A and Smith TJ. (1998). Development of walking, swimming and neuronal connections after complete spinal cord transection in the neonatal opossum, Monodelphis domestica. *Journal of Neuroscience* **18**: 339-355.

Schneider H. (1991). Placental transport function. *Reproduction, Fertility, & Development* **3**: 345-353.

Schulze C and Firth JA. (1992). Interendothelial junctions during blood-brain barrier development in the rat: morphological changes at the level of individual tight junctional contacts. *Brain Research. Developmental Brain Research* **69**: 85-95.

Schwarze SR, Ho A, Vocero-Akbani A and Dowdy SF. (1999). In vivo protein transduction: delivery of a biologically active protein into the mouse. *Science* **285**: 1569-1572.

Sedlakova R, Shivers RR and Del Maestro RF. (1999). Ultrastructure of the blood-brain barrier in the rabbit. *Journal of Submicroscopic Cytology and Pathology* **31**: 149-161.

Serot JM, Foliguet B, Bene MC and Faure GC. (2001). Choroid plexus and ageing in rats: a morphometric and ultrastructural study. *European Journal of Neuroscience* **14**: 794-798.

Shivers RR, Betz AL and Goldstein GW. (1984). Isolated rat brain capillaries possess intact, structurally complex, interendothelial tight junctions; freeze-fracture verification of tight junction integrity. *Brain Research* **324**: 313-322.

Shuangshoti S and Netsky MG. (1966). Histogenesis of choroid plexus in man. *American Journal of Anatomy* **118**: 283-316.

Simionescu M, Ghinea N, Fixman A, Lasser M, Kukes L, Simionescu N and Palade GE. (1988). The cerebral microvasculature of the rat: structure and luminal surface properties during early development. *Journal of Submicroscopic Cytology and Pathology* **20**: 243-261.

Simionescu N and Siminoescu M and Palade GE. (1975). Permeability of muscle capillaries to small heme-peptides. Evidence for the existence of patent transendothelial channels. *Journal of Cell Biology* **64**: 586-607.

Smith QR and Stoll J. (1998). Blood-brain barrier amino acid transport. In: *Introduction to the blood-brain barrier: methodology, biology and pathology.* WM Pardridge (ed). pp 207-213. University Press, Cambridge.

Speake T, Whitwell C, Kajita H, Majid A and Brown PD. (2001). Mechanisms of CSF secretion by the choroid plexus. *Microscopy Research and Technique* **52**: 49-59.

Stern L and Peyrot R. (1927). Le fonctionnement de la barriere hémato-encéphalique aux divers stades de développement chez divereses espèces animales. *Comptes rendus des séances de la société de biologie* **96**: 1124-1126.

Stewart PA. (2000). Endothelial vesicles in the blood-brain barrier: are they related to permeability? *Cellular and Molecular Neurobiology* **20**: 149-163.

Stewart PA and Hayakawa EM. (1987). Interendothelial junctional changes underlie the developmental 'tightening' of the blood-brain barrier. *Brain Research* **429**: 271-281.

Stewart PA and Hayakawa K. (1994). Early ultrastructural changes in blood-brain barrier vessels of the rat embryo. *Brain Research. Developmental Brain Research* **78**: 25-34.

Stewart PA and Wiley MJ. (1981). Developing nervous tissue induces formation of blood-brain barrier characteristics in invading endothelial cells: a study using quail-chick transplantation chimeras. *Developmental Biology* **84**: 183-192.

Stonestreet BS, Patlak CS, Pettigrew KD, Reilly CB and Cserr HF. (1996). Ontogeny of blood-brain barrier function in ovine fetuses, lambs, and adults. *American Journal of Physiology* **271**: R1594-1601.

Sturrock RR. (1979). A morphological study of the development of the mouse choroid plexus. *Journal of Anatomy* **129**: 777-793.

Takeda H and Tsukita S. (1995). Effects of tyrosine phosphorylation on tight junctions in temperature-sensitive v-src-transfected MDCK cells. *Cell Structure and Function* **20**: 387-393.

Tauc M, Vignon X and Bouchaud C. (1984). Evidence for the effectiveness of the blood--CSF barrier in the fetal rat choroid plexus. A freeze-fracture and peroxidase diffusion study. *Tissue and Cell* **16**: 65-74.

Tennyson VM. (1971). The differences in fine structure of the myelencephalic and telencephalic choroid plexuses in the fetuses of man and rabbit, and a comparison with the mature stage. *Acta Neurologica Latinoamericana* **1**: 11-52.

Tennyson VM and Appas GD. (1968). The fine structure of the choroid plexus adult and developmental stages. *Progress in Brain Research* **29**: 63-85.

Tschirgi RD. (1950). Protein complexes and the impermeability of the blood-brain barrier. *American Journal of Physiology* **163**: 756.

Ueda F, Raja KB, Simpson RJ, Trowbridge IS and Bradbury MW. (1993). Rate of ^{59}Fe uptake into brain and cerebrospinal fluid and the influence thereon of antibodies against the transferrin receptor. *Journal of Neurochemistry* **60**: 106-113.

van Deurs B. (1979). Cell junctions in the endothelia and connective tissue of the rat choroid plexus. *Anatomical Record* **195**: 73-94.

van Deurs B, Moller M and Amtorp O. (1978). Uptake of horseradish peroxidase from CSF into the choroid plexus of the rat, with special reference to transepithelial transport. *Cell and Tissue Research* **187**: 215-234.

van Deurs BV. (1978). Microperoxidase uptake into the rat choroid plexus epithelium. *Journal of ultrastructure research* **62**: 168-180.

Wakai S and Hirokawa N. (1978). Development of the blood-brain barrier to horseradish peroxidase in the chick embryo. *Cell and Tissue Research* **195**: 195-203.

Wakai S and Hirokawa N. (1981). Development of blood-cerebrospinal fluid barrier to horseradish peroxidase in the avian choroidal epithelium. *Cell and Tissue Research* **214**: 271-278.

Weston JA. (1970). The migration and differentiation of neural crest cells. In: *Advances in Morphogenesis*. M Abercombie, J Brachet and TJ King (ed). pp 41-114. Academic Press, New York.

Wilting J and Christ B. (1989). An experimental and ultrastructural study on the development of the avian choroid plexus. *Cell and Tissue Research* **255**: 487-494.

Wislocki GB. (1920). Experimental studies on fetal absorption. *Contributions to Embryology* **11**: 45-60.

Xu J and Ling EA. (1994). Studies of the ultrastructure and permeability of the blood-brain barrier in the developing corpus callosum in postnatal rat brain using electron dense tracers. *Journal of Anatomy* **184**: 227-237.

Yoshida Y, Yamada M, Wakabayashi K and Ikuta F. (1988). Endothelial fenestrae in the rat fetal cerebrum. *Brain Research. Developmental Brain Research* **44**: 211-219.

Zaki W. (1981). Ultrastructure of the choroid plexus and its development in the mouse. *Zeitschrift für Mikroskopisch-Anatomische Forschung* **95**: 919-935.

Appendix A

Fixation and processing tissue for paraffin sections

1) Perfuse with PBS solution containing 5000 units heparin /100ml PBS for approximately 1-2 min. In smaller pups that cannot be perfused fixed, the tissue is processed from step 3.
2) Perfuse fix with fresh cool 4% paraformaldehyde solution.
3) Immerse tissue in Bouin's fixative for 24 hours.
4) 3x1hour changes in 70% ethanol.
5) 3x1 hour changes in 95% ethanol.
6) 3x1 hour changes 100% ethanol.
7) Leave tissue in chloroform overnight.
8) Leave in paraffin for 1 hour.
9) Transfer tissue to fresh paraffin and leave under –10 inches of mercury for 1-2 hours.
10) Decrease pressure to –20 inches of mercury and leave for 1-2 hours.
11) Embed in fresh paraffin and leave cool to harden.

Dewaxing and rehydrating paraffin sections

1) Melt paraffin in 60°C oven for 30 min.
2) 10 min in xylene.
3) 5 min in xylene.
4) 5 min in xylene.
5) 5 min 100% ethanol.
6) 5 min 100% ethanol.
7) 5 min 95% ethanol.
8) 5 min 70% ethanol.

Rehydrating and mounting paraffin sections

1) 5 min 70% ethanol.
2) 5 min 95% ethanol.
3) 5 min 100% ethanol.
4) 5 min 100% ethanol.
5) 5 min in xylene.
6) 5 min in xylene.
7) Mount slides.

Appendix B

Processing paraffin sections for BDA-3000 histochemistry

1) Dewax and rehydrate sections according to appendix A.
2) 3x5 min wash in 0.2% Tween20 PBS.
3) Incubate in peroxidase blocker (Dako) for 30 min.
4) 3x5 min wash in 0.2% Tween20 PBS.
5) Incubate in protein blocker (Dako) for 30 min.
6) 3x5 min wash in 0.2% Tween20 PBS.
7) Apply avidin-horseradish peroxidase complex using a Vectastain Elite ABC kit (Vector). Solution A and B must be mixed 30 min before incubation.
8) 3x10 min wash in Tween20 PBS.
9) Process sections with the diaminobenzidine tetrahydrochloride reaction (DAB Kit, Dako) for about 3-10 min.
10) Rinse briefly in distilled water.
11) Wash 10 min in tap water.
12) Dehydrate sections according to appendix A.
13) Mount slides with DPX.

Processing paraffin sections for BDA-3000 and endogenous albumin double labelling

1) Dewax and rehydrate sections according to appendix A.
2) 3x5 min wash in 0.2% Tween20 PBS.
3) Incubated in rabbit antibodies against human albumin (Dako) diluted 1:100 overnight in fridge.
4) 3x10 min wash in 0.2% Tween20 PBS.
5) Incubate in a mixture of 1:30 dilution of swine anti-rabbit fluorescein conjugated antiserum (FITC) antibodies (Dako) and 1:70 dilution of streptavidin Texas-Red (Vector) overnight in fridge.
6) 3x10 min wash in 0.2% Tween20 PBS.
7) Mount sections in an aqueous mounting medium (Dako).

Appendix C

Processing of choroid plexus for standard electron microscopy

1) Choroid plexus fixed in 2.5% glutaraldehyde cacodylate buffer (0.1 M, pH 7.3) and left in fixative for 2-3 hours at 4 C.
2) 3x10 min washes of tissue in buffer.
3) Osmicate in 50/50 mixture of osmium tetroxide (4%) and 0.05 M potassium ferrocyanide 0.2 M PBS solution for 45 min.
4) 3x10 min washes of sections in buffer.
5) Leave tissue in a 1% uranyl acetate solution for 30 min.
6) 10 min in 50% Ethanol.
7) 10 min in 75% Ethanol.
8) 10 min in 95% Ethanol.
9) 2x15 min in 100% Ethanol.
10) Rinse tissue 2x15 min in Propylene oxide.
11) Transfer to a 50/50 mixture of Procure 812/Propylene oxide for at least 1 hours.
12) Transfer to a 75/25 mixture of Procure 812/Propylene oxide for at least 1 hours.
13) Transfer to 100% Procure and leave overnight.
14) Transfer to fresh Procure and leave for 6-7 hours.
15) Embed in fresh procure and leave in 37°C for 12 hours.
16) Increase heat to 60°C and leave for 48 hours.

Appendix D

Biotin-dextran labelling of choroid plexus for electron microscopy

Injection: Intraperitoneal injection of BDA-3000 (0.7 mg/g body weight) and wait 30-45 min. Choroid plexuses dissected out and fixed in 2.5% glutaraldehyde phosphate buffered saline (0.1M, pH 7.3). Leave tissue in fridge for 2-3 hours.

1) 3x10 min washes of sections in large amounts of PBS.
2) Leave sections in 50% ethanol PBS solution for 30 min.
3) 3x10 min washes of sections in PBS.
4) Apply avidin peroxidase complex using an ABC kit (Vector). Leave A and B solution for 30 min in room temperature before incubation. Incubate for 30-60 min.
5) 3x10 min washes of sections in PBS.
6) Carry out DAB reaction. Try keeping the reaction time as short as possible to minimise precipitation.
7) 3x10 min washes of sections in PBS.
8) Osmicate in a 50/50 mixture of osmium tetroxide (4%) and 0.05 M potassium ferrocyanide 0.2 M PBS solution for 45 min.
9) 3x10 min washes of sections in PBS.
10) Leave tissue in a 1% uranyl acetate solution for 30 min.
11) 10 min in 50% Ethanol
12) 10 min in 75% Ethanol.
13) 10 min in 95% Ethanol.
14) 2x15 min in 100% Ethanol.
15) Rinse tissue in 2x15 min in Propylene oxide (for Procure 812).
16) Transfer to a 50/50 mixture of Procure 812/Propylene oxide for at least 1 hours.
17) Transfer to a 75/25 mixture of Procure 812/Propylene oxide for at least 1 hours.
18) Transfer to 100% Procure and leave overnight.
19) Transfer to fresh Procure and leave for 6-7 hours.
20) Embed in fresh procure and leave in 37°C for 12 hours.
21) Increase heat to 60°C and leave for 48 hours.